DESY 96-116

A Renormalization Group approach to Self-Organized Criticality

Dissertation
zur Erlangung des Doktorgrades
des Fachbereichs Physik
der Universität Hamburg

vorgelegt von
Bernhard Mikeska
aus München

Hamburg
1996

Gutachter der Dissertation:	Prof. Dr. G. Mack Priv. Doz. Dr. K. Jansen
Gutachter der Disputation:	Prof. Dr. G. Mack Prof. Dr. W. Buchmüller
Datum der Disputation:	2. Juli 1996
Sprecher des Fachbereichs Physik und Vorsitzender des Promotionsausschusses:	Prof. Dr. B. Kramer

Zusammenfassung

In dieser Arbeit untersuchen wir die Erweiterung der Renormierungsgruppen (RG)-Methode auf selbst-organisiert kritische Systeme. Wir beschränken uns auf extremale Modelle, in denen nur der Gitterpunkt (und seine rechten/linken Nachbarn) eine zeitliche Änderung pro Zeitschritt erfährt, dessen Wert extremal ist, d.h. der ein Minimum oder ein Maximum unter allen Gitterpunkten annimmt. Im RG-Zugang kommt es darauf an, die relevanten makroskopischen Variablen zu finden, die das System auf einer gröberen Skala beschreiben. Damit zusammenhängend ist eine makroskopische Dynamik zu finden, die aus den mikroskopischen Zusammenhängen der Variablen auf der feineren Skala erwächst (Blockverfahren). Um einen erfolgreichen Renormierungsgruppen-Ansatz zu entwickeln, fordern wir die Kommutativität des Blockverfahrens als ein wesentliches Element.

Wir erörtern den Zusammenhang zwischen gewöhnlichen und selbst-organisiert kritischen Systemen, insbesondere die Frage nach einem Mechanismus, der ein gewöhnliches kritisches System in ein selbst-organisiert kritisches System verwandelt. Im Hinblick auf unsere Anwendung eines RG-Zugangs auf ein Modell biologischer Evolution führen wir kurz in die biologischen Aspekte ein und geben einen Überblick über bisherige Arbeiten auf diesem Gebiet.

Anhand des Bak-Sneppen (BS) Modells für biologische Evolution entwickeln wir eine neue Technik um einen kürzlich vorgeschlagenen RG-Zugang zu verwirklichen. Damit gelingt es uns, frühere Ergebnisse zu verbessern und zu korrigieren. Darüberhinaus beschleunigt die neue Methode die RG-Iteration um wenigstens eine Größenordnung. Wir berechnen semi-analytisch die kritischen Exponenten des räumlichen und zeitlichen Skalenverhaltens der Lawinengrössen. Die Ergebnisse stimmen mit numerischen Studien auf 4% überein. Ferner haben wir sehr genaue numerische Simulationen für das isotrope BS-Modell durchgeführt und gute Übereinstimmung mit anderen Messungen neuerer Arbeiten festgestellt.

Die Anwendung der neuen Renormierungsgruppen-Methode auf das verwandte Phänomen von Grenzflächen in ungeordneten Medien wird diskutiert. Wir beschreiben das physikalische Problem, ein Blockverfahren zu definieren, das die Kommutativität respektiert. Jenseits dieses Problems stellen wir ein Verfahren zur Verfügung mit dem ein RG-Zugang realisiert werden könnte.

Wir analysieren ein kürzlich vorgeschlagenes ökonomisches Modell im Hinblick auf seinen SOC-Charakter. Obwohl es viele Eigenschaften von SOC-Modellen aufweist, ist es wahrscheinlich nicht selbst-organisiert kritisch. Wir untersuchen seine Beziehungen zu q-Zustands-Spinmodellen und betrachten ein einfaches Spielzeugmodell, das auf diesem Zusammenhang beruht, mit dem Ziel ein selbst-organisiert kritisches Modell zu konstruieren.

Abstract

In this paper we investigate the extension of the renormalization group (RG) method to self-organized critical (SOC) systems. We restrict ourselves to extremal models in which only one site (and its right/left neighbors), whose value is extremal, i.e. represents the minimum or maximum among all sites, evolves per time step. In the RG-approach one has to find the relevant macroscopic variables which describe the system on a coarser scale *and* the corresponding coarser dynamics obtained from the relations of the variables on the fine scale in a self-consistent way (blocking scheme). To design a successful renormalization group approach we postulate the commutativity of such a blocking scheme as an essential ingredient.

We discuss the correspondence of ordinary critical systems and self-organized critical systems, especially the question of a mechanism turning an ordinary critical system into a self-organized one. In view of our application of a RG-approach to a model of biological evolution, we give an introduction concerning the more biological aspects and review some work done in this field.

Using the example of the Bak-Sneppen (BS) model of biological evolution we develop a new technique to realize a recently proposed RG-approach for extremal models. Thereby we are able to improve and correct previous results. Moreover our new method speeds up the performance of the RG-iteration at least one order of magnitude. We calculate semi-analytical the critical exponents describing spatial and temporal avalanche scaling in the BS-model. The results coincide up to 4% with numerical studies. In addition we perform high precision numerical simulations for the isotropic BS-model and obtain good coincidence with the measurements of other recent publications.

The application of the new renormalization group method to the related phenomenon of interfaces in disordered media is discussed. We isolate the physical problem of how to define a blocking procedure respecting commutativity. Beyond this problem, we provide a scheme within which a RG-approach could be performed in principle.

We analyze a recently proposed model of an economic system with respect to its SOC-character. Though it contains many features common to SOC-models, it is probably not self-organized critical. We studied its connections to q-state spin models and consider a simple toy model based on this correspondence, aiming at construction of a self-organized critical model.

Contents

Introduction 4

I Self-Organized Criticality 6

1 Modeling Self-Organized Criticality 6

1.1 Self-Similarity and $1/f$ Noise 6

1.2 Cellular automata - type models 7

1.3 Extremal models 9

2 Self-Organized vs. Ordinary Criticality 10

2.1 Depinning transition 10

2.2 Role of order- and control parameter 13

2.3 Constructing a SOC-depinning model 14

II Biological Evolution as an SOC - Phenomenon 16

3 Evolution and Fitness Landscapes 16

3.1 Viewpoint of a Paleologist 16

3.2 Modeling Biological Evolution using Fitness Landscapes 19

3.3 NK-Landscapes 20

3.4 Coevolution of Species 21

3.5 Other approaches 23

4 Bak-Sneppen model 24

4.1 Definition of the Bak-Sneppen model 24

4.2 Interpretation in a biological context 25

4.3 Properties of the BS-model 30

4.4 Numerical Results 35

4.5 A local version of the BS-model 41

III Renormalization group approach to Self-Organized Criticality 42

5 Renormalization group method for the BS-model 42

5.1 The Idea 42

5.2 Construction of the Renormalization group approach 43

5.3 Calculating fundamental exponents τ and z 47

6 Run-Time-Statistics approach 48

6.1 The RTS-Equations 48

6.2 The renormalization group iteration 50

7 A new Monte-Carlo approach 51

7.1 The idea 51

7.2 Advantages and Disadvantages 54

7.3 Analysis of fixed point properties 55

8 Interfaces in Disordered Media 59

8.1 Linear Interface Model and "Robin Hood"-Model 60

8.2 Discussion of an RG-approach 64

IV Self-organized criticality in economical systems **67**

9 A simple model of money exchange **67**

9.1 Description of the model 67

9.2 Evolutionary money exchange model 68

10 Self-organized criticality in the model of money exchange **68**

10.1 Avalanche analysis 68

10.2 Analogies and differences with spin models 72

10.3 A simple economical model at criticality 73

Conclusions and Outlook **76**

Bibliography **77**

Introduction

Since the early days of science[1], the question for a deeper understanding of the emergence of macroscopic phenomena, arising from interaction among smallest elements fascinates philosophers and scientists, among them especially physicists. Uncovering composite objects *and* the macroscopic dynamics describing their interaction goes in parallel with growing physical insight into the system [Mac 94].

This fact is elucidated when one applies such multiscale tools as the renormalization group (RG) method [Wil 71] or numerical multiscale algorithms [Mac 87]. Both methods are successful only if a good understanding of the relevant macroscopic excitations is provided. In RG-methods one usually deals with block spins, in numerical multigrid methods as an example of a multiscale algorithm the same information is included in the restriction kernel.

A very well understood example in this sense is the magnetic property of certain metals. At low temperatures the microscopic elementary units behave in an ordered fashion and align their spins in the same direction thereby producing a macroscopic magnetization. Renormalization group methods as well as efficient numerical multiscale methods achieved a good understanding of ordered systems [Itz 89].

However, most systems occuring in nature are not of this friendly ordered type. We think of spinglasses, neural networks modeling brain function, interfaces in disordered media, ecosystems, biological evolution and economical processes like stock market dynamics. These are fundamentally different from ordered systems. They account for a very rich macroscopic description, while ordered systems may be described by only a few variables and may assume only a few macrostates.

Consider two examples: water can be specified by temperature and pressure without ambiguities, it can assume three macrostates (solid, liquid and gaseous). On the other hand consider a biological protein. Mostly the protein may fold in many different ways and each folding may have a totally different function due to its three dimensional structure. Each of the possible foldings represents a macrostate and hence the macroscopic description is very rich. Following Parisi [Par 94], we denote such a system as a *complex system.*

Ordered systems are well understood since it is relatively clear in which way macroscopic observables are composed from microscopic elements. The renormalization group or efficient numerical methods open the possibility of an intensive study of these systems. In the case of disordered and complex systems it is much more difficult to extract the relevant composite objects and their macroscopic dynamics emerging from microscopic elements and their local interactions [Mac 94].

One of the most interesting examples of complex systems is the class of the *self-organized*

[1] Around 340 B.C. Aristoteles thought about the relation of the whole to its parts, "The whole is greater than the sum of its parts".

critical (SOC) systems. They evolve intrinsically towards a critical state without any fine tuning of an external parameter. It is believed that such systems are abundant in nature, consider e.g. the structure and growth of interfaces, earthquake dynamics, ecological and economic processes [Bak 87]. In the past decade there was a great effort in designing and studying simplified models of such systems.

However, they have been studied only via large scale computer simulations until recently. Such an approach is expensive and moreover it does not provide a deeper understanding of the *self-organized* nature of the dynamics. The aim of this thesis is to study and develop a tool inspired from the renormalization group designed for a better understanding of self-organized critical systems and to provide an analytical method to calculate critical exponents that could be measured only numerically up to now.

For a special class of SOC-models, which are similar to cellular automata, such an RG-approach was proposed in [Pie 94] for the first time. We concentrate on a different class of models which we call *extremal models*. The most popular representative among these models is the Bak-Sneppen (BS) model of biological evolution [Bak 93], which will be our main actor throughout this work.

The thesis is organized in four main parts:

Chapter I introduces the reader to the phenomenon of Self-Organized Criticality. The first section explains the original idea of self-organized criticality and categorizes different approaches of modeling SOC-systems. The second section illuminates the self-organized nature of such systems by considering their relation to ordinary critical phenomena.

Chapter II prepares the reader for the study of the biological evolution model. Section 3 provides some biological background information on competing evolution theories, introduces basic concepts like fitness landscapes and the principle of coevolution, earlier approaches to model biological evolution are shortly reviewed. Section 4 is devoted to the introduction and discussion of the BS-model of biological evolution. Numerical and analytical results are summarized.

Chapter III, the heart of this thesis, considers the possibilities of a renormalization group analysis of the BS-model. Based on work of Marsili [Mar 94b] the necessary ingredients for a multiscale analysis are discussed (section 5), his technical approach to this concept is reviewed and at some points corrected (section 6). We propose a new independent method and present the results obtained with this new approach in section 7. The application of the same procedure to the problem of self-organized critical behavior of interfaces in disordered media is considered in the last section of this chapter.

The thesis is completed by reporting some of our research on the dynamics of economic systems (Chapter IV). Though it is widely believed that such systems are also self-organized critical, there is no major breakthrough in this direction up to today. The ideas contained in this chapter might be a first step towards an economical SOC-model.

I Self-Organized Criticality

This chapter introduces the reader to the concept and main ideas of self-organized criticality. An overview on the research activities of the past decade is given. We propose to divide the models studied into two classes (Section 1). The connections of self-organized criticality and ordinary critical phenomena are considered in section 2 using the class of extremal models, especially models of interfaces in disordered media.

1 Modeling Self-Organized Criticality

We give an introduction to the phenomenon of Self-Organized Criticality (SOC). In the first paragraph it is postulated that self-similarity and $1/f$-noise are the spatial respectively temporal fingerprint of one underlying mechanism which is called self-organized criticality. In the remaining two paragraphs we present some examples out of the variety of SOC-models invented so far. These models may be divided into cellular automata type models (1.2) and extremal models (1.3). The latter case is discussed only shortly since extremal models will be the main actor throughout this work and we will become more familiar with them during later chapters.

1.1 Self-Similarity and $1/f$ Noise

Self-similarity and $1/f$ noise are widespread phenomena observed in nature. The term self-similarity may be defined in the following way [Man 83]. A shape (e.g. a curve, a coastline, the branching structure of a tree), as well as the mechanism generating it, is *self-similar* if each piece of the shape is geometrically similar to the whole. In other words: self-similarity means geometrical invariance under spatial scale transformations. Such shapes are ubiquitous in nature: coastlines and mountain landscapes, Brownian motion, the structure of the human lung, turbulence phenomena [Man 83]. An example from astrophysics is the distribution of galaxies [Pie 92]. New data and reanalysis of old experimental data on the large scale structure has shown that the distribution of visible matter in the universe appears to be fractal up to the observational limits.

Though much work has been done on construction and generation of self-similar objects, their physical background and the reason why they are so abundant in nature remains dark. The idea of self-organized criticality marks a step towards a better understanding of these phenomena as we will discuss below.

Besides self-similarity the so called *flicker noise* is a widely occuring temporal phenomenon [Dut 81]. It denotes the power law behavior of a power spectrum $M(f)$ scaling as $M(f) \sim f^{-\alpha}$, $\alpha \approx 1$ and is also known as $1/f$ noise. Such noise is observed in current flow through resistors, flow of rivers, stock exchange price indices [Man 83], music [Vos 75, Boo 95] and light emission from quasars [Har 87]. Let us be a bit more concrete and consider for the last case a light intensity $I(t)$ observed from an active

galactic source. The power spectrum $M(f)$ is defined as fourier transformation of the correlation function $M(\tau) = \langle I(t)I(t+\tau)\rangle$,

$$M(f) = \int M(\tau)e^{-i\tau f}d\tau \sim \frac{1}{f} \ , \tag{1.1}$$

which is measured in [Har 87] for a frequency range of nearly three decades. Noteworthy are also results from the analysis of temporal correlations of music literature from the 18th to the 20th century. In [Vos 75] power spectra of the loudness and pitch fluctuations for Bach's 1st Brandenburg Concerto and for the output of 12 hours of different radio stations (classical, jazz, rock) are calculated. The authors claim to find a $1/f$ spectrum. A recent work containing more detailed analysis of this question [Boo 95] is at variance with this claim. They find for pitch fluctuations a power spectrum $M(f) \sim 1/f^{\alpha}$ with $\alpha \approx 2$. They explain the difference with the fact that Voss and Clarke used long sequences containing different pieces, different composers and styles as well as spoken announcements. They argue that a single piece is normally the largest unit of artistic significance and it therefore does not make sense to use larger recordings containing several pieces.

To resolve the puzzle of the ubiquitous existence of $1/f$ noise as well as self-similarity, Bak, Tang and Wiesenfeld [Bak 87, Bak 88] proposed in 1987 that both phenomena are the spatial resp. the temporal signature of the same underlying phenomenon: Self-Organized Criticality. A self-organized critical system is a critical system with all usual properties like scale invariance, spatial and temporal correlations on all length scales and obeying universality. Moreover the critical state is an attractor of the dynamics, i.e. no fine tuning of any parameter to a critical value is needed. This property accounts for the abundant observations of self-similarity and $1/f$ noise; many natural systems are driven to the critical state by their own dynamics.

The concept of SOC has been studied in computer experiments, sometimes in real experiments and we will give a short overview on research activities of the last decade in the next two paragraphs.

1.2 Cellular automata - type models

All models of this class are similar in structure and dynamics to deterministic or stochastic cellular automata [Wol 84]. Among them is the classical sandpile model [Bak 87], forest-fire models (for a review see [Dro 94]), earthquake models [Ola 92] and also the 'Game of Life' [Bak 89]. Each of these models is defined on a d-dimensional lattice, the lattice cell assumes a discrete state and the time evolution of a cell is governed by stochastic or deterministic rules depending on the state of the neighbor cell.

We want to discuss the main properties of self-organized criticality using the prototype of all SOC-models, the classical sandpile, originally introduced in [Bak 87]. The idea is to perform the following experiment: take an amount of sand and drop from above one single grain after another onto the same place. After some time we will observe a small hill with a shallow slope. The hill becomes larger with time and the slope increases.

Eventually the pile will reach a state in which the slope no longer grows. The sandpile becomes unstable in the sense that adding a grain would increase the slope beyond this instability and will thus trigger an avalanche of grains sliding down. The size s of this avalanche is given by the number of grains involved. Once the avalanche stops one may add the next grain. The avalanche size distribution obeys a power law

$$P(s) \sim s^{-\alpha} \quad , \alpha > 0 \quad , \tag{1.2}$$

thus avalanches occur on all length scales. This scale invariant, critical state is an attractor of the dynamics. If we start the experiment with a flat surface, we will observe for a certain time interval more often smaller avalanches and the pile builds up. If we start with a pile steeper than the critical slope we will observe for a short time interval a larger number of very large avalanches thereby decreasing the slope of the pile. Besides the exponent α describing critical fluctuations several other exponents can be defined describing spatial and temporal correlations. The hope is that these exponents are universal and do not depend on microscopic properties but only on symmetry and dimension. Of course the critical slope itself may depend on the details, e.g. on the sort of grains or their size. For wet grains we expect a larger critical slope than for dry grains, but the exponent α and other possible exponents should be the same. If this universality holds, it is possible to use simple models (suitable for computer simulations) for predictions on the behavior of realistic systems.

We now sketch the construction of a simplified computer model for a sandpile. On a $2d$-array one defines a height variable h_i for each site i and a height difference z_i, the local slope, to the neighboring sites[2]. Adding a grain to site i these variables have to be updated for this site. If the new slope exceeds a critical value z_c, the site relaxes and one grain is moving to neighbor sites. In turn this may cause the neighbor sites to become critical and to relax by their self. A chain reaction sets in that is an avalanche of sliding grains. When all local slopes are smaller than the critical slope the avalanche comes to rest and one may add a grain and thereby trigger an avalanche anew.

The main mechanism is the 'transportation of slope' from one critical cell to the neighbor cells, thereby opening the possibility of becoming critical by their self and inducing a "domino" effect. Essentially the same mechanism is responsible for the SOC-behavior of earthquake models (transportation of frictional energy) and forest-fire models (transportation of fire). Earthquake models have been considered to explain the Gutenberg-Richter law for the distribution of earthquakes $P(E)$ in which an amount of energy E is released, $P(E) \sim E^{-b}$, $b \approx 1.5$ [Bak 90]. However, in earthquake models the critical exponents depend on details of the specific model, e.g. on the level of energy conservation [Ola 92] and are thus somewhat problematic and not truly self-organized critical.

The forest-fire model [Dro 94] is an example of an stochastic cellular automaton, it contains a lightening probability and a tree-growth probability. The forest-fire model turned out to be self-organized critical only in the limit of vanishing lightening probability and it is thus at least questionable if it is really a self-organized critical system.

[2]The slope could be defined as the height difference in diagonal direction, thus adding height differences in x- and y-directions. For details see [Bak 88].

The question of a fractal structure of the universe is investigated by a toy model in [Che 89]. It describes propagating active particles interacting with passive static particles following cellular automata like rules. The authors observe, that an initially homogeneous mass distribution evolves towards a fractal distribution of active 'bright' sites. This model is very similar to the 'Game of Life' [Bak 89].

A real experiment with sandpiles has been reported in [Hel 90]. The experimental findings confirm the picture obtained by computer experiments at least for sufficiently small sandpiles that show scale invariant avalanche events. However, the power spectrum of the mass fluctuations is proportional to $1/f^2$ and not to the $1/f$ behavior as was the original idea of Bak and coworkers. This finding has also been confirmed theoretically by [Jen 89].

Recently a renormalization group approach has been invented for cellular automata type models, applied to sandpiles [Pie 94, Ves 95, Ves 96] and forest-fire models [Lor 95, Ves 96]. With this method it is possible to demonstrate the attractive *self-organized* nature of the critical state for the sandpile model and to calculate the main critical exponents. The values coincide with the simulation results up to four percent. For the forest-fire model, the RG-method detects the lightening probability as a relevant parameter, thus emphasizing the point that the forest-fire model is not really self-organized. The exponents are calculated with similar precision as for the sandpile model. This renormalization group approach is suitable for models using discrete states and a cellular automata type dynamics. For the completely different class of *extremal models* this approach is not applicable and the remainder of this work is dedicated to the development and discussion of a renormalization group tool for these models. We give a short overview on this class of models in the next paragraph.

1.3 Extremal models

This class contains models whose dynamics relies on the global search of a minimal or maximal value of a specific variable ϕ_i among all sites i of the system. The site with extremal value at time t is denoted as active site $i(t)$. Its extremal value is denoted $\varphi_{i(t)}$. The updating is done only for this active site and the sites interacting with it. We will see that this setup guarantees an infinitesimal driving rate which is essential for self-organized criticality.

Most popular examples that fit into this scheme are interfaces in disordered media [Gal 95] and the BS-model of biological evolution [Bak 93]. Both models are discussed in detail throughout this work and we refer the reader to the corresponding sections (for interfaces see section 8, for the biological evolution model section 4). The next section elucidates the connection between infinitesimal driving rate in extremal models and self-organized criticality.

2 Self-Organized vs. Ordinary Criticality

In this section we want to elucidate some connections between ordinary critical phenomena and self-organized critical systems. An understanding of this connection will provide us with a deeper insight into the mechanisms leading to self-organized criticality. To this end we introduce the well known depinning transition of an interface in a disordered medium as an example in paragraph 2.1. The pinning and depinning of interfaces by random impurities occurs in many circumstances: the motion of a domain wall in the random field Ising model [Ji 92], the fluid flow through porous media [Kop 85], the growth of bacteria colonies [Vic 90], burning paper [Zha 92] or fluid penetration in paper [Bul 92]. In the following paragraph (2.2) we discuss a new view of the role of order- and control parameter in ordinary critical phenomena as presented by Sornette *et al.* [Sor 95]. Finally we apply this scenario in 2.3 to the classical depinning transition and show how to turn this ordinary critical phenomenon into a self-organized critical system.

2.1 Depinning transition

Among the huge variety of systems showing a depinning transition we would like to concentrate on the fluid flow through porous media. Consider an oil-water interface in a porous material separating both phases. Let us assume a constant pressure exerted on the oil from below. Thus the oil displaces the water and the interface moves upward, see Figure 2.1. We assume further, that the interface is well described by a solid-on-solid model, i.e., it has no overhangs. Eventually we consider the displacement of the water by the oil as an irreversible process, i.e. the interfaces can move only upward. An interesting question for technical applications is the scaling of the interface roughness w^2 with the linear dimension L of the system. This is commonly characterized by the roughness exponent χ,

$$w^2 = \langle h^2 \rangle - \langle h \rangle^2 \sim L^{2\chi}. \tag{2.1}$$

Such an interface may be described by the Hamiltonian [Bru 84]

$$\mathcal{H}[h(x), f] = \frac{\sigma}{2} \int_0^L dx |\nabla h(x)|^2 + \int_0^L dx \int_0^{h(x)} dh'(\eta(h', x) - f)) \tag{2.2}$$

The first term describes the energy due to the usual surface tension, the second term involves the energy contribution of the disorder. $\eta(h, x)$ is a random pinning force of the surface at site x and height $h(x)$ preventing the interface from moving further upward. The physical origin of this random force might be for example a locally varying surface tension of the oil-water interface due to more or less small holes in the porous material, see Figure 2.1. The force f acting in the opposite direction as η is induced by a constant pressure that is exerted on the oil invading from below.

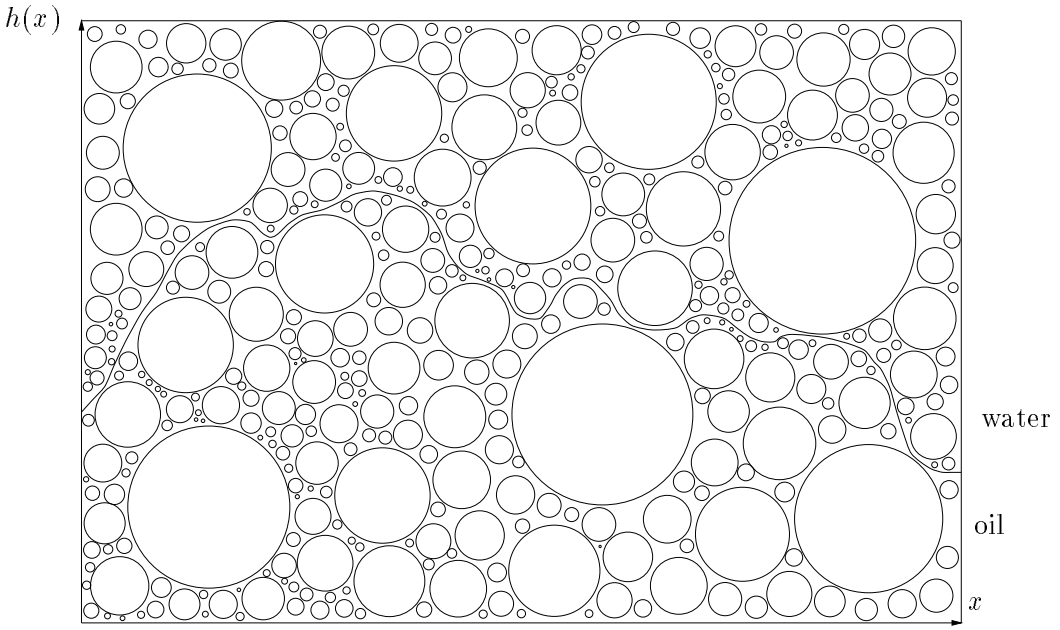

Figure 2.1: Example of a interface (line) separating oil and water in a porous rock (symbolized by circles). The oil invades from below and displaces the water. The disorder is induced via a more or less strong surface tension due to different hole sizes in the porous rock, thus preventing the oil with a more or less strong force from moving upward.

The equation of motion for the interface $h(x)$ is obtained via a variational ansatz

$$\dot{h}(x,t) = -\frac{\delta \mathcal{H}[h,f]}{\delta h} \quad . \tag{2.3}$$

The variation $\delta h(x)$ with boundary condition

$$\delta h(0) = \delta h(L) = 0 \tag{2.4}$$

leads to

$$\begin{aligned}
\delta\mathcal{H}[h,f] = \; & \mathcal{H}[h+\delta h, f] - \mathcal{H}[h,f] \\
= & \int_0^L dx \frac{\sigma}{2} |\nabla h(x) + \nabla \delta h(x)|^2 + \int_0^L dx \int_0^{h(x)+\delta h(x)} dh'(\eta(h',x) - f)) \\
& - \frac{\sigma}{2} \int_0^L dx |\nabla h(x)|^2 - \int_0^L dx \int_0^{h(x)} dh'(\eta(h',x) - f) \\
= & \int_0^L dx (\sigma \nabla h(x) \nabla \delta h(x)) + \int_0^L dx \int_{h(x)}^{h(x)+\delta h(x)} dh'(\eta(h',x) - f) + o(\delta h^2) \\
= & \int_0^L dx \left[-\sigma \nabla^2 h(x) \delta h(x) + (\eta(h,x) - f) \delta h(x) \right] \\
= & \int_0^L dx (-\sigma \nabla^2 h(x) + \eta(h,x) - f) \delta h(x) \quad .
\end{aligned} \tag{2.5}$$

This is valid for arbitrary functions $\delta h(x)$, thus we obtain

$$\dot{h}(x,t) = \sigma \Delta h(x,t) - \eta(h,x) + f \quad , \tag{2.6}$$

which is known as the BAKL-equation (Bruinsma,Aeppli,Koplik,Levine).

Due to the disorder it is possible that the interface becomes trapped in a configuration where all $\eta(h,x)$ are large enough to balance the surface term plus the contribution from f, i.e. $\dot{h}(x,t) < 0$. In general the interface will move forward by an infinitesimal amount δh if $\dot{h}(x,t) \geq 0$, i.e. if $f \geq -\sigma \Delta h(x,t) + \eta(h,x)$. Discretizing in space and time we obtain for the irreversible motion of the interface

$$h(x, t+\delta t) = \begin{cases} h(x,t) + \delta h & f \geq -\sigma \Delta h(x,t) + \eta(h,x) \\ h(x,t) & \text{else} \quad . \end{cases} \tag{2.7}$$

For large f, the probability that the interface becomes stuck in a local minimum vanishes. Then we expect a moving interface with constant velocity v

$$v \equiv \lim_{\delta t \to 0} \left\langle \frac{1}{\delta t} \int_0^L h(x, t+\delta t) - h(x,t) dx \right\rangle_{\text{disorder } \eta} \quad . \tag{2.8}$$

For vanishing external force, $f \equiv 0$, the interface becomes trapped in a meta-stable state, i.e. in a configuration where all $\eta(h,x)$ are large enough to balance the surface term. Then the velocity v will be zero.

Imagine that we increase f starting from $f = 0$ slowly. At some critical value f_c the interface will become depinned and start to move with a finite velocity $v > 0$. A phase transition from the pinned to the depinned state occurs at the critical value f_c. Above the critical point the velocity v behaves according to [Nar 93] (see also Figure 2.2)

$$v \sim (\frac{f}{f_c} - 1)^{\beta} \quad . \tag{2.9}$$

The depinning transition is an ordinary critical phenomenon [Fis 85]. A control parameter exits that has to be tuned externally to its critical value. However, it is possible to turn this ordinary critical phenomenon into self-organized criticality. A systematic way how to achieve this will be introduced in the following paragraph.

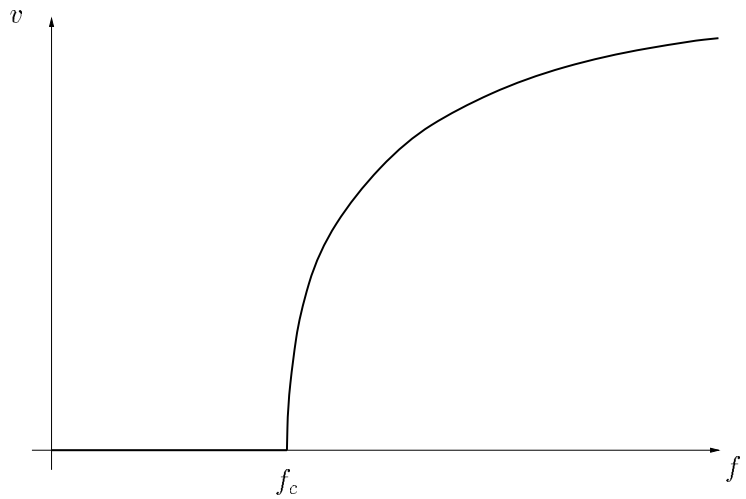

Figure 2.2: Depinning transition of an interface in a disordered medium. At a critical value f_c the interface starts to move forward with finite velocity v. Below f_c the interface is trapped in meta-stable state.

2.2 Role of order- and control parameter

In ordinary critical phenomena there always is a control- and an order parameter. In the standard ferromagnetic Ising model with zero external field the order parameter is the total magnetization M which is zero above the critical temperature T_c and behaves like $M \sim (T_c - T)^\beta$ below T_c. The temperature T is the control parameter that has to be tuned to T_c for the system to be critical, i.e. to show infinite correlation length.

Sornette *et al.* now make the following proposal [Sor 95]: It may turn out to be natural for a system, instead of controlling the control parameter T, that the order parameter M is tuned and moreover it is tuned to a positive but arbitrarily small value. In other words: the order parameter M is tuned to $M \to 0^+$. This has the consequence that the former control parameter is driven to $T \to T_c^-$. Note the two ingredients of this mechanism:

- exchange the role of order- and control-parameter
- tune the former order-parameter (now control-parameter) to an arbitrarily small positive value.

This procedure is applicable to *every* ordinary critical phenomenon. In our opinion, however, this does not mean that every ordinary critical phenomenon may be turned into a self-organized critical phenomenon. This is only possible if controlling the former order parameter and its tuning to 0^+ is *natural. Natural* means that nature itself acts in this way. This is the case if it is possible to define an experimental setup realizing a the system with the former order-parameter now acting as control-parameter, i.e. if the experimentator is able to to adjust the former order-parameter to 0^+ by hand. Of course this is an ambivalent definition since it often depends on the interpretation of

the experimentator studying the system. As the essence of this discussion we want to propose here the following definition:

Self-Organized Criticality is an ordinary critical phenomenon for which it is natural to tune the order parameter to 0^+ .

A natural tuning of the order parameter to 0^+ is at least sometimes equivalent to the condition of driving the system at an infinitely small rate [Sor 95, Gri 95]. Obviously the ferromagnetic Ising model is *not* self-organized critical in the sense of our definition: it is not possible to find a parameter, that controls the total magnetization directly (one cannot control the direction of single spins), thus it is not natural to tune the former order-parameter to 0^+ and the Ising model is not a candidate for SOC. For a discussion of sandpile- and forest-fire-models that have been described shortly in section 1.2, see [Sor 95].

In the next section we consider the previously described depinning transition, for which we will see that it is natural to exchange the role of order- and control-parameter and to tune the former order-parameter to 0^+. In paragraph 4.5 we give some remarks on the Bak-Sneppen model of biological evolution in this context.

2.3 Constructing a SOC-depinning model

Following the discussion of the previous paragraph, we will now explain how to turn the depinning transition of an interface in a disordered medium into a self-organized critical phenomenon. In this case the order parameter is the velocity of the moving interface v, defined in (2.8). The control parameter is the external force f. Applying the concept discussed above, one has to tune the velocity to an arbitrarily small but positive value, $v \to 0^+$, thereby adjusting f to the critical value f_c.

This may be achieved as follows: one has to move upward only one site of the interface by one unit δh per time step δt. This results in the smallest possible velocity $v > 0$. The next question arising is, which site of the interface should be moved upward ? A natural choice is to move the site x of the interface pinned with minimal pinning force $-\sigma\Delta h(x,t) + \eta(h,x)$. Or equivalently, look for the site x with maximal value of $\sigma\Delta h(x,t) - \eta(h,x)$ and change $h(x,t) \to h(x,t+1) = h(x,t) + \delta h$ [3]. The force $f(t)$ that has to act for this movement (see equation (2.7)) is

$$f(t) = min_x \{-\sigma\Delta h(x,t) + \eta(h,x)\} \quad . \tag{2.10}$$

$f(t)$ will then fluctuate in time around the critical value f_c. This kind of dynamics, moving only the least pinned site, is realized in real experimental situations [Gal 95]. In a typical experiment with a water-air interface in a porous medium, the water displacing the air, water is pumped at constant but infinitesimally slow rate into the system. Thus a pressure in the water phase builds up until eventually a breakthrough occurs at the minimally pinned position of the interface. Due to the volume gain of the water phase

[3] We will see in section 8 that this maximum definition is the basis of all SOC-depinning models.

and the infinitesimally slow pumping, the pressure in the water phase drops. Now it takes some time pumping more water into the system, building up higher pressure slowly until the next breakthrough of the interface occurs. This procedure is exactly the tuning of $v \to 0^+$ described above. Thus it is natural for a interface in an disordered medium to move with infinitely small velocity v and hence we are allowed to consider it as a self-organized critical phenomenon in the described experimental context.

A discussion of some models describing SOC-depinning will be introduced in section 8 with an application of a renormalization group procedure in mind. Before, a possible RG-method for extremal self-organized critical models will be introduced and applied to a simple model of biological evolution.

II Biological Evolution as an SOC - Phenomenon

This chapter is devoted to the study of biological evolution as a self-organized critical phenomenon. The reason why it is appealing to consider biological evolution as a self-organized critical process is the following. Consider extinction events in an ecology as avalanches: A small perturbation of the ecology may be able to induce extinction events of all sizes due to the connectivity of the ecological system. Thus one could explain mass extinction events such as the famous demise of the dinosaurs as an intrinsic property of the underlying system and its dynamics. There would be no need for some extraterrestrial influences, e.g. meteorite crashes[4]. We give a short introduction to the basics from a biologist's point of view and discuss some earlier approaches to model biological evolution aiming at the reproduction of paleological data and the construction of a self-organized critical model (section 3). However, none of the presented models turned out to be self-organized critical until Bak and Sneppen introduced their very simple BS-model. This model is defined and discussed analytically and numerically in section 4.

3 Evolution and Fitness Landscapes

We give a comprehensive overview on the biological background of the theory of biological evolution. In the first paragraph we take a look at the extinction rates of species in earth history. Following these observations, we explain the concept of punctuated equilibrium which is in contrast to Darwinism. In the second paragraph 3.2 we introduce the idea of a fitness landscape used to model main aspects of biological evolution. This paragraph already leads us to a more physical point of view. The following paragraphs 3.3 and 3.4 deal with a model proposed by Kauffman *et al.* [Kau 87] which was refined in the early nineties by Flyvbjerg, Lautrup and Bak [Fly 92, Bak 92] with the hope to detect self-organized criticality therein. In 3.4 we discuss the coevolution principle applied to this model. The last paragraph gives a short overview on some more recent approaches to model biological evolution mainly inspired from spinglass physics. All models in this section are based on the concept of a fitness landscape and none of them turned out to be self-organized critical.

3.1 Viewpoint of a Paleologist

Over the past 600 million years, which is approximately the period of life on earth, about 4×10^9 species of plants and animals have lived on earth. Only a few millions are living on our planet today[Rau 86]. From these numbers it is obvious that extinction of species is at least as important as their origination and in the following we want to take a closer look onto the dynamics and size of extinction events.

[4]Of course this would not exclude such catastrophes.

Because of the extremely small probability of preservation and discovery of species, the database for extinction analysis consists of only approximately 250 000 known fossil species [Rau 86]. This is of course a negligible small fraction of all species that ever lived on earth and the conclusions from these data should be handled with caution. Nevertheless it is possible to deduce some interesting facts on extinction dynamics.

Let us start considering extinction events; well known and most popular is the mass extinction at the end of the Cretaceous that includes the demise of the dinosaurs[5]. During this terminal Cretaceous extinction approximately 15% of all species became extinct. Besides this famous event, we know from the fossil record of four more events of similar or larger order, the largest one being the late Permian mass extinction with a percentage of approximately 60% of all species that did not survive [Ben 95].

On the other hand small extinction events with only a few species or families involved are also observed. These events are sometimes considered as "background" or "spontaneous" extinction [Rau 86]. They occur much more often than larger events. In Figure 3.1 we show data from [Rau 86] describing the varying intensity of extinction events. Based on the data of 2316 extinct families of marine animals from the 600 million years, the probability of an extinction event of size s is shown. The size s of an extinction is defined as the number of marine families that became extinct during one of the 79 known geological stages of earth history, each one lasting about 7 million years on average.

From these data we conclude that extinction events of every size are possible. The double logarithmic plot reveals that the extinction size probability does not follow a strict power law, at least if we use our usual precision standards. However, one has to keep in mind, that the fossil record provides us with very incomplete and unsatisfying data. So – to our opinion – a power law decay of extinction probabilities cannot be ruled out from this plot and should be still considered as a valid possibility.

Looking onto the extinction events depicted in Figure 3.1 from a dynamical point of view, one detects some more interesting features. Plotting the percentage of families that still exist after time t as a function[6] of t one obtains a step like pattern of this function, see Figure 3 in [Rau 86]. This indicates a cumulative nature of extinction events. Between such events, the function behaves constant for large time intervals, thereby indicating long periods of stasis. Raup suggests that the step like patterns might have a fractal quality of self-similarity with changing scale, which is already a hint to self-organized criticality.

The discussed data from the fossil record imply that the extinction process and thus biological evolution is an episodic process rather than a continuous one. This supports the famous concept of *punctuated equilibrium* proposed by Gould and Eldredge in the early seventies, for a more recent review see [Gou 93]. This concept is in contrast to the picture of a gradual and continuous transformation of populations as it is believed by the Darwinian school. The observation of long periods of phenotypical stability had

[5]This extinction made the evolution of mammals in the Tertiary possible, eventually leading to human evolution.

[6]The function is equals 1.0 at $t = 0$ and decays monotonically.

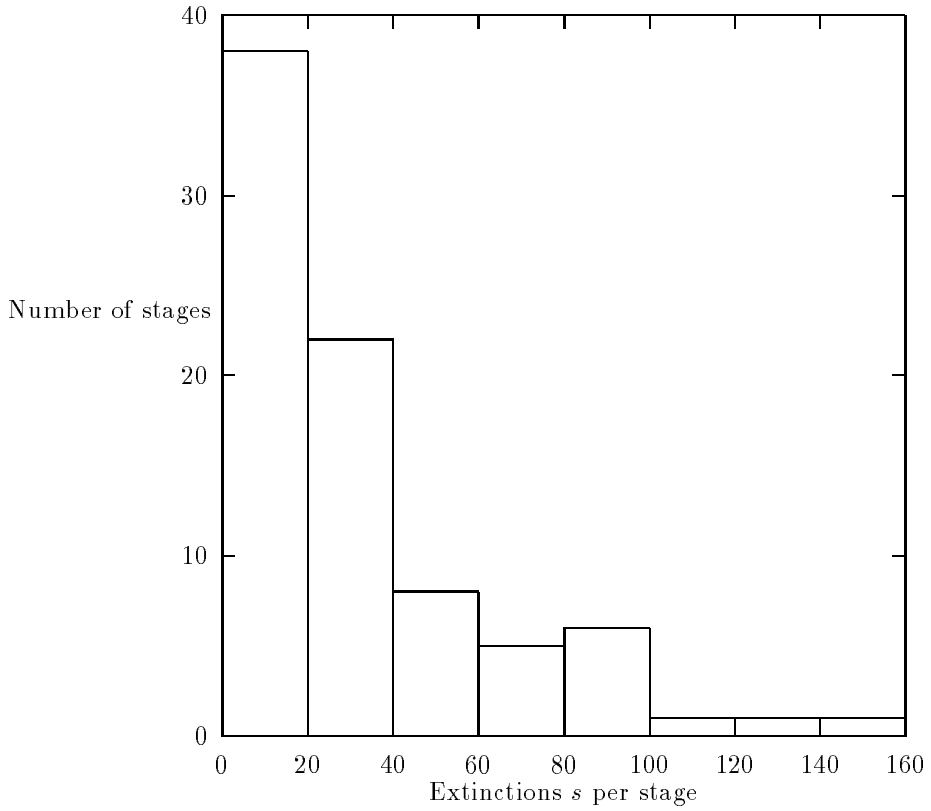

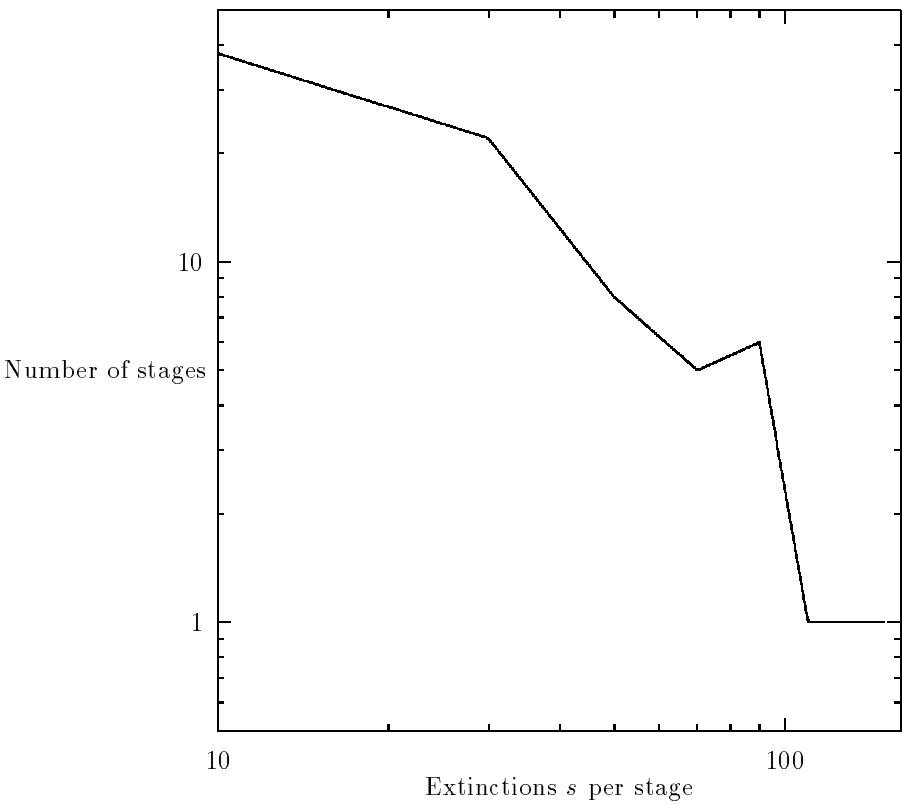

Figure 3.1: (a) Distribution of extinction events of size s. The size is measured as the number of marine families that became extinct during one geological stage of approximately 7 million years. Data from [Rau 86]. (b) Same as Figure (a) but with a double logarithmic scale. Further discussion see text.

long been ascribed by the Darwinian school to the imperfection of the fossil record and was interpreted simply as missing information. The theory of punctuated equilibrium postulates that most phenotypical changes occur at speciation but that the species are stable over millions of years, typically three to six millions of years [Kau 93].

After this short introduction to some main features of biological evolution we turn to the more physical part of the section, the modeling of evolution via fitness landscapes.

3.2 Modeling Biological Evolution using Fitness Landscapes

Consider an individual with a specific genetic information. Its genetic message is mapped via a genotype-phenotype mapping characterizing all properties of the individual. The process of evolutionary selection is based on the "survival of the fittest", thus on a phenotype-fitness mapping. The most common choice to define *fitness* of an individual is to couple it to the number of its offsprings: the fitness of an individual is proportional to the number of its offsprings [Pel 95].

Figure 3.2: Mapping from the genotype, which is a sequence of nucleotide bases to the phenotype and mapping this onto a fitness value F. In most models of biological evolution, the intermediate step via the phenotype is neglected, i.e. one assumes $genotype \equiv phenotype$.

The genetic information is contained in the sequence consisting of four nucleotide bases: adenin (A), guanin (G), thymine (T) and cytosin (C), that are arranged in the two strands of the DNA in matching pairs A-T and G-C. It is well known that replication is achieved by completion of each of the two strands using the corresponding matching pairs. However, sometimes errors occur during this process, which are most probably point mutations: one of the nucleotide base is substituted by another one. Sometimes insertion and deletion of longer strands are occuring. In the following discussion only point mutations are taken into account.

To define a genotype space one considers genetic sequences of a given length N consisting of the four letter alphabet ACGT. The distance of two sequences σ and σ' may then be defined as the *Hamming distance*: the number of points in the sequence, in which different bases are found. Assigning to each point in this space a fitness value $F \in \mathbb{R}$, we obtain a fitness landscape.

Due to the Fundamental Theorem of Natural Selection [Pel 95], the average fitness of a population increases if its variance is nonzero. For a proof see [Pel 95]. Thus populations always climb up to the hills of the fitness landscape and maximize their fitness value. This is – up to the sign – the same as for physical systems, that are moving downwards the energy landscape to minimize their energy.

Without mutations, the populations will reach sooner or later a local maximum and will then stop evolving, although there might exist higher maxima in sequence space that are separated by valleys. By allowing mutations it is possible for a population to jump into a new basin of attraction and to reach a higher fitness peak as before. This is the basis of a class of adaptive walk models.

Such models mainly consist of two steps [Pel 95]. For simplicity we assume only two possible alleles (± 1) for each gene instead of the four-letter alphabet. We provide a fitness landscape as a mapping from genotype space $\mathcal{G}$ to fitness $F \in \mathbb{R}$. In the first step one chooses a gene of the genome $\sigma(t)$ at random, changes its sign and denotes the new genome $\sigma'(t)$. In the second step one evaluates the fitness of the new and the old genome and keeps the genome with higher fitness value: If $F(\sigma'(t)) > F(\sigma(t))$, then $\sigma(t+1) = \sigma'(t)$; otherwise $\sigma(t+1) = \sigma(t)$. This is equivalent to zero temperature Monte-Carlo dynamics in physics, with *fitness* $\sim -$ *energy*.

The model discussed in the next two paragraphs is a specific example of an adaptive walk model.

3.3 NK-Landscapes

Consider a genome sequence of N genes as representative for a whole population. We neglect intraspecies evolution which is justified if the time scale of selection is much shorter than the time scale on which mutations occur. Each of the N genes may be in the state of A different alleles. We choose $A = 2$ and label the possible alleles by ± 1. The genome of each species lives in the configuration space of $A^N = 2^N$ different states. The fitness landscape on this configuration space is defined as follows [Kau 91].

Each gene i, $1 \leq i \leq N$ contributes to the total fitness $F(\sigma)$ of genome σ an amount w_i

$$F(\sigma) = \frac{1}{N} \sum_i w_i \quad . \tag{3.1}$$

The value of w_i depends on the state of gene i itself *and* on the state of K other genes labeled $g_i(j)$, $1 \leq j \leq K$ of the same genome σ. Of course $K \leq N-1$. Hence, w_i can take 2^{K+1} different values depending on the state of gene i and K other genes. These values of $w_i = w_i(g_i(1), g_i(2), \ldots, g_i(K))$ are determined randomly from an uniform distribution in the interval $[0,1]$, $\mathcal{P}(w_i) = \Theta(w_i)\Theta(1-w_i)$. The model is named by its two parameters N and K.

We now want to discuss the two limiting cases of this fitness landscapes, $K = 0$ and $K = N-1$. For the first case, $K = 0$, each gene has a favored state, $+1$ or -1, the one with the higher fitness contribution. This contribution is independent of all other genes. The fitness landscape has a single global maximum and is highly correlated. The mutation of one single gene j alters only the contribution w_j of this gene and therefore does not change the fitness value of the genome σ very much.

In the other limiting case, $K = N - 1$, the fitness landscape is totally uncorrelated. The mutation of a single gene j changes all contributions w_j to the total fitness value since the contribution of every gene depends on the state of *all* genes. Hence one-mutant neighbors in configuration space have totally uncorrelated fitness values. The fitness landscape has many local maxima and is totally rugged. Thus, *NK*-Landscapes provide a tunable family of fitness functions ranging from high correlation (low K) to low correlation (high K). The totally uncorrelated case $K = N - 1$ has been discussed and analyzed by [Fly 92].

Once the *NK*-landscape is defined in the described way, we may initialize some species with a randomly chosen genome and start with adaptive walks as discussed at the end of the previous paragraph. There are several interesting observables to be calculated such as the number of local maxima, the number of species that live in the same basin of attraction, the ratio of accepted to rejected mutations or the average length of an adaptive walk to a local maximum. For a detailed discussion we refer the reader to [Kau 93] or the analytic work of [Fly 92].

In the discussion of the coevolution concept in the next paragraph we need to know the average length $\langle l \rangle$ of adaptive walks to a local maximum (i.e. the number of successful mutations) in the case of $K = N - 1$. Therefore we give the result of [Kau 93, Fly 92]

$$\langle l \rangle \sim \log N \quad . \tag{3.2}$$

A reader familiar with spinglass physics will already have noticed that the *NK*-Landscapes are very similar to spinglass energy functions. Especially the Random energy model (REM) of B. Derrida [Der 81] is very close to Kauffmans *NK*-model. It is defined by the Hamiltonian

$$\mathcal{H}^{(p)}(\sigma) = \sum_{\{i_1, i_2, \ldots, i_p\}} J_{\{i_1, i_2, \ldots, i_p\}} \sigma_{i_1} \sigma_{i_2} \cdots \sigma_{i_p} \quad , \tag{3.3}$$

and one has to sum over all different subsets of p indices. p plays the role of K in the *NK*-model. The coefficient $J_{\{i_1, i_2, \ldots, i_p\}}$ is chosen at random for each combination of indices from the same distribution. For $p = 2$ the model reduces to the SK-spinglass-model of Sherrington and Kirkpatrick.

3.4 Coevolution of Species

Let us simulate an ecosystem with S species living therein using the *NK*-model, $K = N - 1$. This means that we define S fitness landscapes in the way described in the previous paragraph. At the beginning the species will have random positions in configuration space, but as the adaptive walks are going on, they approach local maxima of their fitness landscapes. They will reach local maxima on average after $\log N$ successful mutations as we see from equation (3.2). But then nothing more will happen, the species will live at their local maxima (that might have a very low value) and have no possibility to evolve further and to explore a greater part of the configuration space. It is a dead state and surely not a good description of biological evolution.

What has been omitted is the interaction among species or in other words, the idea of *co*evolution. Each species lives in an environment that is also populated by other species. The interaction arises from predator-prey relations or competition among species for food. If a species a changes its genome, this changes also the fitness landscapes of all species interacting with species a. Thus they find themselves no longer on a fitness maximum but have to adapt anew in their changed fitness landscape.

The ideas sketched here have been cast into a model by [Kau 91] and [Bak 92]. It turns out that such a system shows a phase transition from a frozen state, where all species live at local maxima, to a chaotic state, where a finite fraction of species always evolves towards local maxima. In the following we stick to the notation and argumentation of [Bak 92] which is slightly different from Kauffman's approach [Kau 91].

In the so called NKC-model, we consider S species each characterized by a genome of N genes. Each gene may occur in two alleles. The fitness landscape for each species is defined as follows. For each possible state of the N genes we choose independently a random number uniformly distributed in the interval $[0, 1]$. This would correspond to the NK-model with $K = N - 1$, i.e. it describes a totally uncorrelated landscape. Now we extend the model to include interaction among species. The fitness of each species does not only depend on the state of its own genes, but in addition on the state of C more genes chosen at random (and then fixed) among the genes of all other species. Thus, to define the fitness landscape of a species, one has to choose 2^{N+C} random numbers.

In the case $C = 0$ the model reduces again to the NK-model and the stationary state consists of all species at their local maxima without further evolution. The probability[7] A to accept a mutation vanishes. This state is known in economics as a *Nash equilibrium* [Kau 93]. At the other extreme, $C/N \gg 1$, all species change their fitness if one mutation occurs. Hence the fitness values of the species are randomly distributed and the probability to accept a mutation is $A = \frac{1}{2}$.

At intermediate values of C we expect a finite fraction of species at local maxima, while the rest of the species evolves towards their local maxima. The number of species set back from their local maxima due to the coevolutionary character and the number of evolving species reaching their local maxima may balance and sustain a finite probability $A > 0$.

It might also be possible that C is too small to sustain a finite $A > 0$ and that the species become all trapped at local maxima. The threshold C_{crit} where the transition from a frozen state with $A = 0$ ($C < C_{\text{crit}}$) to a state with a finite fraction of species evolving ($A > 0$, $C < C_{\text{crit}}$) occurs, can be determined by a quite simple consideration [Bak 92].

Let us assume a state where all species have evolved to local maxima. Now we perturb the system by changing the genome of one species and hence changing its fitness to a random value. This species evolves back to a local maximum, by changing $\langle l \rangle$ genes on

[7] This probability is called 'activity' in [Bak 92]

its way. The probability that a gene of a species impinges upon the fitness of another species is by construction of the model C/N. The process is supercritical if the number of such genes changed during the adaptive walk is greater than unity. It is sub-critical if this number is smaller than unity. The process will sustain itself exactly if on average one other species is set back in its evolution during the adaptive walk. This defines the value of C_{crit}

$$\frac{C_{\mathrm{crit}}}{N}\langle l\rangle \equiv 1 \quad , \tag{3.4}$$

from which follows

$$C_{\mathrm{crit}} = \frac{N}{\langle l\rangle} \quad . \tag{3.5}$$

The value of $\langle l\rangle$ has been calculated in [Fly 92]. This argumentation can be made more exact by analytical calculations [Bak 92]. Moreover it is shown by [Bak 92] that C_{crit} is critical in the sense that the relaxation time to the asymptotic state diverges for this value.

The *NKC*-model discussed in this paragraph is a model for biological coevolution and shows a phase transition at C_{crit} from a frozen, dead state to a state with a finite fraction of species evolving. It would be very nice to turn this model into a self-organized critical model, i.e. to invent a mechanism treating N and C as dynamical parameters that are driven by the dynamics onto their critical value. Maybe this could be done along the guidelines of section 2 exploiting the results on the role of order- and control-parameters. We do not know of any progress in this direction.

3.5 Other approaches

In paragraph 3.3 we already mentioned the similarity between the *NK*-model and spinglass-Hamiltonians. Indeed a large amount of literature on possible connections between spinglass physics and the modeling of biological evolution exists. We want to mention only a very few points of interest and refer the interested reader to the original papers given in the bibliography.

In [Bak 92] the authors claim that the *NKC*-model cannot be driven from its frozen phase to the critical state using perturbations, because after a response to a perturbation the system is back in the same state as it was before (all species at local maxima). They conclude that this is due to the fact that there is no possibility to impose a *small* perturbation of the fitness value. For a totally uncorrelated landscape ($K = N - 1$) the change of only one gene necessarily results in a finite change of the fitness value. Moreover it eliminates all memory of the previous fitness value. On the other hand the authors do not want to abandon the uncorrelated landscape since it is necessary for deducing analytical results. In this context we have thought of considering the $p = 2$ random-energy-model (REM) of equation (3.3) as fitness landscape. This model, which is also known as the SK-spinglass, allows for small perturbations due to higher correlations and is analytically tractable. Preliminary simulations of such coupled SK-landscapes show qualitatively the same features as the NKC-model discussed in 3.4.

A generalization of the random-energy-model, the "G-REM" has been proposed to describe the hierarchy of species within genera within families within orders [Eps 89]. The idea is to map this branching into hierarchies onto similar structures that occur in spinglass models as the G-REM. It is believed that the equilibrium states in such models are also organized in valleys within super-valleys etc. . For further details see [Eps 89] and references therein.

Finally we want to mention an interesting work done by Leuthäusser [Leu 85, Leu 87], who has mapped an evolution model for self-replicating molecules [Eig 77] onto a two-dimensional Ising system. The evolution model consists of a constant number of molecules (or genomes of different species) of length N using two alleles ± 1. Each molecule i out of the 2^N possibilities, $1 \leq i \leq 2^N$, replicates itself via a replication rate (fitness) $A(i)$. During the replication process point-mutations occur with probability $1 - q$.

Leuthäusser shows that this model can be mapped onto an anisotropic two-dimensional Ising model with nearest neighbor interaction in one direction (which is the time direction in the evolution model) and an interaction described by the replication rates A in the perpendicular direction. The mutation rate $1 - q$ is mapped onto the temperature $T^{-1} = \beta = |\ln((1-q)/q)|$. For low mutation rate $1/2 < q \leq 1$ one obtains ferromagnetic interaction, a high mutation rate $0 \leq q < 1/2$ corresponds to the antiferromagnetic case. To observe a macroscopic occupation of some molecules sequences q must exceed a threshold value q_{crit}. This error threshold of replication is related to the critical temperature of the Ising system. A detailed description is contained in [Leu 85, Leu 87]. The ideas and results of this work might be helpful for constructing self-organized critical evolution models.

4 Bak-Sneppen model

The first model of biological evolution exhibiting self-organized criticality is the Bak-Sneppen (BS) model [Bak 93]. In the first paragraph of this section we define its statics and dynamics. Then a detailed interpretation of its biological meaning is given (4.2). Critical properties of the model are then investigated and discussed in 4.3. Also the critical exponents are defined herein. Finally we present numerical results for the avalanche dynamics of the model (4.4). We discuss shortly some evidence for the breakdown of self-organized criticality in the absence of an infinitesimal small driving rate (4.5).

4.1 Definition of the Bak-Sneppen model

We define the one-dimensional BS-model. The generalization to higher dimensions is straightforward. Consider N real variables distributed in the interval $[0, 1)$

$$\boldsymbol{\phi} = (\phi_i) \quad , \quad i \in \{1, \ldots, N\} \quad , \quad 0.0 \leq \phi_i < 1.0 \tag{4.1}$$

arranged in a one dimensional array. We use periodic boundary conditions. Furthermore we define the probability distribution $\mathcal{P}(\phi) = \Theta(\phi)\Theta(1-\phi)$ [8]. The dynamical rule is then defined as follows.

1. Initialize each variable ϕ_i by choosing its value randomly with probability $\mathcal{P}(\phi_i)$. Time $t = 0$.

2. Determine the index $i(t)$ of the random variable with the smallest value among all variables ϕ_j
$$\phi_{i(t)}^{(t)} \leq \phi_j^{(t)} \quad \forall \ 1 \leq j \leq N$$

3. Replace the value of $\phi_{i(t)}^{(t)}$ by the new value $\phi_{i(t)}^{(t+1)}$
$$\phi_{i(t)}^{(t+1)} = \varphi \text{ with probability } \mathcal{P}(\varphi).$$

4. Replace the values of the nearest neighbors $i(t) \pm 1$ by new values $\phi_{i(t)\pm 1}^{(t+1)}$
$$\phi_{i(t)\pm 1}^{(t+1)} = \varphi_\pm \text{ with probability } \mathcal{P}(\varphi_\pm).$$

5. The values of all other variables remain unchanged
$$\phi_j^{(t+1)} = \phi_j^{(t)} \ \forall\ j \neq i(t), i(t \pm 1)$$

6. $t \to t+1$. Goto 2.

Though this is an extremely simple dynamical algorithm, we will see in paragraph (4.3) that it shows a very rich and interesting dynamical behavior. Before studying its critical properties let us have a look at the interpretation of these dynamics from a biologists point of view.

4.2 Interpretation in a biological context

As already discussed in section 3 let us consider an ecosystem with some species living therein. We make the following assumptions

- neglect the mapping from RNA sequences to protein structure or assume *genotype* $\equiv$ *phenotype*
- neglect population dynamics.

[8] Though the explicit use of this trivial distribution seems not necessary here, we introduce it for better compatibility with the RG-approach in section 5.

What does that mean for the evolutionary dynamics ? Due to our first assumption *genotype* $\equiv$ *phenotype*, it is possible to describe a species via a fitness function F which is a mapping from genome space $\mathcal{G}$ to real numbers $\mathbb{R}$, $F : \mathcal{G} \mapsto \mathbb{R}$. The second assumption allows us to consider only one individual as a representative for all individuals of that species. We neglect small fluctuations caused by point mutations in the intraspecies genome material. But how will species evolve in this model and on what time scale does evolution then take place ?

Let us look at the system at the level of population dynamics for a moment: Individuals of a species that are not positioned on a maximum of the fitness landscape are driven by a selection pressure (due to small fluctuations in the intraspecies genome material) in the direction of the gradient ∇F towards the next maximum. If a species living at a maximum of the fitness landscape is hit by a mutation, it evolves typically back to the old maximum forced by the selection pressure. These adaptive processes take place on a short time scale $\tau_{selection}$. In rare events, however, it is possible that a mutation moves a species into the attractive region of another maximum. This may happen e.g. if a sufficient number of point mutations occur in a short time interval. Then interspecies competition sets in and if the new maximum is higher, the mutated species will survive, the old one will become extinct. Significant mutations take place at a time scale τ_{mutation} and we may assume

$$\tau_{\text{selection}} \ll \tau_{\text{mutation}}, \tag{4.2}$$

i.e. the time taken to move species toward maxima is much shorter than the time scale of a mutation from one stable genotype to a different stable genotype.

This is basically the same assumption as to neglect population dynamical effects and may be also considered as a coarse-graining of time. It means that we only must consider species living at maxima of the fitness landscape. When a significant mutation occurs, the species moves to a new better maximum more or less far away from the present one. All intermediate steps taking place on the level of population dynamics are not taken into account. This process of coarse-graining is illustrated in Figure 4.1.

The interpretation of the Bak-Sneppen model in this framework is the following [Bak 93]: The distance that is overcome by a significant mutation moving a species from one fitness maximum to another one in genome space is called *barrier value*. To be concrete, the barrier value ϕ_i is defined as the distance in genome space for species i to the next higher fitness maximum of the fitness landscape $F(\mathcal{G})$. A measure for the barrier value could be the number of genes that have to be hit by point mutations during a short time interval.

The barrier value ϕ_i will be correlated with the fitness of species i. Small barriers are generally connected to low fitness values, since the next higher fitness values are usually nearby. Higher barriers are connected to high fitness values since a species that has already a high fitness value has to change many genes to find an even higher value. Thus the barrier ϕ_i may also be considered as a measure for the fitness of species i. Furthermore, a significant mutation, involving $n \sim \phi_i$ point mutations takes place typically after a real time

$$\tau_{\text{real}} \sim \text{const}^n \sim e^{n \text{ const}} \sim e^{\phi_i/\tau_c} \tag{4.3}$$

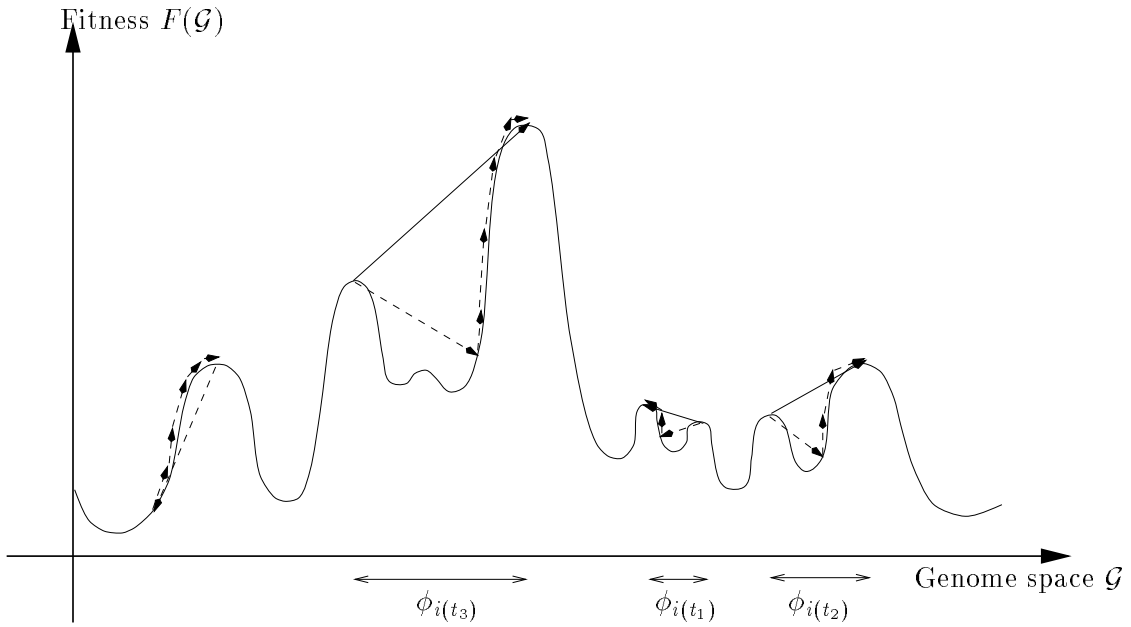

Figure 4.1: Mutations from one fitness maximum to another maximum define the fundamental time step (solid lines). Intermediate steps (dashed lines) on the level of population dynamics are not taken into account. The distance from one maximum to the next higher one defines barrier values ϕ_i. Such events occur on a time scale $\tau_{\text{real}} \sim e^{\phi_i/\tau_c}$, eq. (4.3).

with some constant τ_c. The first species to mutate is therefore with high probability the species $i(t)$ with the lowest barrier value $\phi_{i(t)}$. It is obviously possible to identify the barrier values in this simple picture with the random numbers ϕ_i of the BS model. The coevolution principle is taken into the model by changing the fitness landscape and thus the barrier values of the neighbors of the active species with minimal ϕ_i.

To see how the model evolves in time let us turn off the coevolution first: At each time step only the species with minimal barrier value is updated and *not* its neighbors. Clearly all species evolve towards $\phi = 1.0$ (infinitely slow). The system ends up in a static dead state that no longer evolves. But this contradicts the concept of life: Life is synonymous with volatility and evolution [Bak 93]. The principle of coevolution is indispensable.

Using the full BS-algorithm including coevolutionary interaction we find a much more interesting behavior. The stationary distribution of barrier values ϕ, $P(\phi)$ behaves like a step function $P(\phi) \sim \Theta(\phi - \rho_c)$, $\rho_c \approx 0.667$, see Figure 4.2.

To get an idea of temporal and spatial distribution of mutating species we mark in Figure 4.3a at each time step the species with minimal fitness. In addition, if in two consecutive time steps neighboring species mutate they are connected by a line. After some transient time we observe the development of species-clusters of different size that are involved in the coevolution process. From time to time the activity stops and starts somewhere else anew. These clusters will be identified as avalanches in the sense of SOC in the next paragraph.

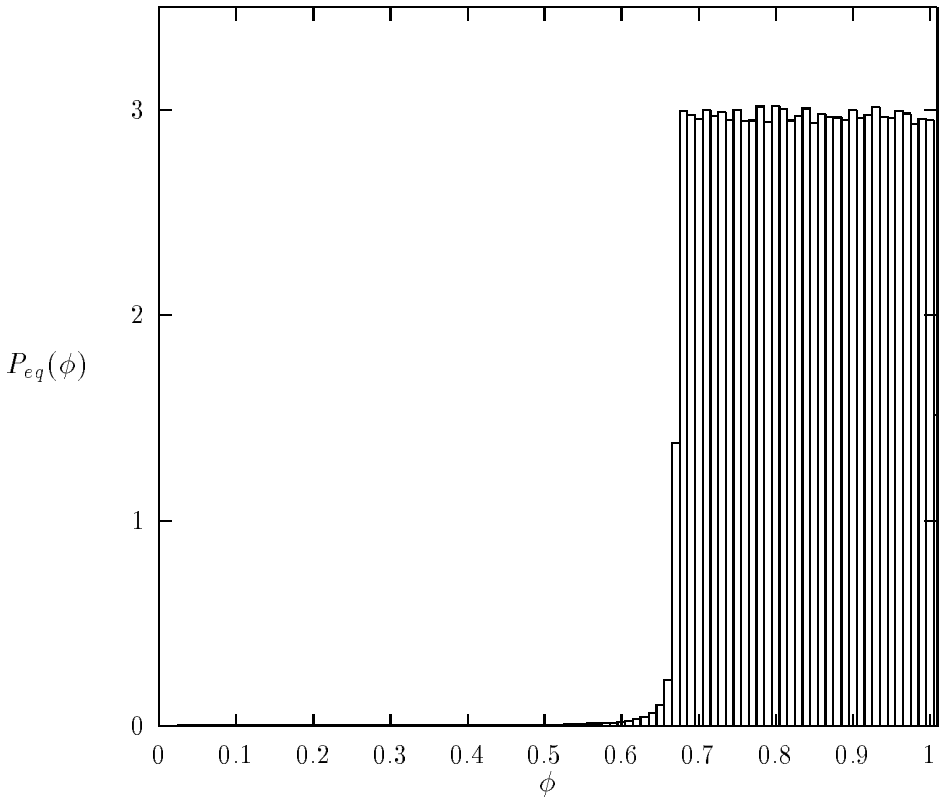

Figure 4.2: The equilibrium distribution of all barriers in the nearest neighbor Bak-Sneppen model $P(\phi) \sim \Theta(\phi - \rho_c)$, $\rho_c \approx 0.66$, $N = 2048$ species, statistics $= 2 \times 10^9$.

But before let us apply the real time scale of eq.(4.3) to Figure 4.3a

$$\tau_{\text{real}}(t) = \sum_{t'=0}^{t} e^{\phi_{i(t')}/\tau_c} \tag{4.4}$$

When we apply eq.(4.3) to the time axis this shrinks the time duration of such coevolutionary avalanches and extends the time in between, as is illustrated in Figure 4.3b. The same effect is seen more clearly when plotting real-time τ as function of computer time. During coevolutionary avalanches only a little real time elapses. These are the flat regions of the graph in Figure 4.4. Between such clustered activity we have long periods of stasis in real time. These are the vertical regions of the graph in Figure 4.4.

If one considers the avalanches as extinction events, the real time activity diagram shows the punctuated equilibrium picture of biological evolution: Mostly we have stasis but from time to time extinction events occur on a small or larger scale again to be followed by a long period of stasis. We may also remark that a species that was not involved in a coevolutionary avalanche is likely to have a high barrier value ϕ and will probably still be stable for a long time. On the other hand, a species that took part in an avalanche recently is likely to mutate on the coarse time scale in the near future again[9]. After

[9]The interpretation of this fact with view on cockroaches and humans is left to the reader.

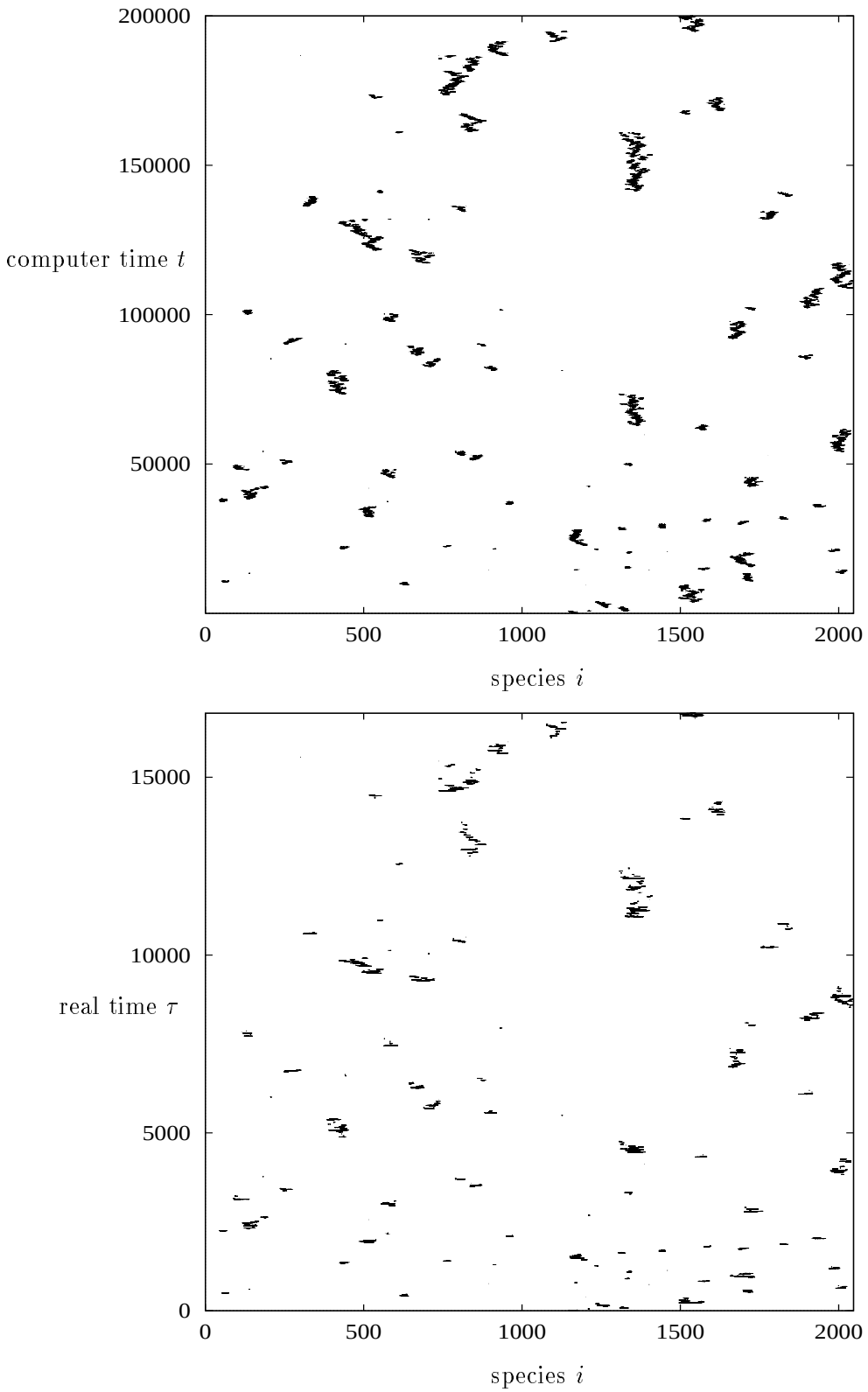

Figure 4.3: Activity diagram for the nearest neighbor Bak-Sneppen model: (a) computer time units, (b) real time units. Neighboring species that have minimal fitness in subsequent time steps are connected with lines. A clustered activity is observed.

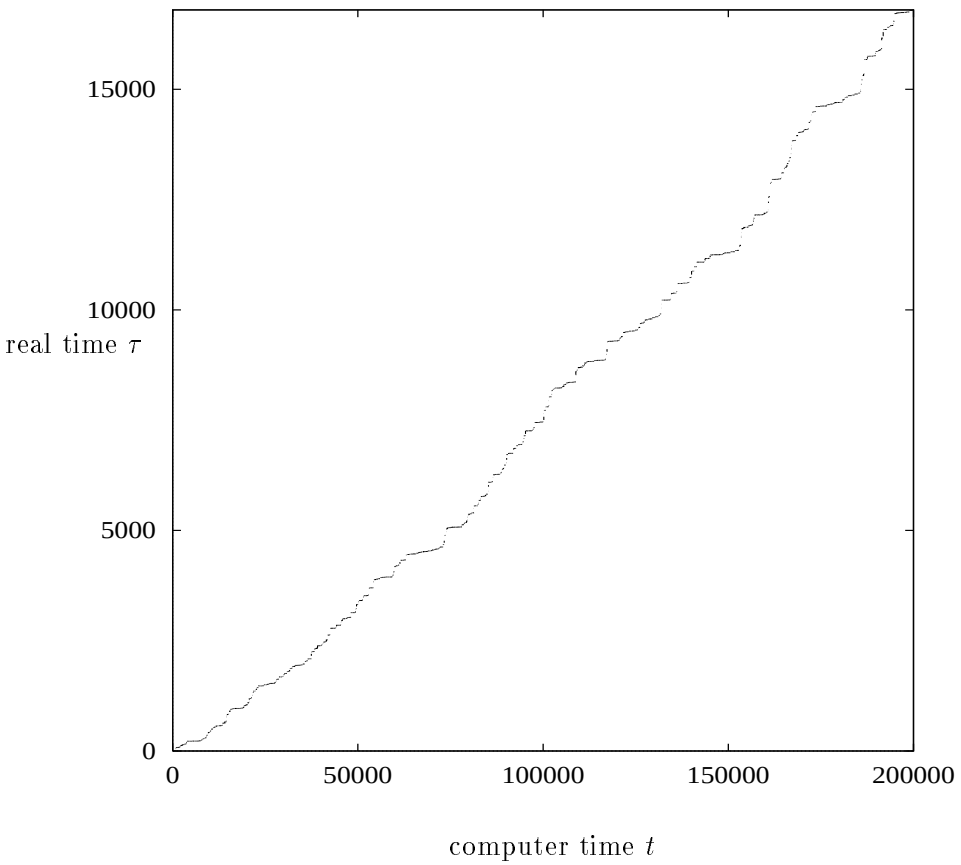

Figure 4.4: Real time flow versus computer time. Flat regions of the graph correspond to coevolutionary avalanches, while vertical parts of the graph represent periods of stasis.

looking at the BS-model from a phenomenological point of view we will go into a more serious discussion in the following paragraph.

4.3 Properties of the BS-model

We discuss in detail the transient to the critical state described by a gap-equation as well as the scaling properties of the critical stationary state itself.

Transient Regime

Consider the initial state of a d-dimensional system at time $t = 0$ as given in the algorithm of paragraph 4.1. Since all $\phi_i^{(t)} \in [0, 1)$ are uniformly distributed at $t = 0$ we have

$$\phi_{\min}(t) \equiv \phi_{i(t)} \approx \mathcal{O}(L^{-d}) \text{ at } t = 0. \tag{4.5}$$

The "gap" $G(t)$ is defined

$$G(t) \equiv \max_{0 \leq t' \leq t} \{\phi_{\min}(t')\}, \tag{4.6}$$

thus

$$G(0) \approx \mathcal{O}(L^{-d}). \tag{4.7}$$

From this definition it is clear that G(t) is a stepwise increasing monotonic function, see Figure 4.5. When the gap jumps at time t_1 to a new higher value, all random variables of the system are uniformly distributed in the interval $[G(t_1), 1]$. The length S of a plateau in the gap function between two subsequent jumps at times t_1 and $t_1 + S$ defines the length of an $G(t_1)$-avalanche with $\phi_{\min}(t) < G(t_1)\, \forall t_1 < t < t_1 + S$. This definition of an avalanche is consistent with our later definition of forward-avalanches in the critical state (see below). The mean length $\langle S \rangle_{G(t_1)}$ depends on the start value $G(t_1)$. The smaller $G(t_1)$, the smaller will be the average avalanche length since it is more likely that all random variables lie above $G(t_1)$. The stationary value of $G(t)$ has to be less than one since due to the interaction among nearest neighbors we have always variables $\phi_i < 1.0$. Hence, $G(t)$ will converge to a stationary value $\rho_c < 1.0$.

The avalanche size $\langle S \rangle_{G(t)}$ will diverge as $G(t)$ approaches its stationary value. The relation of the divergence of $\langle S \rangle_{G(t)}$ and the approach of the stationary (critical) state is described by a "gap-equation": The increase of the gap $G(t)$ after an $G(t)$-avalanche is of order $(1 - G(t))/L^d$. This increase is achieved on average in $\langle S \rangle_{G(t)}$ time steps, thus we have [Pac 94]

$$\frac{dG(t)}{dt} = \frac{1 - G(t)}{L^d} \frac{1}{\langle S \rangle_{G(t)}} \tag{4.8}$$

At stationarity $\langle S \rangle_{G(t)} \to \infty$ and $dG(t)/dt \equiv 0$. The gap equation is well defined in the limit $L \to \infty$: Choose an arbitrarily small δG. It is then possible to choose L large enough in order to take into account as many avalanches as wanted to increase the gap from $G(t)$ to $G(t) + \delta G$. Therefore $\langle S \rangle_{G(t)}$ has a well defined value and equation (4.8) is exact. Assuming a power law divergence of the average avalanche size $\langle S \rangle_{G(t)}$

$$\langle S \rangle_{G(t)} \sim (\rho_c - G)^{-\gamma} \tag{4.9}$$

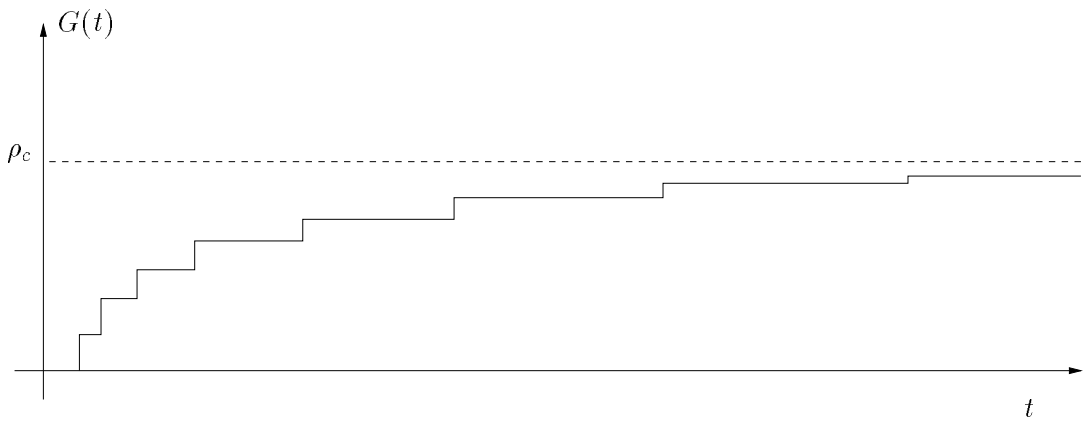

Figure 4.5: A typical function G(t) in the transient regime.

and $\gamma > 1$, inserting this in the gap-equation (4.8), separating variables t, G and integrating it, we are lead to an algebraic approach of the attractor [Pac 94]

$$\tilde{G}(t) \equiv \rho_c - G(t) \sim \left(\frac{t}{L^d}\right)^{-\rho} \qquad \rho = \frac{1}{\gamma - 1} \tag{4.10}$$

Critical State

Let us first define ϕ_0-forward avalanches[10]. Choose an arbitrary $\phi_0 \in [0, 1)$. The temporal size $S \equiv t_f - t_i$ of a ϕ_0-forward avalanche is defined as

$$\phi_{i(t_i)} = \phi_0, \qquad \phi_{i(t_f)} \geq \phi_0,$$

$$\phi_{i(t)} < \phi_0 \quad \forall \quad t_i < t < t_f. \tag{4.11}$$

A ϕ_0-forward avalanche is running as long as there are still variables $\phi_i < \phi_0$.

The probability for ϕ_0-forward avalanches of size S is given by the scaling ansatz [Mas 95]

$$P_f(S, \phi_0) = S^{-\tau} g\left(S(\rho_c - \phi_0)^{1/\sigma}\right) \tag{4.12}$$

with the scaling function

$$g(x) = \begin{cases} \approx 0 & x \gg 1, \\ \text{const.} & x \to 0. \end{cases} \tag{4.13}$$

Critical avalanches start with $\phi_0 = \rho_c$ and we expect a power-law decay $P_S(S) \sim S^{-\tau}$ without cutoff. From equation (4.12) we can calculate the mean size $\langle S \rangle_{\phi_0}$ of an ϕ_0-forward avalanche.

$$\begin{aligned} \langle S \rangle_{\phi_0} &= \int_1^\infty S P_f(S, \phi_0) dS \\ &= \int_1^\infty S^{1-\tau} g(S(\rho_c - \phi_0)^{1/\sigma}) dS \\ &= (\rho_c - \phi_0)^{(-1/\sigma)} \int g(x) \left(x(\rho_c - \phi_0)^{-1/\sigma}\right)^{1-\tau} dx \\ &\sim (\rho_c - \phi_0)^{-\frac{2-\tau}{\sigma}}, \end{aligned} \tag{4.14}$$

$$\gamma = \frac{2 - \tau}{\sigma}. \tag{4.15}$$

Using the observation that a signal $\phi_{i(t)} > \phi_0$ acts as breaking point of ϕ_0-avalanches, we conclude

$$\langle S \rangle_{\phi_0} \times p(\phi_{i(t)} > \phi_0) = \text{const.} \quad \text{for any time } t \tag{4.16}$$

[10] Below we define also backward avalanches. From time to time we will omit the term 'forward'. If we speak only of 'avalanches' we will assume implicit forward-avalanches.

which is equivalent to

$$p\left(\phi_{i(t)} > \phi_0\right) \sim \frac{1}{\langle S\rangle_{\phi_0}}. \tag{4.17}$$

Using the result of equation (4.14) we get

$$\begin{aligned} p\left(\phi_{i(t)} = \phi_0\right) &\sim \frac{d}{d\phi_0} p\left(\phi_{i(t)} > \phi_0\right) \\ &\sim (\rho_c - \phi_0)^{\gamma-1} \end{aligned} \tag{4.18}$$

Now let us concentrate on the connection of $\langle n_{\mathrm{cov}}\rangle_{\phi_0}$, the number of sites involved in an ϕ_0-avalanche with its mean temporal size $\langle S\rangle_{\phi_0}$. Consider a time series of $\phi_{\min}(t)$ in an time interval of length T. Let us assume we observe N ϕ_0-avalanches. We increase ϕ_0 by the amount $d\phi_0$. What is the number $N + dN$ of $\phi_0 + d\phi_0$-avalanches ? After each of the N ϕ_0-avalanches we have $\langle n_{\mathrm{cov}}\rangle_{\phi_0}$ involved sites that are uniformly distributed in the interval $[\phi_0, 1)$. If we increase ϕ_0 by the amount $d\phi_0$ we have $\langle n_{\mathrm{cov}}\rangle_{\phi_0} \times \frac{d\phi_0}{1-\phi_0}$ less breaking points for $\phi_0 + d\phi_0$-avalanches than for ϕ_0-avalanches, therefore

$$dN = -N\langle n_{\mathrm{cov}}\rangle_{\phi_0} \frac{d\phi_0}{1-\phi_0}. \tag{4.19}$$

On the other hand we have conservation of the interval length T,

$$\begin{aligned} (N + dN)\langle S\rangle_{\phi_0+d\phi_0} &= N\langle S\rangle_{\phi_0} \\ \Leftrightarrow \quad \left(1 + \tfrac{dN}{N}\right) &= \frac{\langle S\rangle_{\phi_0}}{\langle S\rangle_{\phi_0+d\phi_0}} \\ \Leftrightarrow \quad \tfrac{dN}{N} &= -d\ln\langle S\rangle_{\phi_0} \end{aligned} \tag{4.20}$$

Using scaling assumption (4.14) and combining equations (4.19) and (4.20) we obtain in the limit $\phi_0 \to \rho_c$

$$\begin{aligned} \frac{\langle n_{\mathrm{cov}}\rangle_{\phi_0}}{1-\phi_0} &= \frac{d}{d\phi_0}\ln(\rho_c - \phi_0)^{-\gamma} \\ \gamma &= \lim_{\phi_0\to\rho_c} \frac{\langle n_{\mathrm{cov}}\rangle_{\phi_0}(\rho_c - \phi_0)}{1-\phi_0} \end{aligned} \tag{4.21}$$

γ may be determined as the inverse slope of a plot of $\frac{1-\phi_0}{\langle n_{\mathrm{cov}}\rangle_{\phi_0}}$ as a function of ϕ_0. ρ_c is given by the intersection of this function with the horizontal axis. For detailed numerical results see next paragraph 4.4.

We are now going to discuss the connection between spatial extent and temporal duration of avalanches. For $d = 1$ the spatial size of a ϕ_0-avalanche of temporal duration $S = t_f - t_i$ is naturally defined as the largest extent of sites involved in this avalanche

$$\xi \equiv \max_{t_i \le t_1, t_2 \le t_f} |i(t_1) - i(t_2)|. \tag{4.22}$$

The dynamical exponent z is then defined by the scaling relation

$$S \sim \xi^z. \tag{4.23}$$

For the distribution of spatial avalanche size ξ we expect a power law for critical avalanches

$$P_\xi(\xi) \sim \xi^{-\tau_\xi}. \tag{4.24}$$

The critical exponents τ, z, τ_ξ are connected via the scaling relation obtained from

$$P_\xi(\xi)d\xi = P_S(S)dS \tag{4.25}$$

from which follows

$$\begin{aligned} \xi^{-\tau_\xi} &\sim \xi^{-z\tau}\xi^{z-1} \\ \Rightarrow \quad -\tau_\xi &= -z\tau + z - 1 \\ \Rightarrow \quad \tau &= \frac{\tau_\xi - 1}{z} + 1 \quad . \end{aligned} \tag{4.26}$$

Note that our definition (4.22) for the spatial extension ξ cannot be generalized for higher dimensions $d > 1$. Instead an alternative definition is given in [Pac 96]. The spatial size of an avalanche is given by the root mean square deviation of the set of all active sites in the avalanche from their center of mass. In this definition each site is counted with the weight given by the number of times it was visited by the avalanche

$$R^2_{PMB} = \frac{1}{t_f - t_i} \sum_{t=t_i}^{t_f} (i(t) - i_{CM})^2 \tag{4.27}$$

with

$$i_{CM} \equiv \frac{1}{t_f - t_i} \sum_{t=t_i}^{t_f} i(t). \tag{4.28}$$

It is apriori not clear that $R_{PMB} \sim \xi$ in $d = 1$. If this is not the case the values of the exponent z will be different for both definitions. This question will be investigated numerically in the next paragraph.

For an efficient numerical measurement of the avalanche exponent τ, it is helpful to introduce ϕ_0-backward avalanches. A ϕ_0-backward avalanche is defined as a ϕ_0-forward avalanche but under time reversal, i.e. we exchange t_i and t_f in (4.11) and $S \to -S$. Since the extremal dynamics of the model is irreversible the backward avalanches will have different statistical properties, especially a backward-avalanche probability

$$P_b(S, \phi_0) = \frac{1}{N} S^{-\tau_b} g_b(S(\rho_c - \phi_0)^{1/\sigma}) \tag{4.29}$$

with different power law exponent τ_b. N is a normalization constant and given by (same calculation as in eq. (4.14))

$$\begin{aligned} N &= \int S^{-\tau_b} g_b(S(\rho_c - \phi_0)^{1/\sigma}) dS \\ &= (\rho_c - \phi_0)^{\frac{\tau_b - 1}{\sigma}} \quad . \end{aligned} \tag{4.30}$$

We are now going to calculate the probability $P_b^{\rm all}(S)$ to have any backward-avalanche of size S, independent of its start value ϕ_0

$$\begin{aligned} P_b^{\rm all}(S) &= \int P_b(S,\phi_0) p(\phi_{i(t)} = \phi_0) d\phi_0 \\ &= S^{-\tau_b} \int (\rho_c - \phi_0)^{-\frac{\tau_b - 1}{\sigma}} g_b(S(\rho_c - \phi_0)^{\frac{1}{\sigma}})(\rho_c - \phi_0)^{\gamma - 1} d\phi_0 \\ &= S^{-\tau_b} \int \left(\frac{x}{S}\right)^{-\tau_b + 1} g_b(x) \left(\frac{x}{S}\right)^{\sigma(\gamma-1)} \left(\frac{x}{S}\right)^{\sigma - 1} \frac{\sigma}{S} dx \\ &\sim S^{\tau_b - 1 + (1-\gamma)\sigma - \tau_b + 1 - \sigma - 1} \int x^{-\tau_b + 1 + (-1+\gamma)\sigma + \sigma - 1} g_b(x) dx \\ &\sim S^{\tau - 3} \end{aligned} \tag{4.31}$$

This surprising result means that the forward-avalanche exponent τ for critical avalanches at $\phi_0 = \rho_c$ is related to the power law exponent of *all* backward avalanches *independent* of their start value ϕ_0 [11]. This opens up the possibility to measure the forward exponent τ more precisely from the backward avalanche distribution $P_b^{\rm all}(S)$ since the statistics is of course much better this way. Results are shown in the next paragraph.

4.4 Numerical Results

We give here the main results of our numerical simulations for the $1d$-Bak-Sneppen model. First, the avalanche exponent τ defined in equation (4.12) is obtained from a fit to the backward avalanche distribution (4.31). This distribution is shown in Figure 4.6, that averages over 2×10^9 backward avalanches. The result for the overall backward avalanche exponent is measured as $\tau_b^{\rm all} = 1.92 \pm 0.01$ from which τ follows via (4.31) $\tau_b^{\rm all} = 3 - \tau$

$$\tau = 1.08 \pm 0.01 \ . \tag{4.32}$$

This is in agreement with the results of [Pac 96] $\tau = 1.07 \pm 0.01$ and $\tau = 1.073 \pm 0.003$ of [Gra 95]. The value of γ defined in (4.15) can be obtained from equation (4.21) as already described above: a linear regression analysis applied to a plot of $1 - \phi_0/\langle n_{\rm cov}\rangle_{\phi_0}$ as function of ϕ_0, see Figure 4.7, gives

$$\gamma = 2.703 \pm 0.004 \ . \tag{4.33}$$

This is in agreement with the results $\gamma = 2.70 \pm 0.01$ [Pac 96], $\gamma = 2.71 \pm 0.03$ [Gra 95], and $\gamma = 2.7 \pm 0.1$ [Jov 94]. ρ_c can be determined from the intersection of the function $1 - \phi_0/\langle n_{\rm cov}\rangle_{\phi_0}$ with the horizontal axis. We obtain $\rho_c = 0.6668 \pm 0.0015$ with this method. However, it is possible to get a much more accurate result from the same measurement, using the already known value of γ [Pac 96]. It is possible to calculate from equation (4.21) the quantity $\rho_c - \phi_0 = \gamma(1 - \phi_0)/\langle n_{\rm cov}\rangle_{\phi_0}$. In the limit $\phi_0 \to \rho_c$,

[11] A similar analysis can be done for the distribution of all forward avalanches $P_b f^{\rm all}(S)$. In this case the corresponding power law exponent $\tau_f^{all} = 2$ [Mas 95].

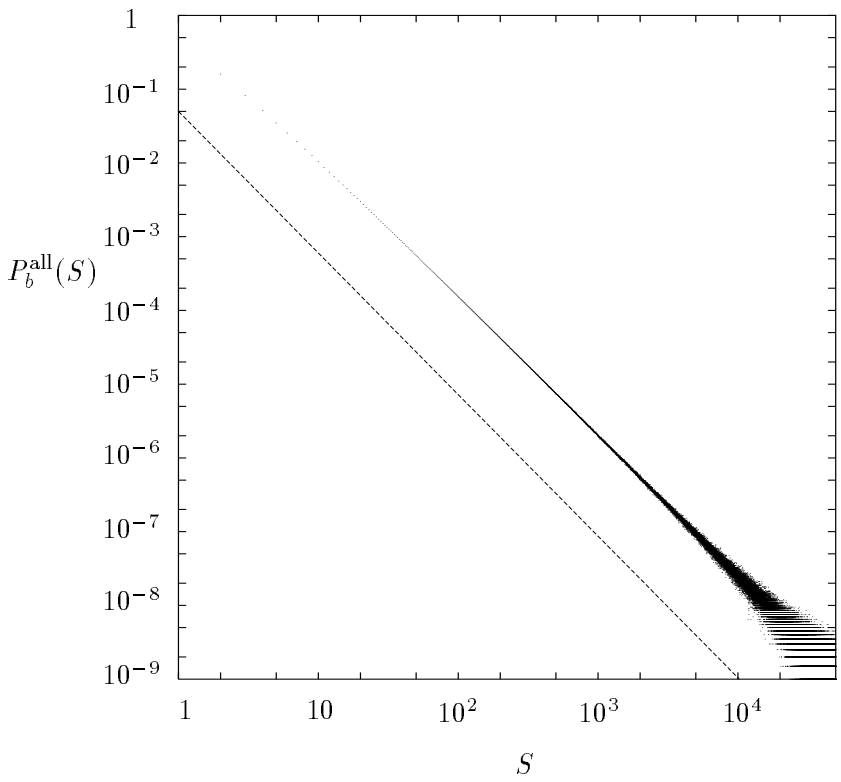

Figure 4.6: Overall backward-avalanche distribution $P_b^{\rm all}(S)$ measured for 2×10^9 backward-avalanches. The dashed line corresponds to a fit $P_b^{\rm all}(S) \sim S^{-1.92}$ in the range $100 \leq S \leq 2{\times}10^4$.

we obtain ρ_c very accurate since the relative error induced by the uncertainty in γ and $\langle n_{\rm cov} \rangle_{\phi_0}$ is in the small difference $\rho_c - \phi_0$ and not in ρ_c itself. For different values of ϕ_0 we show in Figure 4.7 the result for ρ_c using this method. Since equation (4.21) is valid only in the limit $\phi_0 \to \rho_c$, we get for the closest measurement at $\phi_0 = 0.66$

$$\rho_c = 0.66696 \pm 0.00002 \tag{4.34}$$

This value is in agreement with the result $\rho_c = 0.66702 \pm 0.00003$ from [Pac 96] and $\rho_c = 0.66702 \pm 0.00008$ of [Gra 95].

Now we are in the position to check the scaling prediction (4.12) for ϕ_0-forward avalanches of [Mas 95]. In Figure 4.8a we observe clearly the cutoff for large avalanche sizes at small ϕ_0. Plotting $P_f(S, \phi_0) S^\tau$ as a function of $(\rho_c - \phi_0)^{1/\sigma}$ the data of $P_f(S, \phi_0)$ should collapse onto one line (for ϕ_0 close to ρ_c), describing the scaling function $g(x)$, if the scaling assumption (4.12) is correct. This scaling plot is shown in Figure 4.8b. We use our measurements $\tau = 1.08, \gamma = 2.703$, from which follows $\sigma = 0.340 \pm 0.003$. The scaling assumption should be true for $(\rho_c - \phi_0)/\rho_c \ll 1$ and for large avalanches $S \gg 1$. Large avalanches are found at high values of $x = S(\rho_c - \phi_0)^{1/\sigma}$. Figure 4.8b confirms the scaling assumption for that region. For small values of $x = S(\rho_c - \phi_0)^{1/\sigma}$, i.e. small S, we do not expect the scaling assumption to be correct, since the probability distributions $P_f(\phi_0, S)$ show the expected power-law dependence only in the limit of large S.

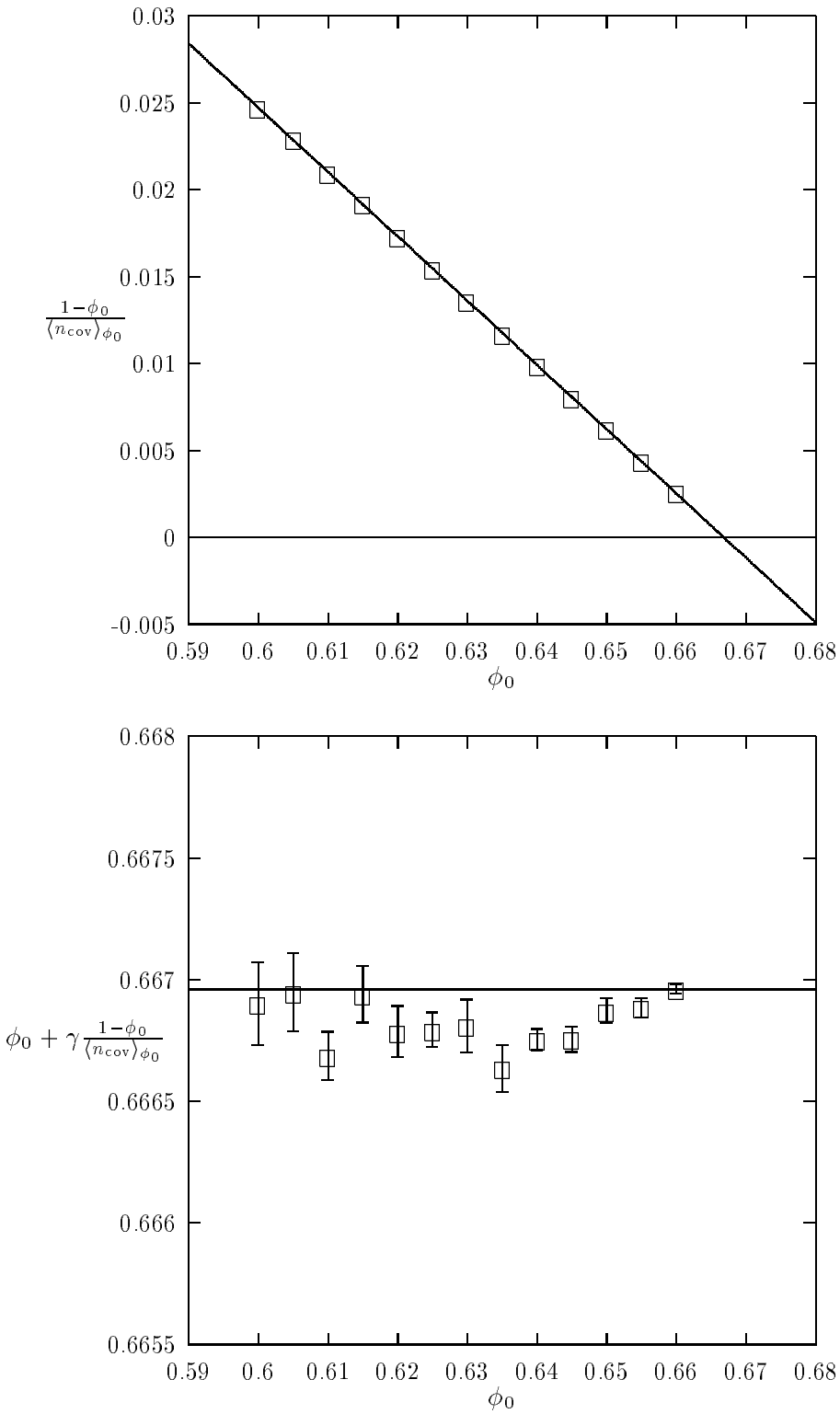

Figure 4.7: (a) According to equation (4.21) the slope of $1 - \phi_0/\langle n_{\rm cov}\rangle_{\phi_0}$ as a function of ϕ_0 is equal $-1/\gamma$. The intersection with the horizontal axis gives ρ_c. The line corresponds to $\gamma = 2.7032$, error bars are invisibly small in this plot. (b) ρ_c extrapolated from different values of ϕ_0. The same data as in figure (a) is used.

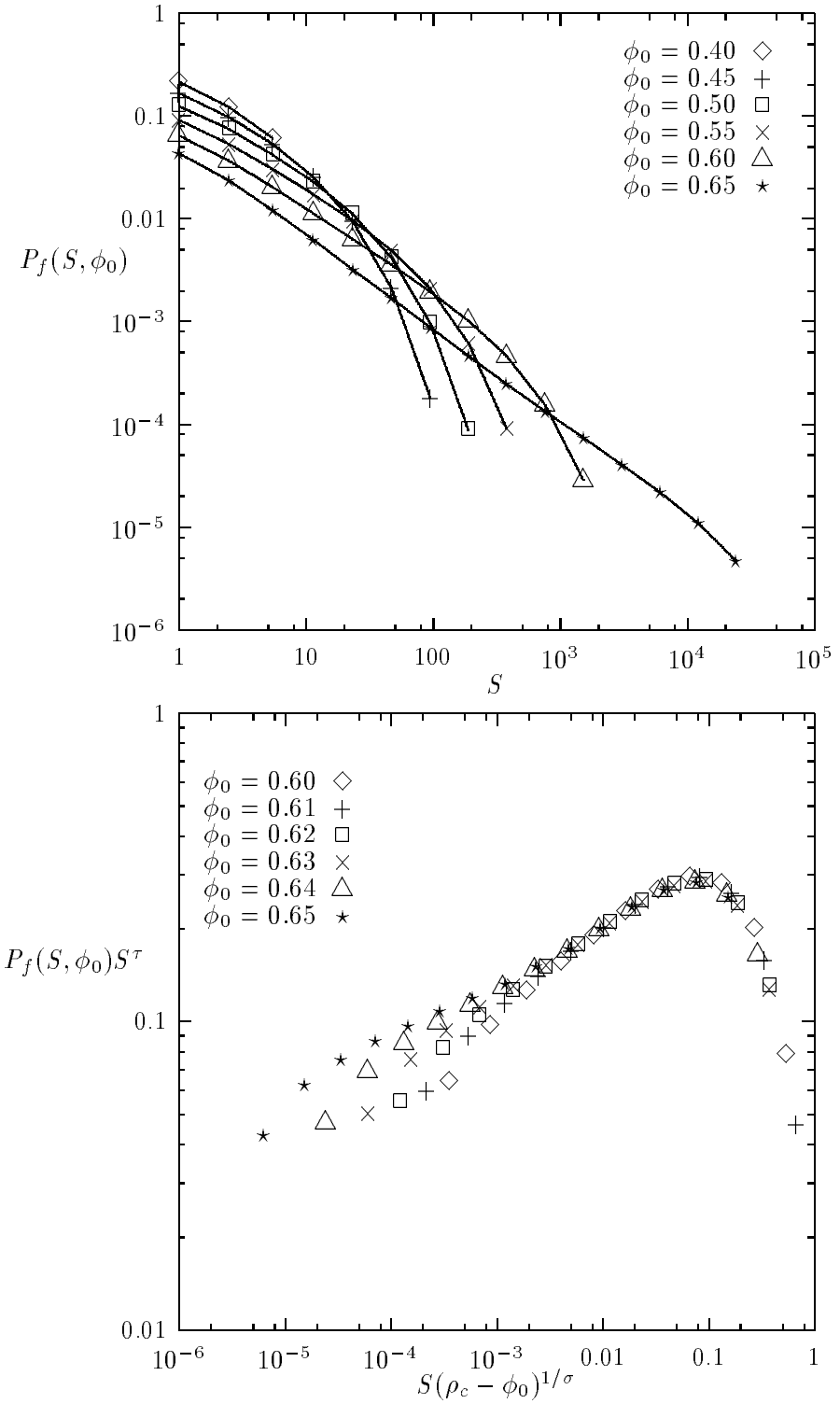

Figure 4.8: Distributions of ϕ_0-forward avalanches. (a) The cutoff at larger sizes S for small values of ϕ_0 is observed qualitatively as expected. (b) Scaling plot to check the scaling prediction (4.12). The data points should collapse onto a single line in the scaling regime.

Using the very accurate value of ρ_c (4.34), we are able to cross-check the value of γ describing the divergence of avalanche size $\langle S \rangle_{\phi_0}$ as given in equation (4.14). We observe good agreement for our value $\gamma = 2.7032$ with the prediction, see Figure 4.9.

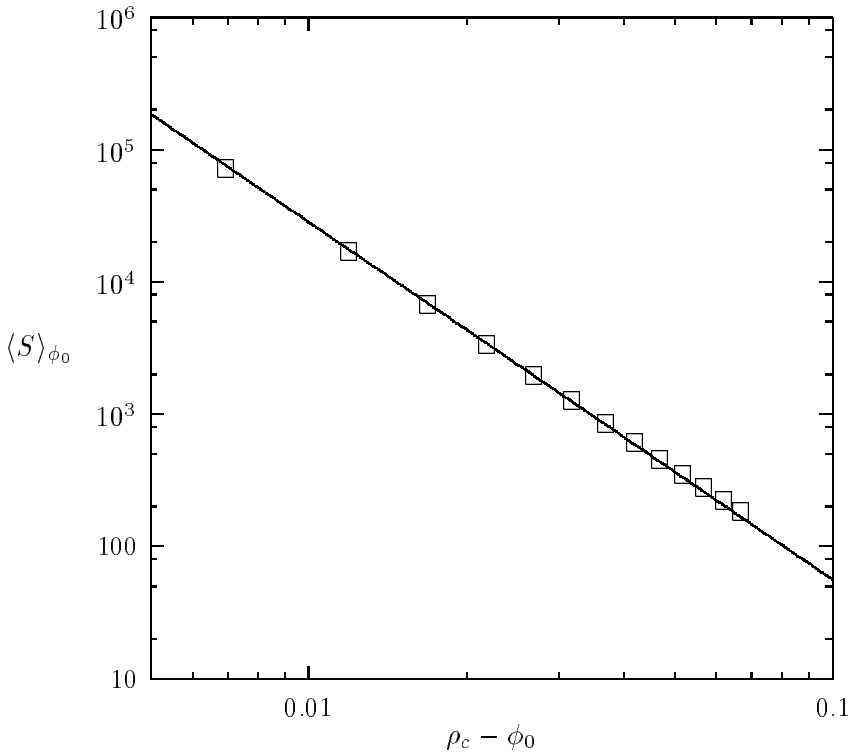

Figure 4.9: Divergence of the temporal extension of ϕ_0-forward avalanches as ϕ_0 approaches ρ_c, $\langle S \rangle_{\phi_0} \sim (\rho_c - \phi_0)^\gamma$. The line corresponds to $\gamma = 2.7032$.

The last numerical investigation concerns the connection of space and time avalanche extension. We defined two possible definitions of the spatial avalanche extension earlier in this section: the spatial size ξ, defined in (4.22), and the alternative definition of a radius of gyration R_{PMB}, given in (4.27). The last one is used in [Pac 96] to obtain the dynamical exponent z, see equation (4.23). At first we want to investigate numerically the relation between ξ and R_{PMB}. We measured both observables for 2.7×10^6 ϕ_0-forward avalanches. The result is shown in Figure 4.10a. Roughly we observe $R_{PMB} \sim \xi^a$, $a = 1.0$, which is indicated by the line. But there are significant differences:$R_{PMB}(\xi)$ oscillates around $R_{PMB} \sim \xi$. At small ξ, a is slightly smaller than 1.0, while it is larger than 1.0 at larger values. The difference is of the order of a few percent. This phenomenon makes it impossible to compare measurements of z obtained with R_{PMB} or with ξ. A measurement of z using $S(\xi) \sim \xi^z$ is shown in Figure 4.10b. Again this plot is based on an analysis of 2.7×10^6 ϕ_0-forward avalanches, $\phi_0 = 0.65$. A fit to the region $10 \leq \xi \leq 100$ gives approximately $z = 2.22$, but it is obvious that data points of larger avalanches are needed for a more reliable value. Our measurements surely contains systematic errors. The value of z given in recent publications is $z = 2.43 \pm 0.01$ [Pac 96] and [Gra 95]. The measurement of [Pac 96] uses R_{PMB} instead of ξ.

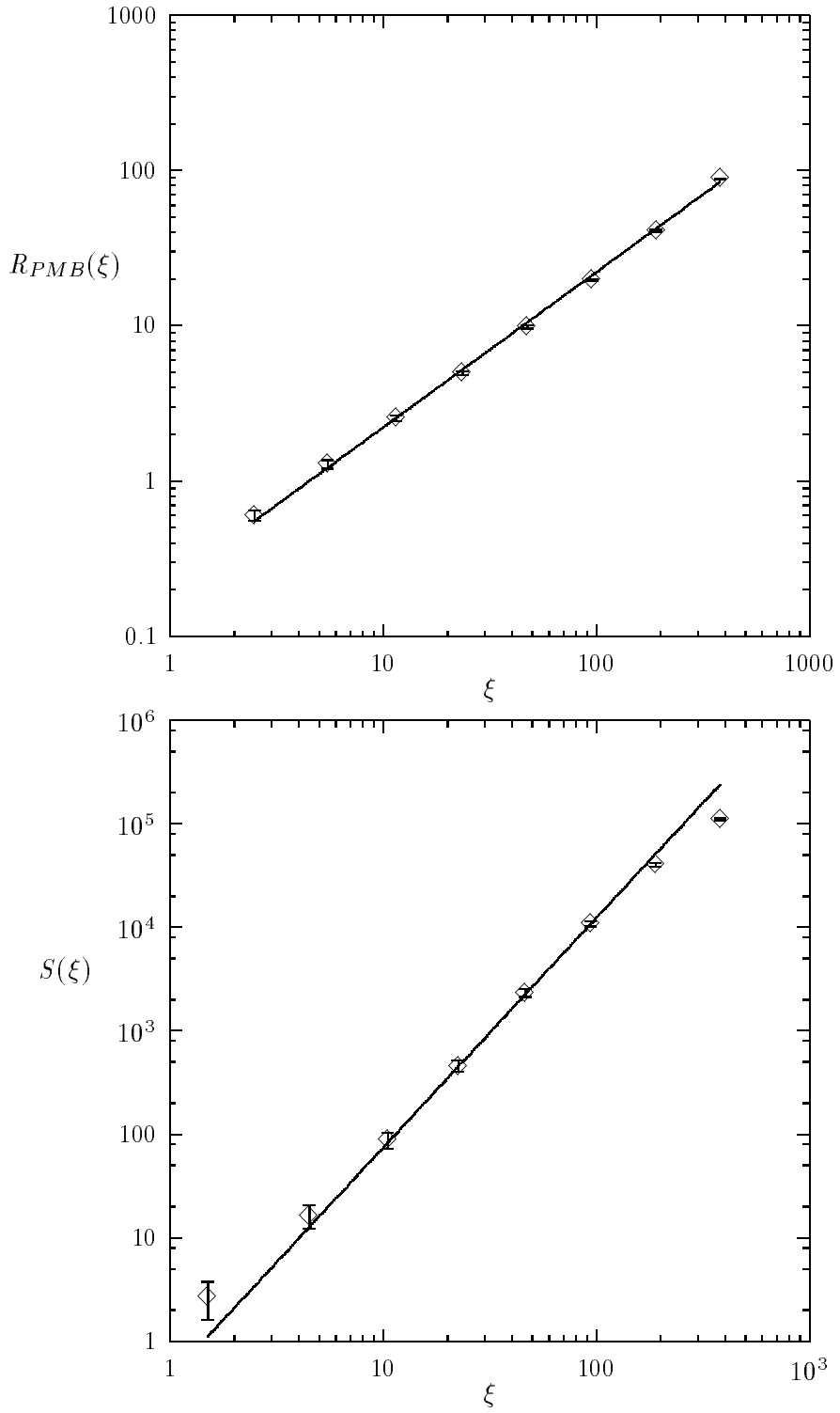

Figure 4.10: Spatial vs. temporal avalanche extension. (a) The relation between two possible definitions of spatial avalanche size ξ and R_{PMB} is shown. Roughly we have $R_{PMB} \sim \xi$ (line), but actually it oscillates significantly. (b) Temporal avalanche extension vs. spatial size ξ. A fit to $10 \leq \xi \leq 100$ gives $S(\xi) \sim \xi^{2.22}$ (line). For further discussion see text.

4.5 A local version of the BS-model

In this final paragraph we would like to make some remarks on a recently proposed local version of the BS-model [Schmo 95a] and the consequences for its self-organized critical behavior. This is especially interesting in the light of our discussions of section 2.2 on the role of infinitesimal small driving rates for SOC phenomena. It confirms our assumption that an infinitesimal driving rate is essential to obtain self-organized criticality.

Schmoltzi proposed to mutate per time step all species j in the model with a barrier (fitness) value smaller than a value η_j^t, which is chosen from a Boltzmann distribution $A(\eta_i^t) = \beta e^{-\beta \eta_i^t}$. As in the original BS-model also the nearest neighbors of these species mutate. Due to this modification it is possible that per time step more than one species is active. There is no need to look for a global minimum. It turns out that this local variant is no longer self-organized critical [Schmo 95b, Schmo 95a]. This observation confirms our proposed view of the role of order- and control-parameter for self-organized criticality as given in section 2.2. The infinitesimal driving rate is indeed essential in the BS-model to obtain self-organized criticality.

In this section we introduced the BS-model, elucidated its biological contents, discussed some of its properties and presented finally our numerical results describing its critical properties. For the rest of this part we turn now to the question of a renormalization group approach designed to calculate exponents analytically from the fixpoint properties and not via computer simulations.

III Renormalization group approach to Self-Organized Criticality

This chapter contains the introduction to a novel type of renormalization group methods. The aim is to recover the properties of self-organized criticality in the RG-application, i.e. the attractive nature of the fixpoint, infinite correlations (power-law exponents) and universality. Using the example of the BS-model the main ideas and principles are given in section 5. The application of this scheme to the BS-model is performed using the Run-Time-Statistics (RTS) method [Mar 94b], which is discussed and slightly corrected in section 6. The calculation is done by a new method combining the RTS-approach and the Monte-Carlo method, thereby improving the performance of the RTS-approach considerably, see section 7. Finally we discuss the possibilities and problems to use the same tool for related models describing interface roughening in disordered media in section 8.

5 Renormalization group method for the BS-model

In this section we give a first idea of how to perform a renormalization group method on the Bak-Sneppen model. We follow the lines of the work of Matteo Marsili [Mar 94b] and consider his modified one dimensional Bak-Sneppen model. The main ideas of the RG approach are given in paragraph 5.1. In 5.2 the concept of the RG transformation is made clearer by picturing it in form of a commutative diagram. Examples of relevant processes are given. Assuming that the Renormalization Group transformation drives the system to a fixed point, it is shown in paragraph 5.3 how to extract the fundamental exponents τ and z from the fixed point properties.

5.1 The Idea

Objects that occur on every scale in the $1d$-Bak-Sneppen model are the temporal and spatial avalanches, their size is denoted by S and ξ as defined in the previous section, see equations (4.11) and (4.22). A renormalization group approach should integrate out small avalanches and provide a mapping of large avalanches onto smaller ones, thereby not changing the scale invariant avalanche distribution. Note that only critical ϕ_0-avalanches, i.e. $\phi_0 = \rho_c$, should be considered for this mapping since only these behave in a scale invariant way.

The mapping of large avalanches onto smaller ones, which depends on the definition of the block transformation, has to respect the dynamical rule: Due to the block transformation a modified dynamics will occur on the coarser level in general. Therefore we have to choose a general dynamical rule that will allow for modifications of the macroscopic dynamics during the RG transformation. This corresponds to choosing a more general hamiltonian in usual RG methods for incorporation of additional terms

that are generated during a RG transformation. In addition the modified dynamics will influence the static threshold ρ_c on the coarser level. We thus have to think about a method to couple the static ρ_c to the dynamical rule governing the avalanche evolution.

The fixed point consists of a dynamical rule and its corresponding $\rho_c^\star$ invariant under further RG-iterations. Before going into details in the next paragraph we define the modified Bak-Sneppen model that will be the subject of the renormalization group transformation.

We change the step 4 of our definition of the BS-model in section 4.1. Instead of choosing the right *and* left neighbor for an update we only update the left *or* right neighbor:

4. Choose $k = i(t) + 1$ or $k = i(t) - 1$ with equal probability $p = 0.5$. Replace the value of the neighbor k by a new value $\phi_k^{(t+1)}$

$$\phi_k^{(t+1)} = x \text{ with probability } b(x).$$

Note that we don't choose the new value $\phi_k^{(t+1)}$ of the neighbor uniformly distributed from the interval $[0, 1)$ as before, but with a general probability $b(\phi_k^{(t+1)})$, $\int_0^1 b(x)dx = 1$. This will allow for the RG proliferation, as we shall see in the following paragraph.

5.2 Construction of the Renormalization group approach

From now on we restrict ourselves to a block factor of two. We denote the fine scale with the index (l) and the next coarser scale with the index $(l+1)$. The block variables are Φ_I, the fine variables are ϕ_i. Let us first think about possible blocktransformation. A general blocktransformation F

$$\Phi_I^{(t)} \equiv F(\{\phi_i^{(t)} | i \in I\}) \tag{5.1}$$

should conserve the information for the position of the minimum: If the minimal value is $\phi_i^{(t)}$ on the fine scale, the minimum on the coarse scale should be $\Phi_{I(t)}$, $i(t) \in I(t)$. Using a block factor of two we have the condition

$$I(t) = J \Leftrightarrow i(t) = 2J \vee i(t) = 2J + 1 \ . \tag{5.2}$$

The simplest block transformation obeying (5.2) is

$$\Phi_I^{(t)} = \min\{\phi_{2i}^{(t)}, \phi_{2i+1}^{(t)}\} \ . \tag{5.3}$$

This choice ensures that the dynamics on the coarser level is again based on the selection of the minimal value $\Phi_{I(t)}$. Applying the block transformation after every time step on the fine scale and monitoring the resulting time evolution of variables on the coarse scale we observe that a couple of time steps is needed to change the block variables Φ_I on the coarse grid. To be sure to perform one update on the coarse grid, i.e. updating

$\Phi_{I(t)}$ and either the left or right neighbor $I(t)\pm 1$, we have to wait until four neighboring variables on the finer scale have been updated. Therefore, in addition to the blocking in space, a blocking procedure in time is needed.

A sequence of T updating steps on the fine scale, changing exactly four neighboring variables, is mapped onto one updating step on the coarse level. We have thus two different time scales: t for the evolution of the fine variables and t' for the evolution of the coarse variables. The mapping from t to t' is dynamic, i.e. it depends on the stochasticity of the temporal evolution. The initial and final state of one updating step on the coarse level is given by applying equation (5.3) to the initial and final configuration of the fine level. This concept, the blocking of the dynamical process in space and time from a fine scale l to a coarser scale $l+1$ is shown in the diagram of Figure 5.1. The blocktransformation and the modified dynamics have to be chosen in such a way that it makes no difference for the final state $\mathbf{\Phi}^{(1)}$ if we apply first T fine updates and then the blocktransformation or if we apply first the blocktransformation and then perform one coarse update using the block dynamics. The space-time diagram of Figure 5.1 has to be commutative.

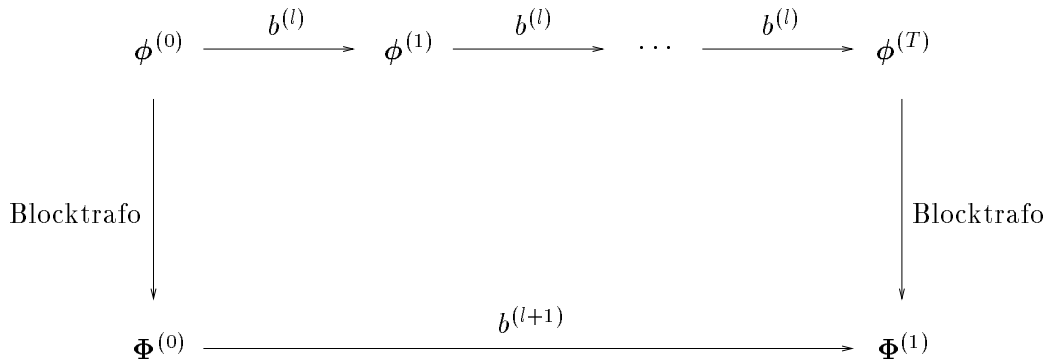

Figure 5.1: Concept of blocking in space and time. T updates on the fine level l are performed until four neighboring variables are changed. The result of this process defines a contribution to one time step on the coarse level $l+1$.

To deduce the dynamics on the coarse level, we have to compute the probability distribution of variables $\Phi_{I(t)}$ and $\Phi_{I(t)\pm 1}$ in the final state on the coarse level. We denote these probability distributions $\tilde{a}^{(l+1)}(x)$ and $\tilde{b}^{(l+1)}(x)$ respectively. They will in general be different from an uniform distribution. However, it is possible to perform a variable transformation $x \to y(x)$

$$y(x) = \int_0^x \tilde{a}^{(l+1)}(x')dx' \tag{5.4}$$

to achieve

$$a^{(l+1)}(y) = \Theta(y)\Theta(1-y) \tag{5.5}$$

$$b^{(l+1)}(y) = \left.\frac{\tilde{b}^{(l+1)}(x)}{\tilde{a}^{(l+1)}(x)}\right|_{y(x)=y} \tag{5.6}$$

Performing this transformation we have reduced the possible proliferation to the distribution $b(x)$ from which a new value of the neighbor of the minimal site is determined.

All other rules (search for the minimum, choose left or right neighbor, replace the value of the minimal variable with a uniformly distributed one) are invariant under this RG-transformation. In the following we would like to discuss more closely the relevant processes that are mapped onto one time step at the coarser scale and thus contribute to $b^{(l+1)}(x)$.

As already noticed above, we expect scale invariant behavior only for avalanches that are critical, i.e. $\phi_{i(t_i)}^{(t)(l)} = \rho_c^{(l)}$. Therefore we have to consider only such processes for the mapping of a sequence of fine updates onto one coarse update. From this initial condition it becomes immediately clear that either we have four neighboring updates on the fine scale after T time steps (contributing to one coarse update) or the process stops earlier because $\phi_{i(t')}^{(t')(l)} \geq \rho_c$ for $t' > t_i$. The latter processes do not contribute since they represent small fluctuations with avalanche size $S \leq 3$ and are neglected in the RG step. Relevant processes α are given as temporal sequence $i_\alpha(t)$, $|i_\alpha(t)|$ indicating the position[12] of the minimal ϕ_i and updating to the right ($i_\alpha(t) > 0$) or to the left ($i_\alpha(t) < 0$). A relevant process starts with the minimal value ρ_c, then it is always smaller than ρ_c. It lasts until four neighboring sites have been updated for the first time. This description may be formalized to the following definition

Definition. A temporal sequence $i_\alpha(t)$ is a relevant process α of length T_α if

$$\phi_{|i_\alpha(1)|} = \rho_c \quad , \quad \phi_{|i_\alpha(t)|} < \rho_c \quad \forall \;\; 1 < t \leq T_\alpha$$

$$T_\alpha = \min_{T'} \{T' : x_{\max}(T') - x_{\min}(T') = 3\} \tag{5.7}$$

with

$$x_{\min}(T') = \min_{1 \leq t \leq T'} \{|i_\alpha(t)| + \text{sign}(i_\alpha(t)), |i_\alpha(t)|\} \tag{5.8}$$

$$x_{\max}(T') = \max_{1 \leq t \leq T'} \{|i_\alpha(t)| + \text{sign}(i_\alpha(t)), |i_\alpha(t)|\} \tag{5.9}$$

The minimal length of a relevant process α is $T_\alpha = 3$, T_α has no upper limit. An example of a relevant process of length $T_\alpha = 4$ is given in Figure 5.2.

In principle we have to compute all processes of arbitrary length, evaluate the probability distributions in the final state and average these results to obtain the probability distributions $\tilde{a}^{(l+1)}(x), \tilde{b}^{(l+1)}(x)$, thereby taking into account the probability μ_α for each process α. In practice it is clear that the probability for long processes will be arbitrary small, so it should be sufficient to calculate only processes up to an order of T_{max}. However, the small weight of long processes is balanced since for longer processes there are much more possibilities to realize a process. The number of processes increases approximately as e^T. For $T_{max} = 20$ we have roughly 10^{12} different possibilities of relevant processes to evaluate.

Intuitively it is plausible that the probability distribution $P(T)$ for a process of length T contains the information for the dynamical exponent z, defined in equation (4.23):

[12] Without loss of generality we may assume to have only positive indices i.

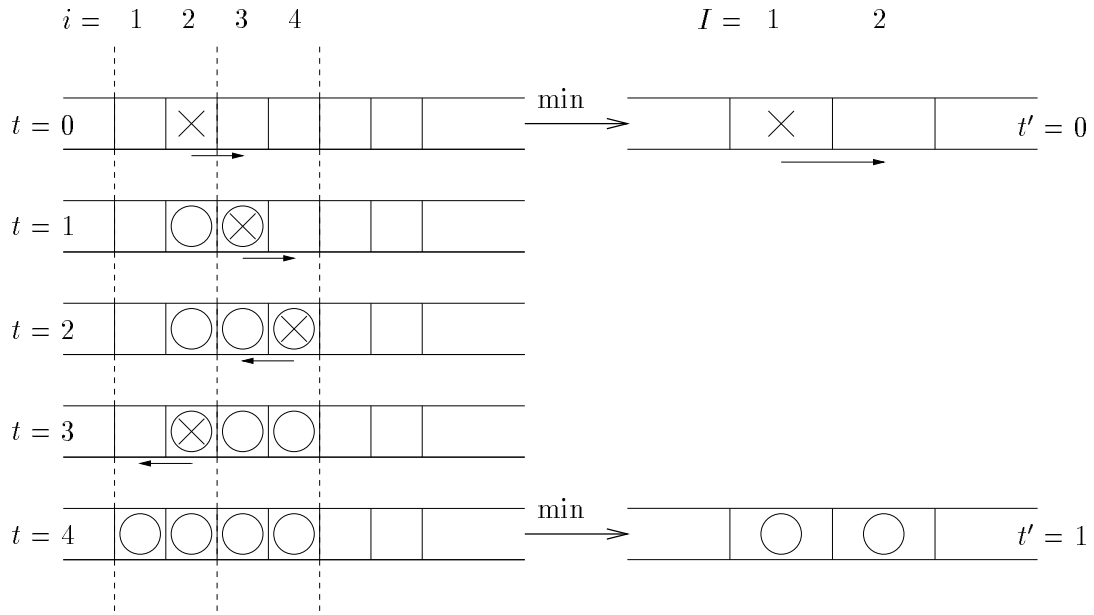

Figure 5.2: An example of a relevant process ($\boldsymbol{i} = (2, 3, -4, -2)$) of length $T = 4$ and its blocking. A $\times$ denotes the position of the minimum, $\rightarrow$ or $\leftarrow$ updating to the right or left and $\bigcirc$ is the symbol for a site updated at least once during this process.

the spatial extension of one process is by definition four sites, the temporal extension is given by $P(T)$. We will discuss this connection in more detail in the next paragraph.

The last point to be discussed is the value $\rho_c^{(l)}$ of the initiator for critical processes. A critical process is defined as an avalanche that in principle could extend over all time scales. Thus, during a critical avalanche we should always have a constant number of variables $\phi_j < \rho_c$. If this number decreases with time, the avalanche cannot extend on all time scales. On the other hand, if it increases, the avalanche will last forever. We therefore demand that the number of variables smaller than ρ_c is constant on average during a critical avalanche. To be more explicit, denote the average number of variables smaller than ρ_c in a ρ_c-forward avalanche started at time $t = 0$ after one time step as

$$\begin{aligned} n_{t=1}(\rho_c^{(l)}, b^{(l)}) &= \left\langle \sum_{i=1}^{4} \Theta(\rho_c^{(l)} - \phi_i^{(t=1)(l)}) \right\rangle_{\text{all processes}} \\ &= \rho_c^{(l)} + \int_0^{\rho_c^{(l)}} b^{(l)}(x)dx \quad . \end{aligned} \tag{5.10}$$

Equivalently we denote the average number of variables smaller than ρ_c in a ρ_c-forward avalanche started at time $t = 0$ in the final state of all processes as

$$n_{t=t_{\text{final}}}(\rho_c^{(l)}, b^{(l)}) = \left\langle \sum_{i=1}^{4} \Theta(\rho_c^{(l)} - \phi_i^{(t=T_\alpha)(l)}) \right\rangle_{\text{all processes}} . \tag{5.11}$$

Note that the average $\langle . \rangle$ in (5.10), (5.11) has to be taken over all processes, including those that stop before four neighboring variables are updated. For given $b^{(l)}(x)$, $\rho_c^{(l)}$ is obtained as solution of the equation

$$n_1(\rho_c^{(l)}, b^{(l)}) = n_{t_{\rm final}}(\rho_c^{(l)}, b^{(l)}) \tag{5.12}$$

5.3 Calculating fundamental exponents τ and z

In the last paragraph we deduce some relations of how to obtain the critical avalanche exponents τ_ξ, z, and τ defined in equations (4.24), (4.23) and (4.12). We assume that the renormalization group transformation is successful and converges to an invariant distribution $b^\star(x)$ and an invariant value $\rho_c^\star$. Let us first calculate the probability $K^\star$, that an avalanche stops exactly at scale 2^j

$$\begin{aligned} K^\star =& \frac{\int_{2^{j-1}}^{2^j} P_\xi(\xi) d\xi}{\int_{2^{j-1}}^{\infty} P_\xi(\xi) d\xi} \\ =& 1 - 2^{1-\tau_\xi} \end{aligned} \tag{5.13}$$

where we used the definition (4.24). In other words: $K^\star$ is the probability that the minimal site is always the same until eventually the avalanche stops. The spatial size is simply $\xi = 1$. This probability can be calculated on the other hand from the fixed point distribution $b^\star(x)$ and $\rho_c^\star$. We find

$$\tau_\xi = 1 - \frac{\log(1 - K^\star)}{\log 2} \quad . \tag{5.14}$$

We turn now to the dynamical exponent z. As noted already above, the information on exponent z is contained in the probability distribution $P(T)$ for the length T of relevant walks. Consider an avalanche of size $\xi = 2^k$. The avalanche duration is one time step on scale 2^k. We would like to know how many time steps $T^{(k)}$ have to be performed on the finest scale 2^0. Going back to finer and finer scales we accumulate at each scale j a factor $t^{(j)}$ that gives the number of time steps on scale j needed to update four neighboring variables. We then have to take the average over all possible realizations of processes of length $t^{(j)}$

$$\begin{aligned} T^{(k)} &= \prod_{j<k} t^{(j)} \\ \Leftrightarrow \quad \log T^{(k)} &= \sum_{j<k} \log t^{(j)} \\ \Leftrightarrow \quad \langle \log T^{(k)} \rangle &= k \langle \log t \rangle \end{aligned} \tag{5.15}$$

with

$$\langle \log t \rangle = \sum_t t P(t) \quad . \tag{5.16}$$

On the other hand we have from definition (4.23)

$$\xi(k)^z = \langle T^{(k)} \rangle = \langle e^{\log T^{(k)}} \rangle \approx e^{\langle \log T^{(k)} \rangle} = e^{z \log \xi(k)} = e^{zk \log 2} \quad . \tag{5.17}$$

The approximation $\langle e^{\log T^{(k)}} \rangle \approx e^{\langle \log T^{(k)} \rangle}$ is valid if the average $\langle . \rangle$ is done over many single measurements (law of large numbers). Using (5.15) we obtain eventually

$$\begin{aligned} k\langle \log t \rangle &= zk \log 2 \\ \Rightarrow \qquad z &= \frac{\langle \log t \rangle}{\log 2} \end{aligned} \tag{5.18}$$

The exponent τ, describing the probability distribution of the temporal extension of critical avalanches can be obtained via the scaling relation (4.26) from exponents τ_ξ and z. Results for these exponents obtained from the renormalization group approach are given in section 7.

6 Run-Time-Statistics approach

In this section we introduce the Run-Time-Statistics (RTS) approach developed by Marsili [Mar 94a]. The purpose of this approach is to transform a deterministic process in a quenched random environment into a stochastic process. The approach is based on the idea, that models in an random environment may be viewed as cognitive processes, that involve testing this environment. This idea may be expressed in a mathematical formalism using the rules of conditional probability, that specifies the evolution of the Run-Time-Statistics of the random environment. The information on the history of the process is stored in a conditional probability distribution. In the first paragraph the main RTS equations for the $1d$-BS model [Mar 94b] are introduced. In the second paragraph we explain how to exploit the RTS-method to perform a renormalization group iteration in the spirit of the last section.

6.1 The RTS-Equations

We use the same notation as introduced in section 4. The probability distribution of ϕ_i at time t will be denoted $p_{i,t}(x)$. The conditional probability that the minimal variable is located at site i is then

$$p^t_{\min,i}(x) = p_{i,t}(x) \prod_{j \neq i} \int_x^1 p_{j,t}(y) dy \quad . \tag{6.1}$$

In the avalanche statistics of relevant processes we are interested in the conditional probability that $\phi_i^{(t)}$ is the minimal site *and* that the avalanche does not stop, i.e. $\phi_i^{(t)} < \rho$ which is

$$\mu_{i,t}(\rho) = \int_0^\rho p^t_{\min,i}(x) dx \quad . \tag{6.2}$$

Once we have determined the site with minimal $\phi_i < \rho$, its probability distribution is no longer $p_{i,t}(x)$ but

$$m_{i,t}(x) = \Theta(\rho - x)\frac{p^t_{\min,i}(x)}{\mu_{i,t}(\rho)} \quad . \tag{6.3}$$

$m_{i,t}(x)$ is normalized. $\mu_{i,t}(\rho)$ may be considered as the normalization factor of the probability distribution of the minimal $\phi_i < \rho$. Once we know the position of the minimum, we also know that all other sites are not the minimum. This information can be used to obtain the conditional probability distributions of all other variables that are not minimal. From $\phi^t_i \leq \phi^t_k \ \forall \ k, j \neq i, \phi^t_i \leq \rho$ we have

$$\tilde{p}_{j,t}(x) = \mathcal{N} p_{j,t}(x) \int_0^\rho p_{i,t}(y)\Theta(x-y) \prod_{k\neq i,j} \int_y^1 p_{k,t}(z)dzdy \quad . \tag{6.4}$$

$\mathcal{N}$ is a normalization factor that has to be computed from the integral. Note that equation (6.4) is different from the corresponding equations in [Mar 94a, Mar 94b] $\tilde{p_{j,t}}(x) = \mathcal{N} p_{j,t}(x) \int_0^x m_{i,t}(y)dy$. Marsili did not take into account the fact, that $m_{i,t}(x)$ and $p_{j,t}(y)$, $j \neq i$ are not mutually independent and it is not allowed to multiply them to obtain the new conditional probability. This leads to different results of the fixpoint properties, see section 7.3 below. We show in the following how to use these RTS equations to evaluate the weight (probability) of a given relevant process $i = i(t)$.

We consider a process α starting at time $t = 1$ of length T_α and a sequence of minima $i(t)$. At time $t = 1$ we have $\phi_{i(1),t=1} = \rho$ while all other variables are larger then ρ. Their exact value is not essential, since in an updating they will acquire a new value, that is completely independent from the old one. The only important information is, that their values are larger than ρ. In this scenario we have

$$\begin{aligned} p_{i(1),t=1}(x) &= \delta(x-\rho) \\ p_{j,t=1}(x) &= \Theta(x-\rho)\frac{1}{1-\rho} \ \ \forall \ j \neq i(1) \quad . \end{aligned} \tag{6.5}$$

After the updating of the minimal site and its left or right neighbor are done, we have at the next time step $t \rightarrow t+1$ the probability distributions $(j \neq i(t), i(t) \pm 1)$

$$\begin{aligned} p_{i(t),t+1}(x) &= \Theta(x)\Theta(1-x) \\ p_{i(t)\pm1,t+1}(x) &= b(x) \\ p_{j,t+1}(x) &= \mathcal{N} p_{j,t}(x) \int_0^\rho p_{i,t}(y)\Theta(x-y) \prod_{k\neq i,j} \int_y^1 p_{k,t}(z)dzdy \ . \end{aligned} \tag{6.6}$$

Now we are able to compute at time $t+1$ the probability that the minimal site is located at $i(t+1)$ as given by process α using equation (6.2). Having calculated the probabilities $\mu_{i_\alpha(t),t}$ for all $1 \leq t \leq T - \alpha$ we get the weight ν_α of process α from

$$\nu_\alpha = \frac{1}{2^{T_\alpha}} \prod_{t=1}^{T_\alpha} \mu_{i_\alpha(t),t} \quad . \tag{6.7}$$

In addition we get the final probability distributions in the four updated variables, from which it is possible to deduce the blocked distributions $\tilde{a}$ and $\tilde{b}$ at the next coarser level. The discussion of this question and other details of the RG-iteration are given in the next paragraph.

6.2 The renormalization group iteration

Let us assume that we start with our renormalization group procedure at scale 2^l denoted (l). We already know $a^{(l)}(x) = \Theta(x)\Theta(1-x)$ and $b^{(l)}(x)$. First, we have to determine the value of $\rho_c^{(l)}$. From condition (5.12) we have to solve

$$n_1(\rho_c^{(l)}, b^{(l)}) = \rho + \int_0^{\rho_c^{(l)}} b^{(l)}(x)dx = n_{t_{\text{final}}}(\rho_c^{(l)}, b^{(l)}) = \sum_\alpha \nu_\alpha \sum_{i=1}^{4} \int_0^{\rho_c^{(l)}} p_{i,t_\alpha}(x)dx \ . \tag{6.8}$$

To solve this equation numerically, one has to look for zero points of

$$f(\rho) \equiv n_1(\rho, b^{(l)}) - n_{t_{\text{final}}}(\rho, b^{(l)}) \ . \tag{6.9}$$

Using an iterative algorithm like the secant method [Pre 89] one has to compute in each iteration the value of $f(\rho)$, thus has to evaluate in each iteration the run time statistics of all relevant processes α for the current value of ρ. Once $\rho_c^{(l)}$ is known, it is possible to compute for this value again the run time statistics of all relevant processes α, their weights ν_α and their final probability distributions $p_{i,t_\alpha}(x)$. For each relevant process one has to apply the blocktransformation (5.3) to the four neighboring updated variables ϕ_i, $i = 1,2,3,4$. The probability distribution of the block variables Φ_I, $I = 1,2$ is given as

$$m_I^\alpha(x) = p_{2I-1,t_\alpha}(x) \int_x^1 p_{2I,t_\alpha}(y)dy + p_{2I,t_\alpha}(x) \int_x^1 p_{2I-1,t_\alpha}(y)dy \ . \tag{6.10}$$

These blocked distributions have to be averaged over all processes with their normalized weight ν_α. The normalization constant W is given as

$$W \equiv \sum_\alpha \nu_\alpha \ , \tag{6.11}$$

and, without loss of generality assuming the minimum in the initial state in ϕ_1 or ϕ_2 (otherwise one has simply to renumber the variables), we obtain the new distributions

$$\begin{aligned} \tilde{a}^{(l+1)}(x) &= \frac{1}{W} \sum_\alpha \nu_\alpha m_1^\alpha(x) \\ \tilde{b}^{(l+1)}(x) &= \frac{1}{W} \sum_\alpha \nu_\alpha m_2^\alpha(x) \end{aligned} \tag{6.12}$$

In a final step the distribution $\tilde{a}^{(l+1)}(x)$ has to be scaled back to an uniform distribution. This is achieved via equation (5.4), leading to

$$\begin{aligned} a^{(l+1)}(y) &= \Theta(y)\Theta(1-y) \\ b^{(l+1)}(y) &= \left. \frac{\tilde{b}^{(l+1)}(x)}{\tilde{a}^{(l+1)}(x)} \right|_{y(x)=y} \ . \end{aligned} \tag{6.13}$$

With $a^{(l+1)}(x)$, $b^{(l+1)}(x)$ one can go to the next coarse level and iterate the procedure. The described iteration needs the generation of *all* relevant processes or at least of processes up to an order $t_\alpha \leq T_{\max}$. Marsili uses $T_{\max} = 20$ and extrapolates to $T_{\max} = \infty$. In the following section we introduce a alternative method that avoids both the explicit generation of all relevant processes and the extrapolation of $T_{\max}$ to infinity.

7 A new Monte-Carlo approach

In this section we introduce a new approach [Mik 96] to Marsili's Renormalization Group Method [Mar 94b], that has been explained in section 5. This new method is inspired from the "importance sampling" - Monte Carlo method and serves as an alternative method to the quite elaborate Run Time Statistics technique of Marsili [Mar 94a] discussed in the previous section. With our new method we are able to cross check Marsili's results and save a lot of computer time. In the first paragraph (7.1) of this section we give a sketch of the main idea and some details concerning the organization of the program. In the second paragraph (7.2) we shortly discuss advantages and disadvantages of the new method compared to Marsili's Run Time Statistics. Eventually we present our results of the fixed point properties and analyze them to extract the critical exponents in paragraph (7.3).

7.1 The idea

The idea is to generate an ensemble of relevant processes as defined in (5.7) in which processes α occur according to their probability ν_α given in (6.7). This way we do not waste time by generating and evaluating processes that occur very seldom. Instead all generated processes of the ensemble contribute with equal probability. This reminds of the concept of the "importance sampling" Monte-Carlo method [Bin 88]. Nevertheless we want to stress the fact that we do not simulate the system. We only evaluate integrals using the Monte-Carlo method, an array of seven neighboring cells is sufficient for this task.

To generate a single relevant process α using a distribution $b^{(l)}(x)$, we start with a variable $\phi_{i_\alpha(0)} = \rho$, do the updating according to the modified Marsili-rule (updating to left *or* right of the minimal site using $b^{(l)}(x)$) until four neighboring sites are updated. For this process we count the number of variables smaller than ρ after the first time step as well as in the final state

$$\begin{aligned} n_1^{(\alpha)} &= \sum_i \Theta(\rho - \phi_{i_\alpha}^{(t=1)}) \,, \\ n_f^{(\alpha)} &= \sum_i \Theta(\rho - \phi_{i_\alpha}^{(t=T_\alpha)}) \,. \end{aligned} \tag{7.1}$$

It is possible that $n_1^{(\alpha)} = 0$ and/or $n_f^{(\alpha)} = 0$. In this case the generated process is not a relevant process, since it stopped, i.e. $\phi_{i(t)} > \rho$, before four neighboring sites are

updated. Using this notation we can easily write down $n_{t=1}(\rho, b^{(l)})$ and $n_{t=t_{\rm final}}(\rho, b^{(l)})$ obtained from the generation of an ensemble of N processes[13]

$$\begin{aligned} n_{t=1}(\rho, b^{(l)}) &= \frac{1}{N} \sum_{\alpha} n_1^{(\alpha)} \\ n_{t=t_{\rm final}}(\rho, b^{(l)}) &= \frac{1}{N} \sum_{\alpha} n_f^{(\alpha)} \end{aligned} \tag{7.2}$$

To determine the critical $\rho_c^{(l)}$ from definition (5.12) we use the function $f^{(l)}(\rho)$ as defined in (6.9)

$$f^{(l)}(\rho) \equiv n_{t=t_{\rm final}}(\rho, b^{(l)}) - n_{t=1}(\rho, b^{(l)})$$

and look for its zero-point. To this end we use the secant method described in [Pre 89]. This method converges in a very few iterations as is illustrated in figure 7.1b. In the upper part of this Figure we show the functions $n_{t=t_{\rm final}}(\rho, b^{(0)})$ and $n_{t=1}(\rho, b^{(0)})$ for the finest level $l = 0$, i.e. $b^{(0)}(x) = \Theta(x)\Theta(1-x)$.

Once we have determined the critical $\rho_c^{(l)}$ at level l for a given $b^{(l)}$, we are able to evaluate all *critical* relevant processes α starting with $\phi_{i_\alpha(0)} = \rho_c^{(l)}$ for their contribution to the blocked distributions $\tilde{a}^{(l+1)}(x)$ and $\tilde{b}^{(l+1)}(x)$. A relevant process contributes to the distributions $\tilde{a}^{(l+1)}(x)$ and $\tilde{b}^{(l+1)}(x)$ for the rules on the next coarser level by

$$\begin{aligned} \tilde{a}_{(\alpha)}^{(l+1)}(x) &= \delta(x - m_{(\alpha)}) \\ \tilde{b}_{(\alpha)}^{(l+1)}(x) &= \delta(x - n_{(\alpha)}) \end{aligned} \tag{7.3}$$

with

$$\begin{aligned} m_{(\alpha)} &= \min\{\phi_{2j}^{(t_\alpha)}, \phi_{2j+1}^{(t_\alpha)}\} \quad i_\alpha(t=0) = 2j \vee i_\alpha(t=0) = 2j+1 \\ n_{(\alpha)} &= \min\{\phi_{2k}^{(t_\alpha)}, \phi_{2k+1}^{(t_\alpha)}\} \quad i_\alpha(t=0) \neq 2k \wedge i_\alpha(t=0) \neq 2k+1 \quad , \end{aligned} \tag{7.4}$$

where the four neighboring sites $2j, 2j+1, 2k, 2k+1$ have been updated. For an ensemble of N' relevant processes α, each occurring with a probability according to their weight ν_α, we obtain

$$\begin{aligned} \tilde{a}^{(l+1)}(x) &= \frac{1}{N'} \sum_{\alpha} \tilde{a}_{(\alpha)}^{(l+1)}(x) \\ \tilde{b}^{(l+1)}(x) &= \frac{1}{N'} \sum_{\alpha} \tilde{b}_{(\alpha)}^{(l+1)}(x) \quad . \end{aligned} \tag{7.5}$$

To these preliminary distributions we apply the variable transformation (5.5), thereby switching back to a uniform distribution $a^{(l+1)}(x)$ and a transformed distribution $b^{(l+1)}(x)$. Now the described procedure may be iterated.

The remaining and central question is, how to generate an ensemble of processes α obeying their probabilities ν_α. But that is straightforward: we just apply the rules of

[13] Including non-relevant processes.

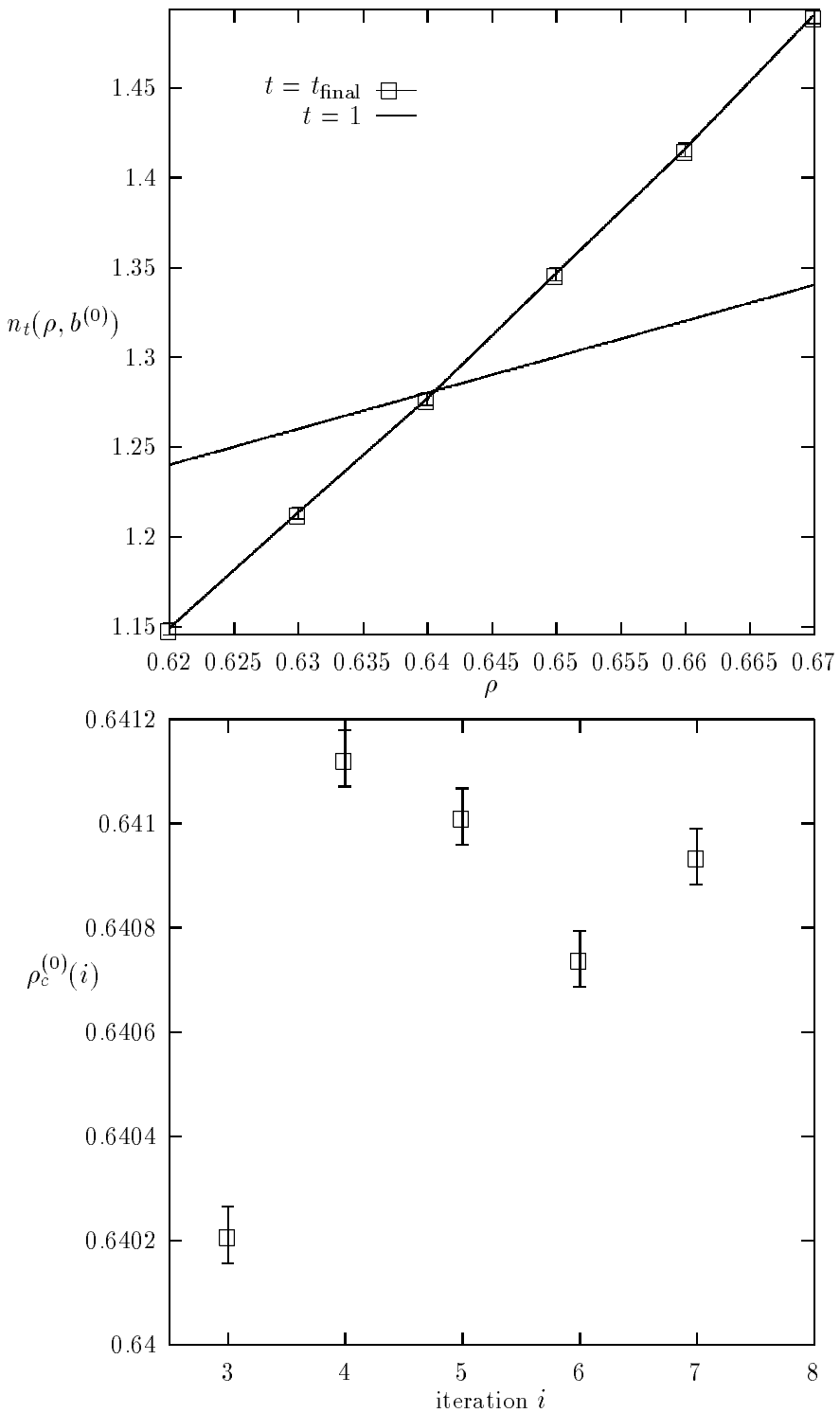

Figure 7.1: (a) $n_{t=t_{\text{final}}}(\rho, b^{(0)})$ and $n_{t=1}(\rho, b^{(0)})$ as a function of ρ for level $l = 0$. (b) Iterative calculation of $\rho_c^{(0)}$ applying the secant method to function $f^{(l)}(\rho)$ as defined in (6.9). The iteration stops if the error in $f^{(l)}(\rho)$ is smaller than the value of $f^{(l)}(\rho)$ itself. Start values of the iteration $\rho_c(i = 1) = 0.65$, $\rho_c(i = 2) = 0.60$ are not shown.

the game to a process starting with $\phi_{i_\alpha(0)} = \rho$ as long as not four neighboring sites have been updated. Once this happens, we stop the process and save its initial and final state[14]. Since we used the correct rules, especially the distributions $a^{(l+1)}(x)$ and $b^{(l+1)}(x)$, the process α occurs with its correct weight ν_α without the need of an explicit calculation of ν_α. Then we start the same procedure again for the next process that is generated completely independently from the previous one.

7.2 Advantages and Disadvantages

After having introduced our new Monte-Carlo approach we now want to discuss shortly some advantages and – of course – disadvantages of our method compared to Marsili's Run-Time-Statistics technique.

The first and most important point to note is that our method is much faster than Marsili's calculation. In his program one has to

- evaluate for each iteration during the determination of $\rho_c^{(l)}$ *all* relevant processes, i.e. iterate equations (6.6) via numerical integration and calculate ν_α for *all* relevant processes using equations (6.1,6.2).
- for each iteration calculate function $f^{(l)}(\rho)$, (6.9), using the expressions for $n_{t=1}(\rho, b^{(l)})$ and $n_{t=t_{\text{final}}}(\rho, b^{(l)})$ given in (6.8).
- evaluate for the critical $\rho_c^{(l)}$ again *all* relevant processes in the same manner, but now with the additional blocktransformation described in (6.10) and the averaging (6.12).

This has to be done on each level l. Taking into account processes up to a length $T_{\max} = 20$, we have about 10^{12} relevant processes. Although it is possible to reduce this number by exploiting symmetry relations [Mar 95], it is clear that such a project will need a huge amount of computer time. On the contrary we are able to reproduce Marsili's results using our alternative method with good accuracy in less than one hour CPU-time on a workstation. In addition Marsili has to extrapolate his results from $T_{\max} = 20$ to $T_{\max} = \infty$. In our approach we effectively consider $T_{\max} = \infty$, since we allow arbitrary long relevant processes.

Of course, our method also has disadvantages. Since we generate a finite number N of processes, we observe statistical fluctuations in the resulting distribution $b^{(l)}(x)$, whereas Marsili's method gives in this sense an exact result (neglecting small errors due to the numerical integration routines). But we think of this as a relatively small drawback compared to the advantage of speeding up the method at least one order of magnitude. Moreover, our alternative method leads to the detection of an error in Marsili's Run-Time-Statistics equations.

[14] We also stop the process if $\phi_{i_\alpha(t)} \geq \rho$ for some $t > 0$.

7.3 Analysis of fixed point properties

In this paragraph we want to present our results obtained with the new 'Monte-Carlo'-approach to the renormalization group scheme for the Bak-Sneppen model. We show that the distribution $b^{(l)}(x)$ converges in the RG-iteration to a fixpoint distribution $b^\star(x)$. Consequently, $\rho_c^{(l)}$ converges to a fixpoint value $\rho_c^\star$. We will calculate the exponents τ and z (4.12, 4.23) from these fixpoint properties and the corresponding probability distribution $P^\star(T)$ for the length T of a relevant process.

Starting with uniform distribution $b^{(0)}(x) = \Theta(x)\Theta(1-x)$

We consider here a uniform distribution $b^{(0)}(x) = \Theta(x)\Theta(1-x)$ at the finest level $l = 0$. This is the BS-model in Marsili's L/R-version. We observe that the distribution $b^{(l)}(x)$ converges very fast. It reaches its fixpoint shape already after one renormalization step, see Figure 7.2(a). Correspondingly the value of $\rho_c^{(l)}$ converges also very fast to its fixed point value $\rho_c^\star$, see Figure 7.2(b). For the calculation of $b^{(l)}(x)$ we have evaluated 10^9 relevant processes at each renormalization step. For the determination of $\rho_c^{(l)}$ we evaluated 10^7 processes per iteration of the secant method and renormalization step. For the fixpoint $\rho_c^\star$ we obtain

$$\rho_c^\star = 0.5954 \ . \tag{7.6}$$

Marsili's results given in [Mar 94b] differ significantly which is probably due to the error in one of his RTS-iteration equations. His fixpoint distribution has roughly the same form as ours, but a higher value at low x, $b^\star(x=0) \approx 3.1$ and lower values at large x, $b^\star(x=1.0) \approx 0.6$. This also changes his value of $\rho_c^\star$ to $\rho_c^\star = 0.5391$.

The probability distribution $P^\star(T)$ for the length T of relevant processes, corresponding to the fixpoint properties $b^\star$ and $\rho_c^\star$, is shown in Figure 7.3. The minimal length of a relevant process (that updates four neighboring sites) is $T = 3$. At $T = 30$ the probability is of order 10^{-5}. The probability for a relevant process of length T decays as

$$P^\star(T) \sim e^{-\text{const}\times T} \ . \tag{7.7}$$

From the probability distribution $P^\star(T)$ we calculate the dynamical exponent z as has been explained in section 5.3. Applying formula (5.18) we obtain

$$z = 2.336(1) \tag{7.8}$$

For the calculation of exponent τ_ξ, describing the spatial scaling of avalanche sizes, the probability $K^\star$, that the site with minimal value is always the same until eventually the avalanche stops, has to be known. The value of $K^\star$ may be obtained in two independent ways: using the Run Time Statistics equations or again our new Monte-Carlo approach.

In the first approach we calculate and sum up the weights ν_β of all processes β, whose minimal site does not change in time and that eventually stop with $i_\beta(T_\beta) \geq \rho_c^\star$. In

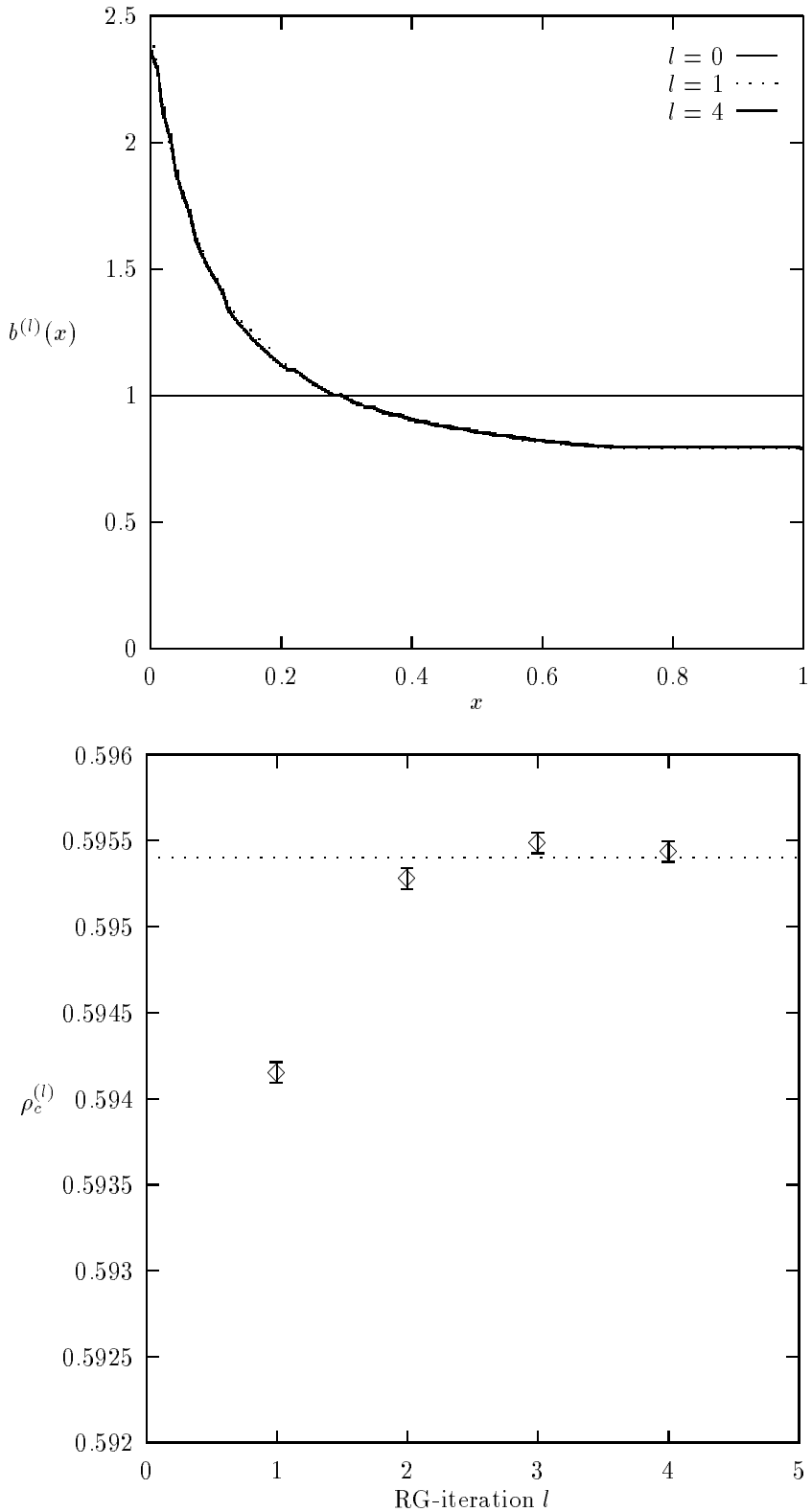

Figure 7.2: (a) Convergence of the distribution $b^{(l)}(x)$ to its fixpoint distribution $b^\star(x)$ is observed already after one renormalization step. For each RG-step 10^9 relevant processes have been generated. (b) Convergence of the critical $\rho_c^{(l)}$ to its fixpoint value (indicated by the dotted line) $\rho_c^\star = 0.5954$. For each iteration of the secant method and each renormalization step 10^7 processes have been evaluated.

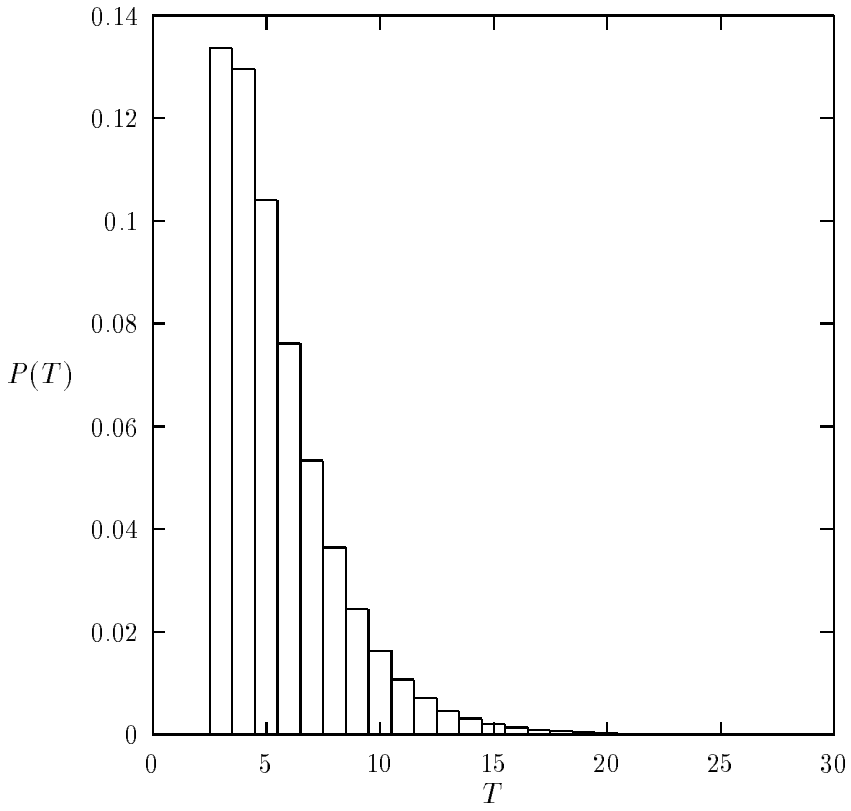

Figure 7.3: Probability distribution $P^\star(T)$ for the length T of relevant processes, corresponding to the fixpoint properties.

our notation introduced in section 5.1 all processes of length $T_\beta \leq 2$ are $\boldsymbol{i} = (2), \boldsymbol{i} = (-2), \boldsymbol{i} = (2,2), \boldsymbol{i} = (2,-2), \boldsymbol{i} = (-2,2), \boldsymbol{i} = (-2,-2)$. For $T_\beta = 3$ we have eight contributing processes, in general we have to evaluate $2^{T_{\max}+1} - 2$ processes for $T_\beta \leq T_{\max}$. The evaluation is done using the iterative Run-Time-Statistic equations (6.6, 6.2). Finally ν_β from (6.7) has to be multiplied by the probability that the process stops after T_β time steps, i.e.,

$$\nu_\beta = \frac{1}{2^{T_\beta}} \prod_{t=1}^{T_\beta} \mu_{i_\beta(t),t} \times \prod_{j \in \boldsymbol{i_\beta}} \int_{\rho_c^\star}^1 p_{j,T_\beta}(x) dx \quad . \tag{7.9}$$

In the second approach we have to count the fraction of processes with the minimum at the same site at each time step until they stop stop due to the condition $\phi_{i_\beta(T_\beta)} \geq \rho_c^\star$. We have to use the fixpoint rules $b^\star(x), \rho_c^\star$. Both methods give consistent results, we find

$$K^\star = 0.1827(1) \ , \tag{7.10}$$

from which follows via equation (5.14)

$$\tau_\xi = 1.2911(1) \ . \tag{7.11}$$

Using our result for the dynamical exponent z and relation (4.26), we obtain for τ

$$\tau = 1.1246(1) \ . \tag{7.12}$$

The values of exponents obtained via the renormalization group approach and via numerical simulation are compared in Table 7.1. Due to the probabilistic nature of our approach the fixpoint distributions fluctuates a little bit. The relative error in $\rho_c^\star$, z, $K^\star$, τ_ξ and τ induced by this fluctuation have been estimated to be very small at the order of 10^{-3}. Thus the table shows that Marsili's results obtained by numerical integration of the RTS-equations differ a little bit but significantly. This results probably from the error in one of the RTS-equations of Marsili, see our discussion in paragraph 6.1. More important is the poor coincidence between exponents obtained via simulations and RG-calculations respectively. It might be the case that the left-or-right (L/R) version of the BS-model is – though widely believed – not in the same universality class as the full isotropic BS-model. We do not know from any precision measurements of exponents for the (L/R)-version of the BS-model. Such measurements are needed and should be done.

	RG method		Simulation
	MC approach	RTS approach	isotropic BS
τ	1.1246(1)*	1.1204*	1.08(1)
τ_ξ	1.2911(1)	1.2766	
z	2.336(1)	2.2975	2.43(1)▲

Table 7.1: Comparison of results for critical exponents using the renormalization group approach and simulations respectively. The renormalization group approach applies to the L/R-version of the BS-model. The original BS model is denoted 'isotropic'. The results marked with $*$ are obtained from equation (4.26). The numerical result marked with ▲ is cited from [Pac 96].

Starting with parabolic distribution $b^{(0)}(x) = 3x^2\Theta(x)\Theta(1-x)$

Finally we would like to demonstrate an example of universality for the Bak-Sneppen model (again in its modified L/R - version). We will show that using a different distribution $b^{(0)}(x)$ does not change the universality class. Thus, simulations of a BS-model with a somewhat modified distribution $b^{(0)}(x)$ will discover the same universal exponents.

To this end we apply the renormalization group method to a BS-model with $b^{(0)}(x) = 3x^2\Theta(x)\Theta(1-x)$. After a few renormalization steps we observe that the distributions $b^{(l)}(x)$ converge to the it same fixpoint distribution $b^\star(x)$ as discovered previously. The same is valid for the value of $\rho_c^\star$. The result of this renormalization group iteration is shown in Figure 7.4.

We have presented a new approach for the realization of Marsili's RG-method, that improves and corrects his results obtained with the RTS-technique. We were able to show in this chapter that the distribution $b^{(l)}(x)$ converges rapidly to the attractive

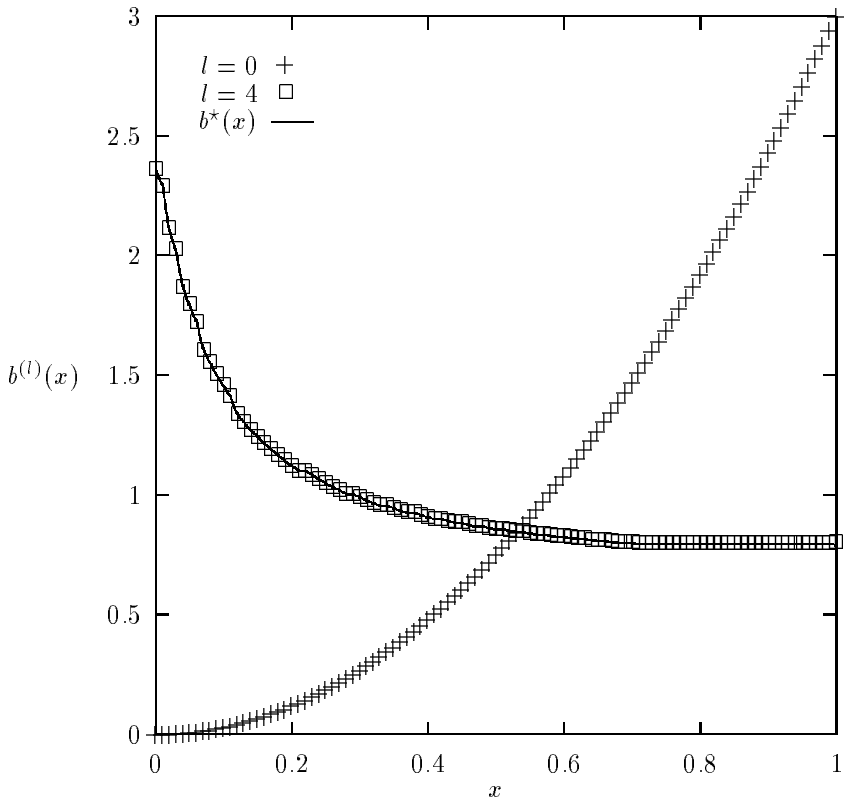

Figure 7.4: Convergence of the distribution $b^{(l)}(x)$ in the renormalization procedure to the fixpoint distribution, independent of its initial form. Here we started with $b^{(0)}(x) = 3x^2$. For each RG-step 10^9 relevant processes have been generated. For the determination of $\rho_c^{(l)}$ we evaluated 10^7 processes per iteration of the secant method and renormalization step.

fixpoint $b^\star(x)$. The attractive nature of the fixpoint can be considered as a manifestation of the fact, that the BS-model is *self*-organized critical. Universality has been shown for different initial distributions $b^{(0)}(x)$. They converge to the same fixpoint $b^\star(x)$. The results for the critical exponents coincide with the numerical results up to differences of about five percent. The reasons for this difference are yet unclear and need further investigations.

8 Interfaces in Disordered Media

The last section of this chapter is devoted to models with a physical background different from the previously discussed BS-model. We return to the second chapter of this thesis and want to give a more detailed overview on different SOC-models describing interfaces in disordered media, e.g. for the fluid flow in porous material. It turns out that these models are constructed in a very similar way as the BS model investigated previously. Their dynamics is based also on the search for an extremal value among all sites to determine the active site at each time step.

Therefore this class of models seem to be natural candidates for a similar RG-approach that was presented and applied to the BS model in the previous sections. In the

following paragraph 8.1 we introduce two related interface models, the "linear interface model" (LIM) [Rou 94] and the so called "Robin-Hood"-Model (RH) [Zai 92]. It has been suggested that both models are in the same universality class [Rou 94]. To decide this question the new renormalization group approach for extremal models might be a good tool and we discuss possibilities and difficulties to extend the RG-approach to these models in paragraph 8.2.

8.1 Linear Interface Model and "Robin Hood"-Model

Following the introduction to interface models given in section 2, it is straightforward to construct a discretized SOC-model for the motion of an interface in a disordered medium. The basis of the model is given by the BAKL-equation (2.6) together with the considerations of paragraph 2.3.

We define the linear interface model (LIM) in $1+1$ dimensions following [Pac 96]. Consider L height variables $\boldsymbol{h} = (h_i), i \in \{0, \ldots, L-1\}$, $h_i \in \mathbb{R}$ and impose periodic boundary conditions. In addition define the discretized Laplacian $d_i = (\Delta \boldsymbol{h})_i$. It is sufficient to consider only the variables d_i, the height function may then be obtained via integration. Furthermore choose L random pinning forces $\boldsymbol{\eta}^{(t=0)} = (\eta_i^{(t=0)})$ with probability $\mathcal{P}(\eta_i) = \Theta(\eta_i)\Theta(1-\eta_i)$ for each i. After these initializations are done the dynamical rule of the model is the following.

1. Time $t = 0$. Initialize $h_i = h$ with probability $\mathcal{P}(h), 0 \leq i < L$.
   Calculate the discretized Laplacian $\boldsymbol{d}^{(t)} = (d_i^{(t)})$

   $$d_i^{(t)} = (\Delta \boldsymbol{h})_i = -(2h_i - h_{i-1} - h_{i+1}) \quad .$$

2. Calculate the depinning forces at time t

   $$f_i^{(t)} = d_i^{(t)} - \eta_i^{(t)} \quad .$$

   Determine the index $i(t)$ with maximal depinning force $f_{i(t)}$

   $$f_{i(t)}^{(t)} \geq f_j^{(t)} \; \forall \;\; 0 \leq j < L \quad .$$

3. Change the value $d_{i(t)}^{(t)}$ of the active site $i(t)$ to

   $$d_{i(t)}^{(t+1)} = d_{i(t)}^{(t)} - 2.0 \quad .$$

   Replace the random pinning force $\eta_{i(t)}^{(t)}$ by the new value $\eta_{i(t)}^{(t+1)}$

   $$\eta_{i(t)}^{(t+1)} = \eta \text{ with probability } \mathcal{P}(\eta) \quad .$$

4. Change the values of the nearest neighbors $i(t) \pm 1$

   $$d_{i(t)\pm 1}^{(t+1)} = d_{i(t)\pm 1}^{(t)} + 1.0 \quad .$$

5. The values of all other variables remain unchanged in the next time step

$$d_j^{(t+1)} = d_j^{(t)} \ \ \forall j \neq i(t), i(t) \pm 1 \ \ ,$$
$$\eta_k^{(t+1)} = \eta_k^{(t)} \ \ \forall k \neq i(t) \ \ .$$

6. $t \rightarrow t+1$, Goto 2.

Step (3.) results from moving the height at the active site with maximal depinning force upward by one unit length. This changes also the Laplacian of the neighbor sites, which is done in step (4.). The random force η is chosen anew only for the active site, since η depends on the height h, see equation (2.6) and not on time t (quenched randomness). Note that we move only one site per time step, which corresponds to a infinitesimally slowly moving surface, $v \rightarrow 0^+$, as it was discussed in section 2.3.

A very similar model has been investigated by Roux and Hansen [Rou 94]. The underlying critical model obtained by changing the role of order- and control-parameter in the spirit of our discussion in section 2 has been studied by Leschhorn [Lesch 93].

In addition to the critical exponents describing backward- and forward-avalanches[15] we also analyze spatial correlations among successive active sites. The correlation function $C(x)$ gives the probability that

$$C(x) \equiv \text{Prob}(|i(t) - i(t+1)| \equiv x) \ \ . \tag{8.1}$$

The spatial correlation function obeys a power law

$$C(x) \sim x^{-\pi} \ \ . \tag{8.2}$$

Our measurements are in good agreement with the results reported in [Pac 96], see Table 8.1. More important for our discussion of a renormalization group approach to this model is the equilibrium distribution of the forces f_i in the LIM, $P_{eq}(f)$. Together with the distribution for the maximal forces at the active sites, this is shown in Figure 8.1(a). As in the BS-model, compare Figure 4.2, we observe a sharp cutoff at a value ρ_c now with nonzero probabilities *below* the this cutoff. This results from using a maximum rule instead of a minimum condition to determine the active site. In addition we note that the equilibrium distribution $P_{eq}(f)$ is not an uniform distribution as in the BS-model. The origin of the different functional dependency is the fact, that an updated value $\phi_i^{(t+1)}$ is no longer independent from its previous value $\phi_i^{(t)}$. Our discussion in the next paragraph will shed a little bit more light on this point.

A very similar model that is less complicated and deals with one variable only (instead of h_i and η_i in the LIM) is the so called 'Robin-Hood'(RH)-model introduced by Zaitsev [Zai 92]. The advancing interface described by the height variables h_i and the effects of the disorder represented by the random variables η_i are concentrated in the RH-model into a single variable. Consider ϕ_i to be the total depinning force acting at site i

$$\phi_i = -2h_i + h_{i+1} + h_{i-1} \ \ . \tag{8.3}$$

[15] Avalanches are defined exactly the same way as in the BS-model. Substitute f_i for ϕ_i and exchange $>$ to $<$ and *vice versa* since we are now looking for a maximal value.

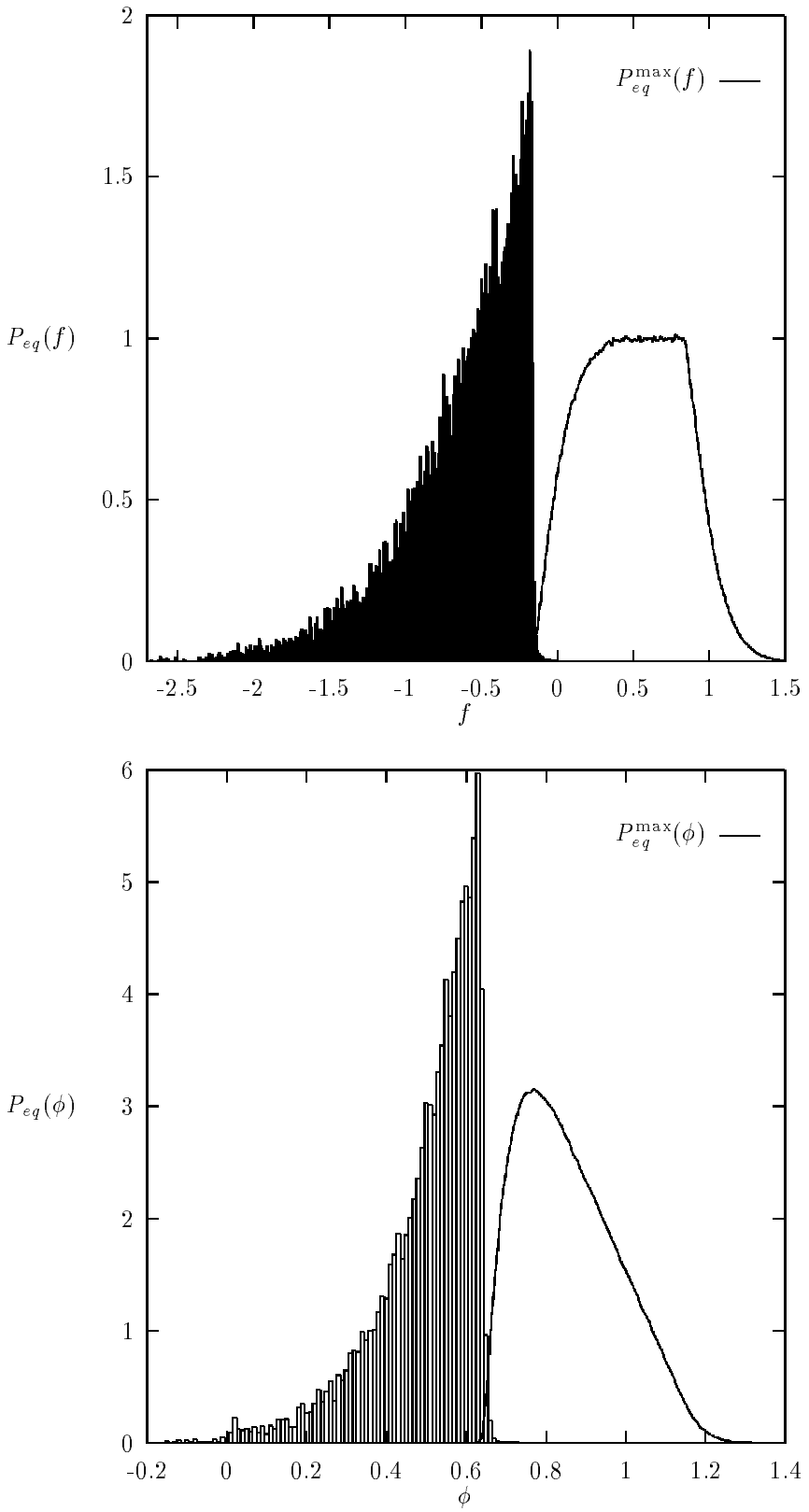

Figure 8.1: (a) The equilibrium distribution of all forces f_i in the linear interface model (LIM) $P_{eq}(f)$. The distribution $P_{eq}^{\max}(f)$ of the maximal forces $f_{i(t)}$ is also shown. (b) Same as Figure (a) but for the Robin Hood (RH)-model. The corresponding distributions are shown for the variables ϕ_i and $\phi_{i(t)}$ respectively. The data has been obtained using $L = 4096$ sites and a statistics of 3×10^6 time steps.

The site $i(t)$ with maximal depinning force at time t relaxes and moves upward to the next pinning center a distance $\tilde{r}$, $\tilde{r} \in [0, \frac{1}{2}]$, apart. Thus

$$\begin{aligned} \phi_i &\rightarrow \phi_i - 2\tilde{r} \\ \phi_{i\pm1} &\rightarrow \phi_{i\pm1} + \tilde{r} \end{aligned} \tag{8.4}$$

The disorder is induced in this model by irregular positions of pinning centers instead of regular positions of obstacles with random pinning strength in the LIM. The value of $2\tilde{r} \equiv r$ is chosen anew for each movement of the interface. Thus the model represents quenched random pinning[16]. The details of the Robin-Hood algorithm are as follows.

We define the RH-model in $1+1$ dimensions. Consider L pinning force variables $\boldsymbol{\phi} = (\phi_i), i \in \{0, \ldots, L-1\}$, $\phi_i \in I\!R$ and impose periodic boundary conditions.

1. Time $t = 0$. Initialize $\phi_i = \phi$ with probability $\mathcal{P}(\phi) = \Theta(\phi)\Theta(1-\phi)$, $0 \leq i < L$.

2. Determine the index $i(t)$ with maximal depinning force $\phi_{i(t)}$

$$\phi_{i(t)}^{(t)} \geq \phi_j^{(t)} \; \forall \;\; 0 \leq j < L \;\; .$$

3. Choose a random number r with probability $\mathcal{P}(r)$. Change the value $\phi_{i(t)}^{(t)}$ of the active site $i(t)$ to

$$\phi_{i(t)}^{(t+1)} = \phi_{i(t)}^{(t)} - r \;\; .$$

4. Change the values of the nearest neighbors $i(t) \pm 1$

$$\phi_{i(t)\pm1}^{(t+1)} = \phi_{i(t)\pm1}^{(t)} + \frac{r}{2} \;\; .$$

5. The values of all other variables remain unchanged in the next time step

$$\phi_j^{(t+1)} = \phi_j^{(t)} \;\; \forall j \neq i(t), i(t) \pm 1$$

6. $t \rightarrow t+1$, Goto 2.

As for the linear interface model it is again possible to measure a variety of exponents, describing the backward-, forward- and critical avalanches as well as the spatial correlations between successive active sites. From our numerics we found good agreement with the values given in [Pac 96, Zai 92], see Table 8.1. Moreover the exponents coincide for the LIM and the RH model, which suggests that both models belong to the same universality class. The equilibrium distribution of pinning forces ϕ and the distribution of maximal forces $\phi_{i(t)}$ is shown in Figure 8.1(b). The distributions show qualitatively the same behavior as the corresponding distributions for the LIM.

[16]The model can be given a completely different interpretation. Imagine Robin Hood, the generous robber, visits a market every day. He looks for the richest agent, takes some (random) amount of his goods and distributes them among the neighbors.

	LIM		RH-model	
	literature	this work	literature	this work
τ_b	1.87(3)*	1.85(1)		1.865(7)
π	2.93(1)*	2.935(28)	2.92▲	2.93(3)
τ_f		1.95(2)		2.01(1)

Table 8.1: Comparison of results for critical exponents The results marked with $*$ are cited from [Pac 96]. The result marked with ▲ is cited from [Zai 92].

8.2 Discussion of an RG-approach

In this paragraph we discuss some problems arising when applying the new RG-approach using Run-Time-Statistics. We try to elucidate the physical background of these problems for better understanding. For this discussion we restrict ourselves to the Robin-Hood model, for its definition see paragraph 8.1.

As for the BS-model it is again useful to modify the RH-model to a *left-or-right* version. This means that we change step 4. of the algorithm at the end of the previous paragraph to

4. Choose $k = i(t) + 1$ or $k = i(t) - 1$ with equal probability $p = 0.5$.

$$\phi_k^{(t+1)} = \phi_k^{(t)} + r \quad .$$

It is possible to establish RTS-equations for the RH-model in almost the same way as it was done for the BS-model in paragraph 6.1. We use an equivalent notation. Let us denote the probability distribution of ϕ_i at time t by $p_{i,t}(x)$.

The conditional probability that, if $\phi_i^{(t)}$ is the site with maximal depinning force, the avalanche does not stop (i.e. it is a relevant process and we have $\phi_i^{(t)} > \rho$) is given by

$$\mu_{i,t}(\rho) = \int_\rho^\infty p_{i,t}(x) \prod_{j \neq i} \int_{-\infty}^x p_{j,t}(y) dy dx \quad . \tag{8.5}$$

Once we know the active site i at time t with $\phi_i^{(t)} > \rho$, the probability distribution of this site becomes

$$m_{i,t}(x) = \frac{\Theta(x-\rho)}{\mu_{i,t}(\rho)} p_{i,t}(x) \prod_{j \neq i} \int_{-\infty}^x p_{j,t}(y) dy \quad . \tag{8.6}$$

The distribution of all non-maximal random variables $\phi_{j,t}$, $j \neq i$, is given by

$$\tilde{p}_{j,t}(x) = \mathcal{N} p_{j,t}(x) \int_\rho^\infty p_{i,t}(y) \Theta(y-x) \prod_{k \neq i,j} \int_{-\infty}^y p_{k,t}(z) dz dy \quad . \tag{8.7}$$

The updating step of the relaxation of the active site $i(t)$ to its left *or* right neighbor is described by

$$\begin{aligned} p_{i(t)}^{(t+1)}(x) &= \int_{-\infty}^{\infty} m_{i,t}(x+\epsilon)a(\epsilon)d\epsilon \\ p_{i(t)\pm 1}^{(t+1)}(x) &= \int_{-\infty}^{\infty} p_{i(t)\pm 1}^{(t)}(x-\epsilon)b(\epsilon)d\epsilon \\ p_{j,t+1}(x) &= \tilde{p}_{j,t}(x) \ . \end{aligned} \tag{8.8}$$

For the first RG-iteration we use $a(\epsilon) = b(\epsilon) = \Theta(\epsilon)\Theta(1-\epsilon)$. We expect that these distributions change under further application of the RG-transformation.

Everything is fine up to now. But when we try to iterate the RTS-equations to evaluate for all processes α their weights ν_α we run into big problems: We do not know the initial condition $p_{i,t=0}(x)$ at the beginning of each process α. The initial state of a variable is important – in contrast to the BS-model – because the updating depends on the old value of the variable. To perform a renormalization procedure as described in section 5.2 by blocking four neighboring cells onto two neighboring block-cells (see Figure 5.2), in principle we have to calculate the weight ν_α of process α for each possible start configuration $(\phi_1, \phi_2, \phi_3, \phi_4)$ of the four neighboring cells, $\nu_\alpha = \nu_\alpha(\phi_1, \phi_2, \phi_3, \phi_4)$. Or – in other words – the probability for the variables in the final state p_{i,t_α} is an average over all possible initial configurations of the cell variables $(\phi_1, \phi_2, \phi_3, \phi_4)$ weighted by the equilibrium probability $P_{eq}(\phi_1, \phi_2, \phi_3, \phi_4)$ for the state of four neighboring cells

$$\overline{p_{i,t_\alpha}(x)} = \iiiint p_{i,t_\alpha}(x|\phi_1, \phi_2, \phi_3, \phi_4) P_{eq}(\phi_1, \phi_2, \phi_3, \phi_4) \prod_{j=1}^{4} d\phi_j \ . \tag{8.9}$$

This averaged probability for the final state could then be used as before to perform the blocking procedure, see below. How is it possible to obtain $P_{eq}(\phi_1, \phi_2, \phi_3, \phi_4)$? The equilibrium distribution has to fulfill a self-consistency condition

$$P_{eq}(\phi_1, \phi_2, \phi_3, \phi_4) = \sum_\alpha \iiiint P_{eq}(x_1, x_2, x_3, x_4) \prod_{i=1}^{4} p_{i,t_\alpha}(\phi_i|x_1, x_2, x_3, x_4) dx_i \ . \tag{8.10}$$

The solution of this equation corresponds to the determination of ρ_c in the RG-analysis for the BS-model. Probably the computation of *all* possible processes, each for all possible initial configurations, will take a huge amount of computing time.

But even if we could solve this technical problem, we immediately would run into a more severe problem. The next step is to think about the blocking procedure. It is well known that the right choice of a blockspin definition is essential for a successful renormalization group application [Mac 92]. For our problem we may postulate two different blocking procedures, each with its own right from the physical background, which contradict each other.

It is essential to conserve the information of the location of the active site $i(t)$ on all scales[17] ,to obtain information on spatial correlations and thus for the correct com-

[17] We made the same argument already at the beginning of paragraph 5.2.

putation of critical exponents. This can only be done by using a maximum definition (blockfactor of 2)

$$\Phi_I^{(t)} = \max\{\phi_{2i}^{(t)}, \phi_{2i+1}^{(t)}\} \quad . \tag{8.11}$$

On the other hand, to conserve the interface fluctuations we should stick to the averaging block transformation

$$\Phi_I^{(t)} = \frac{1}{2}\left(\phi_{2i}^{(t)} + \phi_{2i+1}^{(t)}\right) \quad , \tag{8.12}$$

which is inspired from a geometrical viewpoint. It is obvious that both definitions contradict each other and we found no way to construct a commutative blocking scheme, with one of them, as has been postulated in 5.2, see Figure 5.1.

Besides the more technical problem of computing the equilibrium distribution from a self-consistent condition, the latter point contains the physical problem of an RG-application. Its solution has to be left for future research.

IV Self-organized criticality in economical systems

In the last chapter we want to switch to a different topic that might be more useful for real life applications than biological evolution or sandpiles. Since its introduction in 1987 by Per Bak *et al.* [Bak 87, Bak 88] it has been assumed that stock market behavior and economics are also a candidate for a SOC system. A recent analysis of real data from the stock market [Man 95, Sor 96] confirms this expectation. Nevertheless, up to now there has been no convincing theoretical model in this context. It would be desirable to build a minimal economic model that shows SOC behavior. A first step in that direction might be the model introduced by Yasutomi [Yas 95]. The purpose of this chapter is to discuss this model and some of its properties (section 9) and to analyze a possible self-organized critical behavior (section 10).

9 A simple model of money exchange

We introduce and discuss the model of money exchange (9.1) recently proposed by Yasutomi [Yas 95]. Some numerical results for the extension to an evolutionary model are given in paragraph 9.2.

9.1 Description of the model

The model [Yas 95] consists of N agents trading in N goods. Each agent wants one special good for his own use while he produces another one. Thus, to satisfy their needs, agents have to exchange their goods. Every good has the same unit value, so agents change goods one to one.

Using this setup the exchange rate will be very low, since it is very unlikely to find a pair of two agents with complementary needs and products (this method is known as *barter exchange*). To escape from this unsatisfying situation, agents accept also goods as an exchange medium if they are quite sure that other agents accept these goods also. For that purpose each agent i has an (of course subjective) view, that v_{ij} other agents accept good j. This view is updated every time two agents meet for a trade by accumulating new information from the actual trade and averaging the views of both agents. In addition agents possess a confidence threshold x. If the view v_{ij} that a certain number of other agents accept good j exceeds this threshold x, the agent i will accept good j even if he does not consume it. The idea is that he can exchange it again with another agent for a good then satisfying his needs.

Depending on the threshold x, after some time of low exchange rate, due to fluctuations in the needs of the agents, more and more agents accept one good j_M as a medium of exchange. Eventually the view of every agent on this good j_M exceeds the threshold x and all agents take advantage of the exchange medium: the exchange rate is high, via the exchange medium agents can satisfy their needs and consume a lot. This is

a stable state. The emergence of a good as exchange medium does not occur if the threshold x is to high. If threshold x is very low, almost every good is accepted and the number of consumed units is not as high as it could be. Sometimes a dual money systems emerges. For a detailed algorithm and simulation results see [Yas 95].

9.2 Evolutionary money exchange model

To adjust the threshold value dynamically Yasutomi introduces an individual threshold x_i for each agent i and an evolutionary criterium: The fitness of each agent is measured in terms of consumed units minus the total number of goods he keeps during a fixed time period. Thus agents accepting many goods, that they do not want to consume (due to a low threshold value), will have a low fitness value. Equally, agents accepting almost no good, that they do not want to consume (due to a high threshold), will have a low fitness value since they are bound to the ineffective barter exchange method. At the end of a time period, the fitness of all agents is evaluated and agents with the lowest fitness values choose new random thresholds.

The result of this evolutionary modification is, as before, the emergence of one good as an exchange medium after some time. But now, these happy monetary days do not last forever. It happens that suddenly, triggered by fluctuations, the acceptance of the exchange medium breaks down. Then consumption is again very low and it takes some time until another good emerges as exchange medium. It should be noticed that there is a parameter C in the fitness function, determining the ratio of positive and negative contributions via a carrying cost for all goods kept by an agent. The described results are only valid in a certain range of the carrying cost C. A typical behavior of this evolutionary approach is shown in Figure 9.1.

10 Self-organized criticality in the model of money exchange

To check the presumption that the model of money exchange might be a candidate for self-organized criticality (SOC), several possible avalanche definitions are proposed and investigated in 10.1. The dynamics of the model is compared with the critical behavior of a q-state Potts model (10.2). These analogies might help to construct an self-organized critical economic model. Some very preliminary steps are undertaken in this direction in the last paragraph 10.3

10.1 Avalanche analysis

In his work Yasutomi conjectures that the mechanism of the collapse of money might be related to self-organized criticality. Indeed, the collapse of money involves a typical avalanche process: Consider a situation, where all agents accept a certain good j_M as a

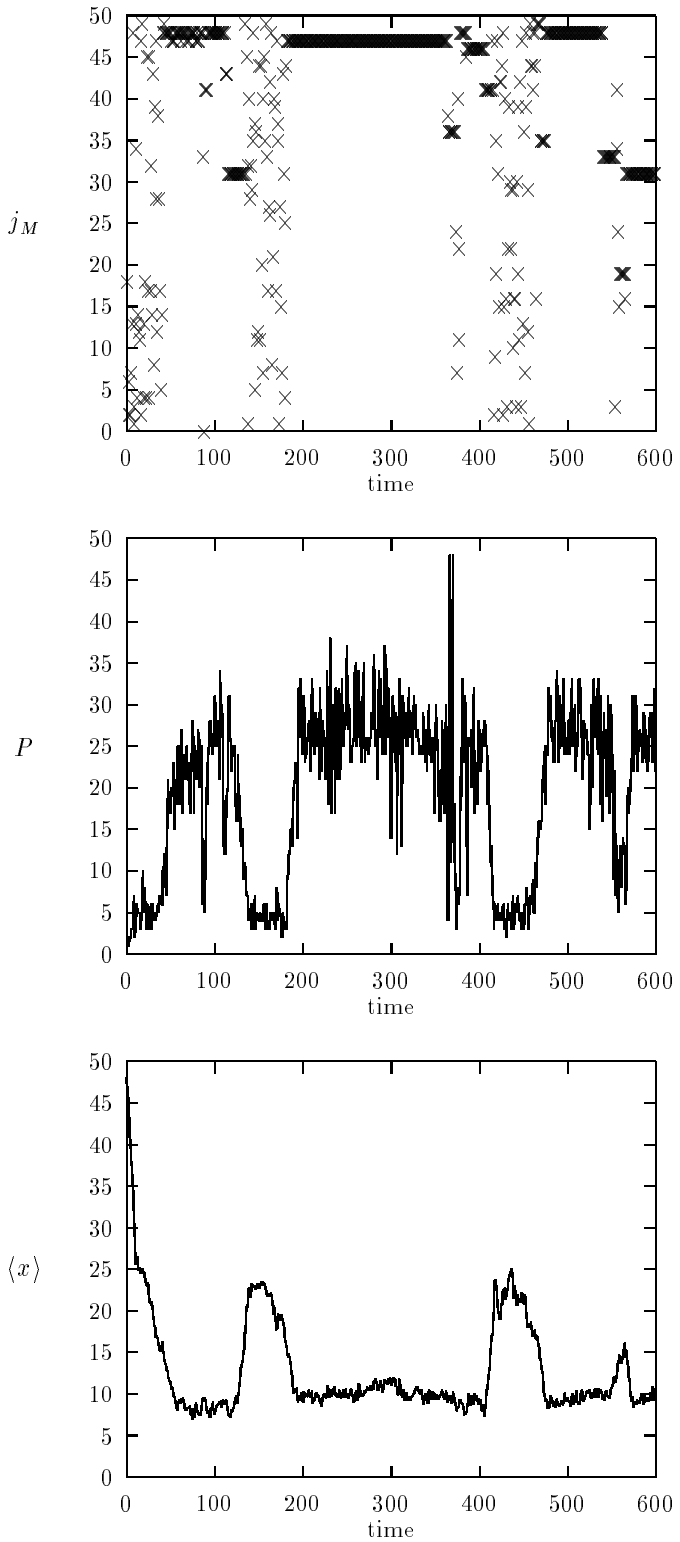

Figure 9.1: A typical run of the exchange model using $N = 50$ agents. One time unit consists of 1000 individual trades among two agents. The carrying cost is $C = \frac{1}{2000}$. The popularity P is defined as $P = \frac{1}{N}\sum_i v_{ij_M}$, the index j_M of the exchange medium is determined as $j_M = \max_j \sum_i v_{ij}$, the average threshold $\langle x \rangle$ is given by $\langle x \rangle = \frac{1}{N}\sum_i x_i$.

medium of exchange. An avalanche is triggered by an agent, whose threshold value x_i becomes higher than his view v_{ij_M} during the evolutionary process. If this agent meets in his next trades other agents and now refuses good j_M as exchange medium, this lowers the view of these agents on good j_M, maybe dropping it below their threshold and leading to a larger fraction of agents refusing good j_M. This process may spread avalanche-like through the marketplace. At the same time an avalanche is spreading, some agents already come back to accept good j_M again as exchange medium. This seems to be a convincing avalanche definition, but there is a serious problem: Time scale separation, that has been recognized as essential[18] for SOC systems [Gri 95], is not fulfilled. Due to fixed time periods for the fitness evaluation (which triggers avalanches) it happens frequently, that the next avalanche is already starting although the previous one has not come to rest. It is not possible to decouple avalanches since the end of an avalanche is not clearly defined: the number of agents accepting good j_M naturally varies due to fluctuations in the needs of agents even without critical initiator[19]. There is no stable stationary state.

Nevertheless we made some analysis for different observables of the model searching for power laws. First let us look at the probability distribution for the length of stable monetary periods. During a stable period, the exchange medium is always the same good j_M [20]. This is shown in the upper graph of Figure 10.1. The data is consistent with a power law but higher precision data is needed.

The lower graph of Figure 10.1 shows the first and all return probabilities of the popularity $P(t)$ for a specified Δt: $P_{first}(\Delta t)$ is is the probability for $P(t_0) = P(t_0 + \Delta t)$ using the condition $P(t) \neq P(t_0) \quad \forall t_0 < t < t_0 + \Delta t$, $P_{all}(\Delta t)$ is the probability for $P(t_0) = P(t_0 + \Delta t)$ without restriction to the intermediate values[21]. We observe fluctuations on all length scales in the index of the popularity $P(t)$ scaling as $P_{first}(\Delta t) \sim \Delta t^{-\tau_{first}}$. For large Δt we find $\tau_{first} \approx 1.8$. A similar analysis has been done recently by Mantegna *et al.* [Man 95]. They analyze the index S&P500 from the New York stock market and also find a power law for the probability of returns, but the different exponent $\tau_{first} = 0.72$. Sornette *et al.* [Sor 96] report also evidence for cooperative behavior and scale invariance found in a study of the same index S&P500 before and after the October 1987 market crash.

From both figures we conclude that there is some evidence for SOC, though it is not very conclusive. More statistical data would make the situation clearer. In view of the above mentioned difficulty to define a non-overlapping clear avalanche process it seems more promising to try to simplify Yasutomi's model and keep only the essential ingredients for a SOC system.

Furthermore, it should not be forgotten that there is still a parameter in Yasutomi's

[18] Basically this is the same condition as the need for a infinitesimal driving rate.

[19] But these fluctuations cannot spread over the whole system.

[20] To exclude unstable short periods of only one or two days we demand, that the popularity P of good j_M exceeds $0.3 \times N$ at least once during a stable period.

[21] The time unit is now on the scale of individual transactions ($\frac{1}{1000}$ of the time in Figure 9.1).

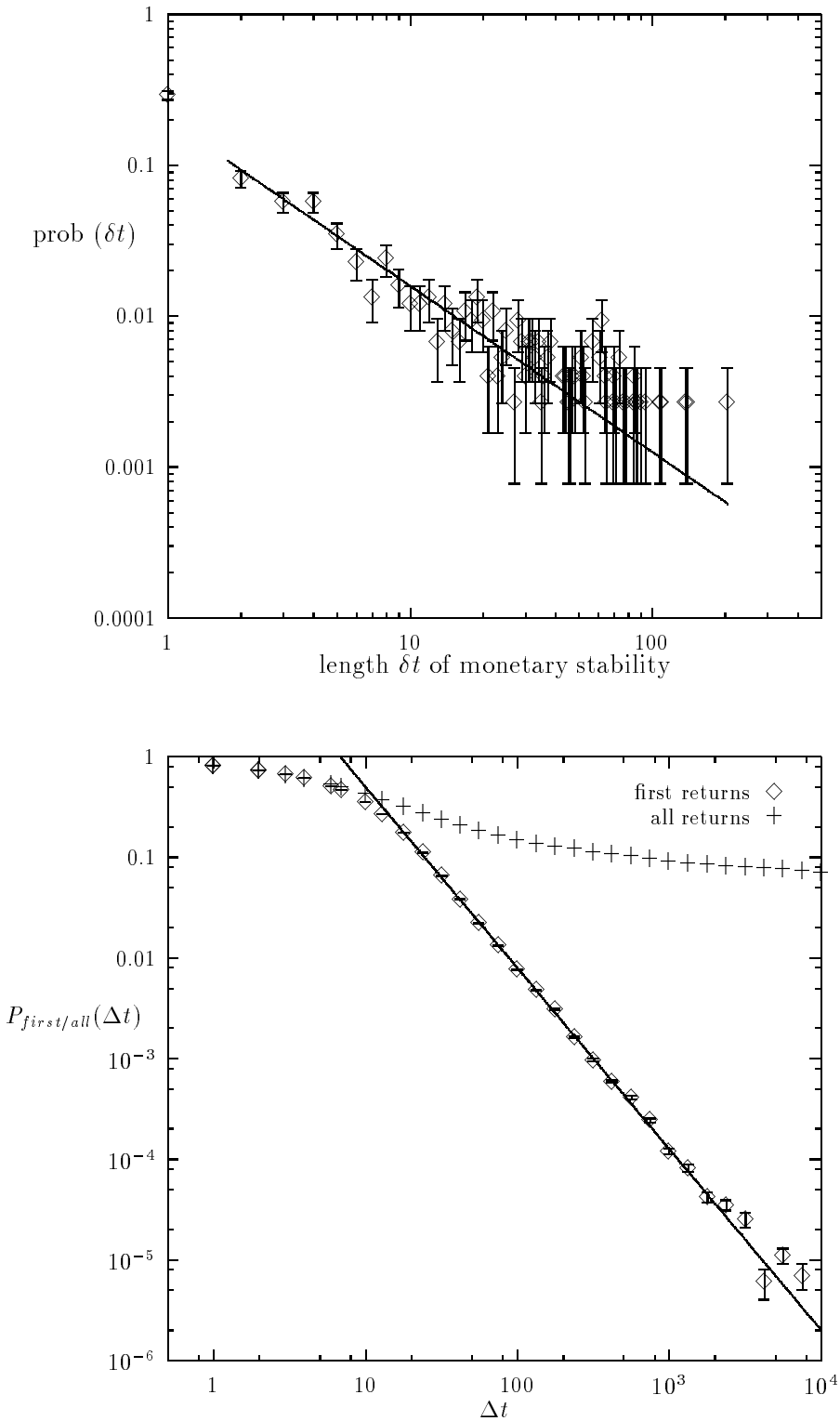

Figure 10.1: (a) The probability distribution prob(δt) for the length δt of stable monetary periods. To suppress short unstable periods of length one or two, we require a minimal popularity of $0.3 \times N = 15$ at least once during the period. (b) First and all return probability $P_0(\Delta t)$ of the Popularity $P(t)$ as a function of the time interval Δt. The line corresponds to an exponent $\tau_{\text{first}} = -1.8$.

model that has to be adjusted: the carrying cost C. Although the behavior of the model is the same for a certain range of C values, this contradicts the general understanding of SOC phenomena that do not need any parameter to be tuned.

10.2 Analogies and differences with spin models

In the previous paragraph it has been investigated if Yasutomi's model is self-organized critical. Even if it was be SOC, it seems not promising to acquire enough statistical data for a reliable analysis based on simulations or to analyze it using the renormalization scheme presented in chapter III or the method for the CA-type models of [Ves 95, Lor 95, Ves 96]. To gain a deeper understanding of SOC in economic systems it might be useful to modify the model to improve and simplify it. In the last two paragraphs we discuss several possibilities and ideas in this direction.

Yasutomi's model contains some key features that are reminiscent of spin models in statistical physics. To begin with, let us consider a system of agents trading with q goods and with fixed threshold $x_i = x$. We define the state S_i of agent i as the index of the good, for which the agent has most confidence, i.e. $S_i = \max_j v_{ij}$. The existence of some agents already accepting the same good j, forces other agents to accept it also (via exchanging information at each trade). The threshold x determines, how large an initial fluctuation of agents demanding the same good should be, to increase the view of other agents above their threshold. If the threshold is below a certain 'critical' value x_c, fluctuations will spontaneously trigger emergence of money. For $x > x_c$ a medium of exchange is not stable. This behavior strongly reminds of the critical behavior of q-state spin models: while for $T > T_c$ spins are uncorrelated, they exhibit a spontaneous magnetization for $T < T_c$.

It should be noted that there are several obvious differences contradicting this maybe oversimplifying picture. First, spin models include a local nearest neighbor interaction defined on a lattice. In Yasutomi's model agents may interact with all other agents. Secondly, if $0 \leq x < x_c$ and x is very small, agents behave again nearly independently since every agent accepts every good. In contrast, spins behave strongly correlated at low temperatures. The first point might be not as serious as the second one. In fact, it would be worthwhile to investigate a lattice version of Yasutomi's model (agents live on a d-dimensional lattice and interact (trade) only with their nearest neighbors).

Nevertheless, it is interesting to see what is happening in the spin model picture if we switch to the evolutionary model using dynamical thresholds. Now the former control-parameter x of the system adjusts itself via a feedback mechanism. Too high values x_i are replaced by lower ones and vice versa. After some equilibration time, the value of $\langle x \rangle$ adjusts at $\langle x \rangle \approx 10$. If it increases too much, the current exchange medium breaks down and the systems undergoes a phase transition. Then $\langle x \rangle$ again decreases and finally the systems switches back to the former phase with a widely accepted exchange medium[22]

[22]The interpretation of emergence/collapse of money as a phase transition is implicitly indicated in

In the corresponding q-state spin model picture, we have accordingly a temperature that adjusts itself via a feedback mechanism to its critical value. This is by definition a self-organized critical system, if the feedback mechanism does not need a new tuning parameter (like the carrying cost in Yasutomi's model). Such a mapping of a critical system onto a self-organized critical systems has been proposed by Sornette *et al.* [Sor 92, Sor 95] and was discussed in section 2 of this work.

To do a small step towards construction of an economical model which undoubtfully exhibits SOC it might be helpful to follow the discussed analogies with spin models. A very simple application is presented in the next paragraph.

10.3 A simple economical model at criticality

We consider N agents living on a $1d$-lattice. Two different currencies A and B are used by the agents when trading with their nearest neighbors. At each time t agent i accepts exactly one currency, either A or B. We denote this state with $S_i(t)$. The state of agent i at time $t+1$ depends on the state of his nearest neighbors at time t. The model is equivalent to a probabilistic cellular automaton with the following rule table.

$S_{i-1}(t)$	$S_{i+1}(t)$	prob	$S_i(t+1)$
A	A	$1-\mu_i$	A
A	A	μ_i	B
B	B	$1-\mu_i$	B
B	B	μ_i	A
A	B	0.5	A
A	B	0.5	B
B	A	0.5	A
B	A	0.5	B

Table 10.1: Rule table for the one dimensional cellular automaton describing the acceptance of money in a very simple trading model. The individual risk factor $0 \leq \mu_i \leq 1.0$ is measure for the risky behavior of agent i. $\mu_i = 0.0$ means no risk, $\mu_i = 1.0$ maximum risk.

Roughly speaking, agents tend to *accept what others accept*, at least for a sufficiently small individual risk parameter μ_i. Agents with higher risk factor try to benefit sometimes from switching to exactly the opposite state. They do not accept money for themselves (and thus don't have the risk of getting nothing to consume for it) but still get consumable goods from their neighbors, since usually the neighbors still accept the current medium of exchange. The case $\mu_i = \mu = 0$ for all i corresponds to a ferromagnetic Ising model at temperature $T = 0$. For $\mu = \mu_i = 0.5$ for all i we have an infinite temperature Ising model, while in the range $\frac{1}{2} \leq \mu = \mu_i \leq 1.0$ the model corresponds to an antiferromagnetic Ising system.

The model is critical in the limit $\mu \to 0$, since it *is* the $1d$-Ising model. It is possible

Fig. 12 of Yasutomi's work as a switching between a double-well and a single-well potential.

to find power laws: consider the number of agents accepting the same currency, $A(t)$, and calculate first and all return probability $P_{\text{first/all}}(\Delta t)$ for $A(t)$. Using $\mu = 10^{-6}$ we have $P_{\text{first}}(\Delta t) \sim \Delta t^{-\tau_{\text{first}}}$, $\tau_{\text{first}} \approx 1.7$ and the same for $P_{\text{all}}(\Delta t)$ with $\tau_{\text{all}} \approx 0.5$. (See Figure 10.2(a)). Increasing μ we observe approximately the same behavior with small deviations from the power law in $P_{all}(\Delta t)$ at large Δt and in $P_{first}(\Delta t)$ at small Δt. The parameter μ could be denoted as 'driving rate', common to all SOC systems. To observe SOC behavior, the driving rate has to be infinitely small.

We find a similar characteristics in the forest-fire model [Dro 94]. The authors claim it to be SOC in the limit of infinitely small lightning probability f. In the light of this discussion it seems more convincing that the forest-fire model is a model with an ordinary critical point: the parameter f has to be tuned to its critical value $f = 0$, otherwise the model is only near criticality. This is supported by the recent RG-approach to the forest-fire model [Lor 95], that identifies the parameter f as a *relevant* parameter in the renormalization group sense.

The art of SOC is either to incorporate this infinitely small driving rate into the system or to invent a mechanism that drives the relevant parameter to its critical value. Following the second possibility we made the following modifications in our simple trading model.

After each time step, agents compare their state with the state of their nearest neighbors. If $S_i(t) = S_{i-1}(t) = S_{i+1}(t)$ agent i increases his risk $\mu_i = \mu_i * 2$, else the risk is lowered $\mu_i = \mu_i * 0.5$. Starting with $\mu_i = 0.25$ for all agents i the average risk factor $\langle \mu \rangle$ converges to its critical value $\langle \mu \rangle \equiv 0.0$. Thus the system may be considered as SOC.

However, this conclusion should be handled with caution, since the one dimensional model is a special case compared to dimensions $d \geq 2$. In $d = 1$ the critical point is equivalent to a macroscopic magnetization. The observed exponents correspond to the (exactly computable) exponents for the equivalent return probabilities in a $1d$-random walk (RW). The results for a $1d$-RW are shown in Figure 10.2(b) for comparison. Thus further studies for higher dimensions of this model are needed.

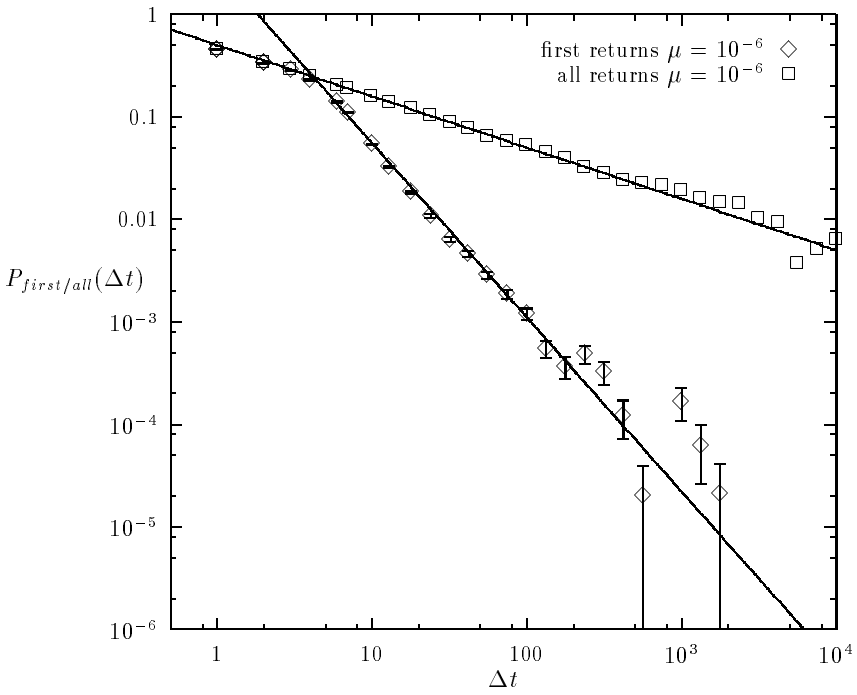

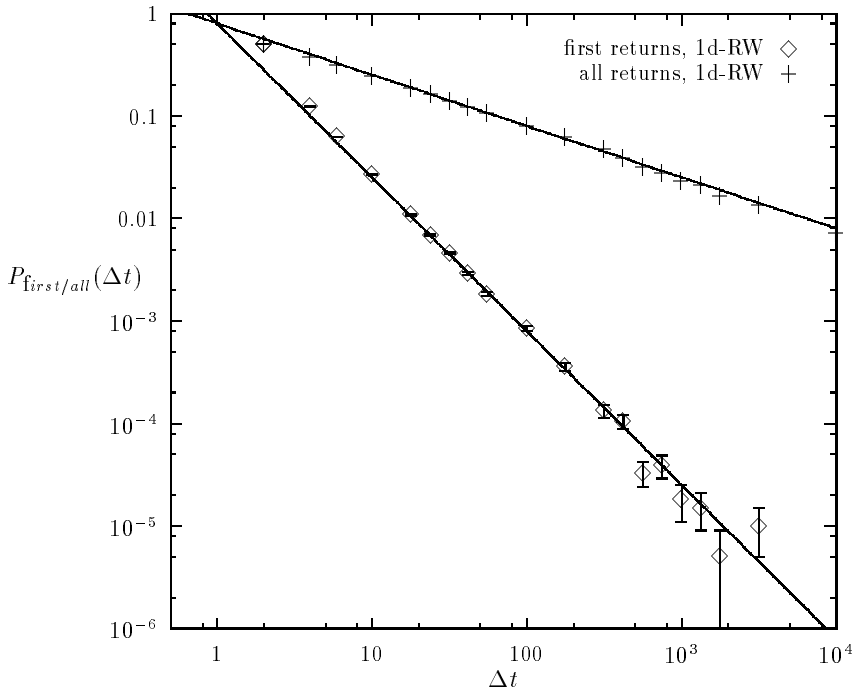

Figure 10.2: (a) First and all return probabilities $P(\Delta t)$ for acceptance of currency A, $A(t)$ as a function of the time interval Δt and risk factor $\mu = \mu_i = 10^{-6}$. Lines correspond to $\tau_{first} = -1.8$, $\tau_{all} = -0.5$. (b) First and all return probabilities $P(\Delta t)$ for a one dimensional random walk. Lines correspond to $\tau_{first} = -1.5$, $\tau_{all} = -0.5$.

Conclusions and Outlook

This thesis was aimed at the development and study of a new renormalization group tool for a specific class of complex systems, which show self-organized critical behavior. Among the variety of SOC-systems we concentrated on the class of extremal models, whose dynamics is based on the global search of an extremal value among all sites of the system.

As a principal property for an RG-method to be applied to SOC we postulated that the diagram picturing the blocking process in space *and* time (see Figure 5.1) has to be commutative: the result of time evolution at the fine level and performing the blocking procedure afterwards should be the same when first performing the blocking procedure and then allowing for time evolution at the coarse level. In other words: macroscopic objects and macroscopic dynamics may only be formulated in a self-consistent way.

Based on this principle we invented a new method to realize the renormalization group approach proposed by Marsili [Mar 94b]. Applied to the Bak-Sneppen model of biological evolution, this new technique improves and corrects Marsili's results. Our calculated fixpoint properties do not coincide with his calculations due to an error in one of his RTS-equations. The new method speeds up the RG-iteration at least one order of magnitude.

The RG-method demonstrates the attractive nature of the critical state for the BS-model. It validates the concept of universality at least in a certain range considering different probability distributions $\mathcal{P}$ for the original BS-model. It is possible to calculate the critical exponents τ and z describing temporal and spatial avalanche scaling. The results show coincidence with the numerical results up to 4%. The reason for the difference to the simulation results is unclear and needs further investigation.

High precision numerical simulations have also been performed for the isotropic BS-model. The results are in good coincidence with other recent publications.

We discussed the application of a similar scheme of multiscale analysis to the related problem of interfaces in disordered media. We provide a principal setup, that should work in the same way as for the BS-model. However, we isolated two problems: a more technical one, the solution of the self-consistency condition for the equilibrium distribution as well as a physical problem, violating the above postulation for a commutative blocking diagram. To overcome this more serious problem new ideas and inspirations are needed.

In a last chapter we have investigated an interesting economical model describing the process of money exchange. It contains at least some ingredients that are typical for SOC models. However, following our numerical results it is unlikely that the model exhibits self-organized criticality. We noticed similarities of the model with a q-state Potts model. Using this observation as a guideline we designed a very simple one-dimensional economical toy model. This model shows critical behavior by construction but might be too trivial. Further studies of a similar approach in higher dimensions are now necessary.

Bibliography

[Bak 87] P. Bak, C. Tang, K. Wiesenfeld, *Self-Organized Criticality: An Explanation of* $1/f$ *Noise*, Phys. Rev. Lett. **59**, 381 (1987)

[Bak 88] P. Bak, C. Tang, K. Wiesenfeld, *Self-Organized Criticality*, Phys. Rev. A **38**, 364 (1988)

[Bak 89] P. Bak, K. Chen, M. Creutz *Self-organized criticality in the 'Game of Life'*, Nature **342**, 780, (1989)

[Bak 90] P. Bak, *Self-organized criticality*, Physica A **163**, 403 (1990)

[Bak 92] P. Bak, H. Flyvbjerg, B. Lautrup, *Coevolution in a rugged fitness landscape*, Phys. Rev. A **46**, 6724 (1992)

[Bak 93] P. Bak, K. Sneppen, *Punctuated Equilibrium and Criticality in a simple Model of Evolution*, Phys. Rev. Lett. **71**, 4083 (1993)

[Ben 95] M. J. Benton, *Diversification and Extinction in the History of Life*, Science, **268**, 52

[Bin 88] K. Binder, D. W. Heermann, *Monte Carlo Simulation in Statistical Physics*, Springer-Verlag, Berlin 1988

[Boo 95] J. P. Boon, O. Decroly, *Dynamical systems theory for music dynamics*, Chaos **5**, 501 (1995)

[Bru 84] R. Bruinsma, G. Aeppli, *Interface Motion and Nonequilibrium Properties of the Random-Field Ising Model*, Phys. Rev. Lett. **52**, 1547 (1984)

[Bul 92] S. V. Buldyrev, A. -L. Barabási, F. Caserta, S. Havlin, H. E. Stanley, T. Vicsek, *Anomalous interface roughening in porous media: Experiment and model*, Phys. Rev. A **45**, R8313 (1992)

[Che 89] K. Chen, P. Bak, *Is the universe operating at a self-organized critical state ?*, Phys. Lett. A **140**, 299 (1989)

[Der 81] B. Derrida, *Random energy model: An exactly solvable model of disordered systems*, Phys. Rev. B **24**, 2613 (1981)

[Dro 94] B. Drossel, F. Schwabl, *Formation of space-time structure in a forest-fire model*, Physica A **204**, 212 (1994)

[Dut 81] P. Dutta, P. M. Horn, *Low-frequency fluctuations in solids:* $1/f$ *noise*, Rev. Mod. Phys. **53**, 497 (1981)

[Eig 77] M. Eigen, P. Schuster, *The Hypercycle*, Naturwissenschaften **64**, 541 (1977)

[Eps 89] H. Epstein, D. Ruelle, *Test of a probabilistic model of evolutionary success*, Phys. Rep. **184**, 289 (1989)

[Fis 85] D. S. Fisher, *Sliding charge-density waves as a dynamic critical phenomenon*, Phys. Rev. B **31**, 1396 (1985)

[Fly 92] H. Flyvbjerg, B. Lautrup, *Evolution in a rugged fitness landscape*, Phys. Rev. A **46**, 6714 (1992)

[Gal 95] S. Galluccio, Y.C. Zhang, *Driven interfaces in quenched disorder at critical depinning*, Phys. Rev. E **51**, 1686 (1995)

[Gou 93] S. J. Gould, N. Eldredge, *Punctuated equilibrium comes of age*, Nature **366**, 223 (1993)

[Gra 95] P. Grassberger, *The Bak-Sneppen model for punctuated evolution*, Phys. Lett. A **200**, 277 (1995)

[Gri 95] G. Grinstein, C. Jayaprakash, *Simple models of self-organized criticality*, Computers in Physics **9**, 164 (1995)

[Har 87] I. McHardy, B. Czerny, *Fractal X-Ray time variability and spectral invariance of the Seyfert galaxy NGC5506*, Nature **325**, 696 (1987)

[Hel 90] G. A. Held, D. H. Solina, D. T. Keane, W. J. Haag, P. M. Horn, G. Grinstein, *Experimental Study of Critical-Mass Fluctuations in an Evolving Sandpile*, Phys. Rev. Lett. **65**, 1120 (1990)

[Itz 89] C. Itzykson, J.M. Drouffe, *Statistical field theory*, Cambridge University Press, 1989

[Jen 89] H. J. Jensen, K. Christensen, H. C. Fogedby, $1/f$ *noise, distribution of lifetimes, and a pile of sand*, Phys. Rev. B **40**, 7425 (1989)

[Ji 92] H. Ji, M. O. Robbins, *Percolative, self-affine and fractal domain growth in random three-dimensional magnets*, Phys. Rev. B **46**, 14519 (1992)

[Jov 94] B. Jovanovic, S. V. Buldyrev, S. Havlin, H. E. Stanley, *Punctuated equilibrium and "history-dependent" percolation*, Phys. Rev. E **50**, 2403 (1994)

[Kau 87] S. A. Kauffman, S. Levin, *Towards a General Theory of Adaptive Walks on Rugged Landscapes*, J. Theor. Biol. **128**, 11 (1987)

[Kau 91] S. A. Kauffman, S. Johnsen, *Coevolution to the Edge of Chaos: Coupled Fitness Landscapes, Poised States and Coevolutionary Avalanches*, J. Theor. Biol. **149**, 467 (1991)

[Kau 93] S. A. Kauffman, *The Origins of Order*, Oxford University Press, Oxford 1993

[Kop 85] J. Koplik, H. Levine, *Interface moving through a random background*, Phys. Rev. B **32**, 280 (1985)

[Lesch 93] H. Leschhorn, *Interface depinning in a disordered medium – numerical results*, Physica A **195**, 324 (1993)

[Leu 85] I. Leuthäusser, *An exact correspondence between Eigen's evolution model and a two-dimensional Ising system*, J. Chem. Phys. **84**, 1884 (1985)

[Leu 87] I. Leuthäusser, *Statistical Mechanics of Eigen's Evolution model*, J. Stat. Phys. **48**, 343 (1987)

[Lor 95] V. Loreto, L. Pietronero, A. Vespignani, *Renormalization group approach to the critical behavior of the forest fire model*, Phys. Rev. Lett. **75**, 465 (1995)

[Mac 87] G. Mack, *Multigrid Methods in Quantum Field Theory*, in: Cargése Lectures, eds: G 't Hooft et al., Plenum, New York 1987

[Mac 92] G. Mack, T. Kalkreuther, G. Palma, M. Speh, *Effective Field Theories*, in: Lecture Notes in Physics **409**, 205 (Schladming 1992)

[Mac 94] G. Mack, *Gauge theory of things alive and universal dynamics*, preprint hep-lat/9411059

[Man 83] B. B. Mandelbrot, *The Fractal Geometry of Nature*, Freeman, San Francisco, 1983

[Man 95] R. N. Mantegna, H. E. Stanley, *Scaling behavior in the dynamics of an economic index*, Nature **376**, 46 (1995)

[Mar 94a] M. Marsili, *Run Time Statistics in Models of Growth in Disordered Media*, J. of Stat. Phys. **77**, 733 (1994)

[Mar 94b] M. Marsili, *Renormalization group approach to the Self Organization of a Simple Model of Biological Evolution*, Europhys. Lett. **28**, 385 (1994)

[Mar 95] M. Marsili, private communication

[Mas 95] S. Maslov, *Time Directed Avalanches in Invasion Models*, Phys. Rev. Lett. **74**, 562 (1995)

[Mik 96] B. Mikeska, *A Monte-Carlo Renormalization group approach to the Bak-Sneppen model*, in preparation

[Nar 93] O. Narayan, D. S. Fisher, *Threshold critical dynamics of driven interfaces in random media*, Phys. Rev. B **48**, 7030 (1993)

[Ola 92] Z. Olami, H. J. S. Feder, K. Christensen, *Self-Organized Criticality in a Continuous, Nonconservative Cellular Automaton Modeling Earthquakes*, Phys. Rev. Lett. **68**, 1244 (1992)

[Par 94] G. Parisi, *Complexity in Biology: The Point of View of a Physicist* Talk, Rome, September 1994, preprint cond-mat/9412018

[Pac 94] M. Paczuski, S. Maslov, P. Bak, *Field Theory for Model of Self-Organized Criticality*, Europhys. Lett. **27**, 97 (1994)

[Pac 96] M. Paczuski, S. Maslov, P. Bak, *Avalanche Dynamics in Evolution, Growth, and Depinning Models*, Phys. Rev. E **53**, 414 (1996)

[Pel 95] L. Peliti, *Fitness Landscapes and Evolution*, Lectures given at the NATO ASI on Physics of Biomaterials: Fluctuations, Self-Assembly and Evolution, Geilo (Norway), March 27 - April 6, preprint cond-mat/9505003 (1995)

[Pie 92] L. Pietronero, *Fractals in Physics: applications and theoretical developments*, Physica A **191**, 85 (1992) (talk given at the conference on *Fractals and Disordered Systems*, Universität Hamburg, July 1992)

[Pie 94] L. Pietronero, A. Vespignani, S. Zapperi, *Renormalization Scheme for Self-Organized Criticality in Sandpile Models* Phys. Rev. Lett. **72**, 1690 (1994)

[Pre 89] W. H. Press, B. P. Flamery, S. A. Teulkowsky, W. T. Vetterling, *Numerical Recipes*, Cambridge University Press, Cambridge 1989

[Rau 86] D. M. Raup, *Biological Extinction in Earth History*, Science **231**, 1528 (1986)

[Schmo 95a] K. Schmoltzi, *Adaptionsvorgänge in Evolution und Neuronalen Netzen*, Dissertation Universität Kiel 1995
K. Schmoltzi, H. G. Schuster, *Introducing a Real Time Scale into the Bak-Sneppen Model*, Phys. Rev. E, **52**, 5273 (1995)

[Schmo 95b] K. Schmoltzi, private communication

[Sor 92] D. Sornette, *Critical phase transitions made self-organized: a dynamical system feedback mechanism for self-organized criticality*, J. Phys. I France **2**, 2065 (1992)

[Sor 95] D. Sornette, A. Johansen, I. Dornic, *Mapping Self-Organized Criticality onto Criticality*, J. Phys. I France **5**, 325 (1995)

[Sor 96] D. Sornette, A. Johansen, J.P. Bouchaud, *Stock Market Crashes, Precursors and Replicas*, J. Phys. I France **6**, 167 (1996)

[Rou 94] S. Roux, A. Hansen, *Interface roughening and pinning*, J. Phys. I France **4**, 515 (1994)

[Ves 95] A. Vespignani, S. Zapperi, L. Pietronero, *Renormalization approach to the self-organized critical behavior of sandpile models*, Phys.Rev.E **51**, 1711 (1995)

[Ves 96] A. Vespignani, S. Zapperi, V. Loreto, *Dynamically Driven Renormalization Group*, cond-mat/9603052 (1996)

[Vic 90] T. Vicsek, M. Cserzo, V. K. Horváth, *Self-affine growth of bacterial colonies*, Physica A **167**, 315 (1990)

[Vos 75] R. F. Voss, J. Clarke, $1/f$*-noise in music and speech*, Nature **258**, 317 (1975)

[Wil 71] K. Wilson, *Renormalization Group and Strong Interactions*, Phys. Rev. D **3**, 1818 (1971)

[Wol 84] S. Wolfram, *Cellular automata as models of complexity*, Nature **311**, 419 (1984)

[Yas 95] A. Yasutomi, *The emergence and collapse of money*, Physica D **82**, 180 (1995)

[Zai 92] S. I. Zaitsev, *Robin Hood as self-organized criticality*, Physica A **189**, 411 (1992)

[Zha 92] J. Zhang, Y. -C. Zhang, P. Alstroem, M. T. Levinsen, *Modeling forest fire by a paper-burning experiment, a realization of the interface growth mechanism*, Physica A **189**, 383 (1992)

Acknowledgements

The continuous interest and constructive criticism of my supervisor Gerhard Mack provided a stimulating working atmosphere. I enjoyed and profited very much from his fascination and understanding of complex systems which he shared in numerous discussions. I am glad to thank him for all of this, especially for his encouragement and support in going unusual ways in physics and elsewhere.

It is a pleasure to thank Karin Horner and Prof. Dr. Heinz Horner as well as Dr. Reimer Kühn for their warm hospitality, interest and stimulating discussions during all my visits to Heidelberg over the past years.

Special thanks go to Prof. Dr. Steffen Meyer for his interest and support of my work on multiscale phenomena with view on multigrid applications.

Without the uncountable inspiring discussions with York Xylander and his patience with my skepticism this work would surely not be in its present shape and probably it would not have been finished at all. He also introduced me to the principles of C++ and shared some of his programs with me.

Valuable discussions on self-organized criticality in the model of money exchange with Daniel Lübbert always raised interesting points and opened new questions worth thinking about.

My understanding of self-organized criticality and the RG-approach to it has profited from interesting discussions with Dr. Matteo Marsili, Dr. K. Schmoltzi and Prof. Dr. H. G. Schuster. Dr. Ayumu Yasutomi was very open for discussions on his model of money exchange and also provided me with a copy of his program for this model. I am grateful to all of them.

For the very careful reading of the manuscript I would like to thank Max Grießl, Hans Lotter, Daniel Lübbert and York Xylander.

The financial and ideal support by the Deutsche Studienstiftung over so many years is gratefully acknowledged.

MARKE: Den unerforschlich tief
geheimisvollen Grund,
wer macht der Welt ihn kund ?

TRISTAN: O König, das kann ich Dir nicht sagen,
und was du frägst,
das kannst Du nie erfahren.

R. Wagner, *Tristan und Isolde*, II/3